# GROWTH AND STRUCTURE OF NICKEL OXIDE SCALE ON POLYCRYSTALLINE NICKEL

By

ANGELA VIOLETA MOISIN MANOLESCU

A Thesis

Submitted to the School of Graduate Studies

in Partial Fulfilment of the Requirements

for the Degree

Doctor of Philosophy

McMaster University

August 1977

# GROWTH AND STRUCTURE OF NICKEL OXIDE SCALE ON POLYCRYSTALLINE NICKEL

To My Parents

DOCTOR OF PHILOSOPHY (1977) McMASTER UNIVERSITY
(Metallurgy and Materials Science) Hamilton, Ontario

TITLE: Growth and structure of nickel oxide scale formed on polycrystalline nickel

AUTHOR: Angela Violeta Moisin Manolescu, Dipl. Chemist
(Bucharest University, Romania)

SUPERVISOR: Professor W. W. Smeltzer

NUMBER OF PAGES: xix, 231

## ABSTRACT

In this thesis the growth and structure of nickel oxide scales formed on polycrystalline nickel during continuous oxidation and oxidation interrupted by vacuum anneals at 800° and $p_{O_2}$ = 400 Torr were studied. The morphological development of nickel oxide formed commencing with early stages of oxidation to scale growth at very long times was studied by thermogravimetry, scanning electron microscopy and X-ray diffraction measurements.

The results demonstrate the influence of the metal structure on the anisotropy of oxidation, the influence of the defect structure of the oxide set up by the growth process itself on the transport mechanism of the reactants, and the preferential growth of oxide grains.

The nickel oxide scales exhibited initially a bilayer structure or a simple equiaxed structure; these structures could be transformed into a monolayer structure of columnar oxide grains by different methods. The early stage cellular structure of nickel oxide developed into inner equiaxed and outer columnar oxide layers by a combined transport of nickel through the oxide lattice and through boundaries of the oxide grains. The structural development of the nickel oxide scale was correlated with the nonparabolic oxidation behaviour of nickel.

ACKNOWLEDGEMENTS

I wish to express my sincerest thanks and gratitude to my Supervisor, Professor W. W. Smeltzer, for suggesting the topic of this research and for his encouragement, continual suggestions and scientific interest during the course of this project. I shall always cherish my scientific association with him.

Professor J. D. Embury is gratefully acknowledged for his suggestions concerning the theoretical aspect of this investigation and especially for the experimental part related to the oxidation at low oxygen pressure.

I wish to acknowledge the helpful discussions and the experimental support accorded by Professor C. Calvo concerning the X-ray experiments.

I am indebted to Professor R. Anderson as a member of my supervisory committee for his interesting comments concerning especially the kinetic aspects of this project.

I am grateful to Professor H. D. Grundy of the Geology Department for allowing me to use their X-ray facilities.

I am endebted to all the faculty, and especially to Professor G. R. Piercy, Professor J. Kirkaldy, Professor M. B. Ives and Professor R. Kelly for their understanding and warm friendship shown during these long years of study at McMaster University. I am indebted to Dr. Peter Mayer and all my

colleagues in the oxidation group for their scientific discussions.

I owe my thanks to the technical staff of both the Department of Metallurgy and Materials Science and the Institute for Materials Research, and in particular for their technical help. I appreciate the help offered by Mr. Frank Gibb in printing my micrographs.

I thank the following for providing the financial assistance: McMaster University, in the form of graduate assistantship and the National Research Council in the form of a research grant to Dr. W. W. Smeltzer.

The manuscript was typed with skill and especially patience by Mrs. Helen Kennelly, to whom I give special thanks. The figures were drawn with talent by my sister, Ms. Mica Moisin, whose constant moral help and understanding in this last most difficult month are gratefully appreciated.

My sincere thanks to two of my special friends for all their friendship and moral support during these years: to Helen Kennelly and Alexandra Perovic.

All my gratitude to some very special people in my life for their moral support, love and understanding: to Muti, Sandra, Anie and Mica.

Last, and by no means least, I owe my special thanks to my husband Dan for his suggesting of applying for a scholarship with McMaster University and for his constant friendship

moral support and counsel, that made my graduate work more enjoyable. To Dan my deepest gratitude.

Finally, to all the colleagues and friends and all the staff of the Department of Metallurgy and Materials Science and the Institute of Materials Research, with whom I spent six years of my life: to all of them I am deeply indebted.

TABLE OF CONTENTS

LIST OF ILLUSTRATIONS

LIST OF TABLES

# CHAPTER I

## INTRODUCTION

Since virtually every metal and alloy reacts with air at ambient temperatures the oxidation resistance must be considered in most chemical and metallurgical engineering applications. Also, the critical property in high temperature application of a material may not be its melting point or strength. It may lie instead with its oxidation resistance, resistance to other active environments, or embrittlement by contamination. It should also be appreciated that an understanding of the oxidation process makes possible a general understanding of the properties of metals. For practical purposes it is very important to know not only the oxidation mechanism but also the amount of protection offered by the respective oxide to the metal surface. Many metals with a high melting point cannot be used at high temperatures due to poor oxidation resistance. However, several nickel alloys are very stable at high temperatures.

Nickel is a transition metal, which combines with other elements to form a host of compounds which range in chemical bonding from ionic (oxides) through covalent (sulphides, arsenides) to metallic (carbides, nitrides). These possibilities promise diverse chemical bonding, structures and transport

processes, offering thus a rich field for theoretical and experimental investigations. On the other hand nickel has many important industrial applications by reason of its good mechanical and physical properties, of its good corrosion resistance (especially in different practical alloys) and also of its catalytic properties (as flake or finely divided nickel). Since it is important to control the behaviour of nickel in an oxidant atmosphere, many studies have been carried out on its oxidation properties. Nickel forms a simple cubic oxide (NiO) which grows at high temperature according to a parabolic rate law by outward diffusion of cations.

Especially marked deviations from the parabolic law have been observed at intermediate temperatures in the range 300-900°. Temperature coefficients of the oxidation rate constant often show an activation energy of less than half the value for lattice diffusion in nickel oxide. Also structural studies of thin films of nickel oxide have shown that they are highly defective containing small oxide grains and line defects. For both polycrystalline nickel and a variety of single crystal orientations, deviations from parabolic oxidation have been explained by diffusion of nickel in the lattice and also along the paths of low resistance to diffusion offered by grain boundaries and dislocations.

The microstructure of nickel oxide scales, especially at intermediate temperatures, is consistently composed of two

layers, an inner equiaxed layer surmounted by a columnar layer. At high temperatures exceeding 1000°C, a single layer of columnar nickel oxide is commonly formed. Despite a considerable amount of research to understand this morphological development of the oxide, there is at present no unified theory to explain the growth of a double or a single layer scale. It therefore appears at this stage that a careful investigation of the morphological development of the nickel oxide scale would permit an analysis, and an understanding of, firstly, the microstructure of the nickel oxide formed under different conditions of oxidation and, secondly, a correlation of the scaling kinetics with the transport of the reactants through a scale.

It is the objective of this work, based on an experimental investigation, to contribute to the development of a model to explain the growth of the single and double layer scale of nickel oxide, to explain the morphological development of the early stage cellular structure into scale formed of an inner equiaxed layer surmounted by a columnar one, and to account for the transport of nickel through this type of oxide scale. To accomplish this objective the morphological development and structure of nickel oxide scales formed during continuous oxidation and oxidation interrupted by vacuum anneals at 800° and $p_{O_2}$ = 400 Torr commencing from the stage of oxide nucleation to scale growth at very long times (240 hours) were determined by thermogravimetry, scanning electron microscopy and X-ray diffraction measurements.

# CHAPTER II

# LITERATURE REVIEW

## II.1 METAL OXIDATION MECHANISM

In spite of the simple chemical reaction representing metal oxidation,

$$Me + \frac{1}{2} O_2 = MeO$$

the mechanism for formation of the oxide products is a very complicated process. In the majority of cases, a solid reaction product is formed on the metal surface and the reaction proceeds by diffusion of reactants across the oxide layer.

The numerous investigations existent on oxidation kinetics of a large number of metals have led to a number of empirical relationships which are often referred to as "oxidation rate laws". Although these equations alone are not sufficient to characterize the oxidation behaviour of the respective metal, they classify the reaction kinetics and limit the number of possible mechanisms. These simple laws are:

$x = k_L t$ linear law (II.1-1)

$x^2 = k_p t$ parabolic law (II.1-2)

$x^3 = k_c t$ cubic law (II.1-3)

$$x = k_{log} \log (t+t_o)+A \quad \text{logarithmic law} \qquad \text{(II.1-4)}$$

$$\frac{1}{x} = B - k_{il} \log t \quad \text{inverse logarithmic law} \qquad \text{(II.1-5)}$$

where alternatively x may represent the amount of oxygen consumed or metal transformed to oxide per unit surface of the oxide layer thickness provided that this layer is uniform, t indicates time, $k_L$, $k_p$, $k_c$, $l_{log}$, $k_{il}$ represent the rate constants and A and B are constants.

Oxidation mechanisms are generally divided into two principal groups related to the formation of thin films (< 1000 Å thick) and oxide scales (> 1 μm thick). This is an arbitrary division but not without basis since it classifies the driving forces responsible for oxide growth. For thin films, the driving force is the electrical field existing across the film due to the transfer of electrons from the metal to adsorbed oxygen atoms. For thick scales, the driving force is the electrochemical potential gradient existing across the scale.

A survey of published experimental data shows that the logarithmic and inverse logarithmic laws are observed for the formation of very thin oxide films, i.e. for low temperature of oxidation. Scale growth generally follows

parabolic or linear kinetics. The attempts made to explain the different empirical oxidation laws have resulted in a series of general theories. All these theories are well known and several monographs cover this subject [1,2,3]. It is important nevertheless, to emphasize that the different processes involved in metal oxidation may be classified. Initially, a phase boundary reaction occurs involving oxygen chemisorption with subsequent formation of the oxide by transfer of the oxygen into the metal or of the metal into the adsorbed oxygen layer. Upon oxide nucleation, predominant transport proceeds into a space charge layer especially during oxidation at low temperatures. Finally, scale growth occurs by diffusion of cations, anions and electrons through the oxide under an electrochemical potential gradient.

It is usually assumed that the reaction product is present on the metal surface as a plane parallel compact plate. The real situation is often very different from these "idealistic cases". Also there are many data reported in the literature where different authors have found different results for the same metal oxidized practically in the same conditions. These discrepancies are due to the multitude of factors that influence the oxidation process and which are not taken into account by the different oxidation theories.

## II.2 FACTORS INFLUENCING METAL OXIDATION

Thermodynamic data are very important in elucidating oxidation mechanisms. Thermodynamics determine whether a reaction is possible under a given set of conditions. As shown above practically all metals and alloys in the presence of oxygen, even at low temperatures, are unstable, a stable compound is formed and the reaction shows a free energy change which is negative. The thermodynamic analysis of the system involved yields information on the stabilities of different oxides, the lattice defect classification of the oxides and the boundary thermodynamic parameters at the metal/oxide and and oxide/oxygen interfaces. It has also been demonstrated that epitaxial restraints at the metal/oxide interface can lead to free energy conditions in a thin oxide film different from those in bulk oxide.

Generally the oxidation rate increases with increasing temperature. Also in some cases increasing pressure of the oxidant increases the oxidation rate. Another important factor in determining the oxidation behaviour is the purity of the metal. Internal trace impurities may not be important at low temperatures, but at high temperatures of oxidation they may diffuse to the surface and thus have a marked effect on the oxidation process. For this reason, it is necessary to work on metals of a high degree of purity or, if not, to work on metals with known impurities in order to appreciate their effects.

The physical condition of the specimen and especially of its surface plays an important role in oxidation. Polycrystalline specimens exhibit different grain sizes, grain boundaries and sub-grain boundaries that provide line defects influencing oxidation rates. The use of single crystals has the advantage of eliminating these effects and providing data on the influence of crystallographic orientation on the kinetics of reaction. In this respect, the oxidation kinetics of a polycrystalline metal leads to an average value for the different crystal faces concerned. There are different methods available for the preparation of the surface free of pits, facets or irregular roughness, contamination or strain. If the specimen is a single crystal the crystallographic orientation must be determined and if it is a polycrystalline metal, grain size and preferred orientation, if any, should be measured.

The rate of oxidation is predominantly dependent on the structural defects existent in the product layer. These defects are classified as point defects, line defects and surface imperfections. The importance of the defect structure of the oxide lies in the fact that the diffusion of the reactant across the oxide layer takes place via defect mechanisms. Diffusion at high temperatures occurs by means of the lattice point defects. At low and intermediate temperatures dislocations and grain boundaries can act as short-circuit diffusion paths for the transport of the diffusing species.

Usually a metal surface is not atomically smooth. It may consist of plane areas, with some regions showing facets, exposing different crystal faces, or with steps, edges and kink sites. These irregularities may arise from the interactions of line imperfections with the surface, or could appear during the surface preparation. The real situations are still more complicated due to the fact that the character of a surface can change during the process. For example, the atoms in a surface step upon increasing the temperature can evaporate and absorb at other sites on the surface, thus generating kink sites. At high temperatures, the surface may show a thermal etching.

Nucleation of the oxide and epitaxial restraints between the oxide and metal influence the oxidation processes, making the mechanism more complicated than considered in the "ideal cases". In 1952 Bardolle and Bénard[4] showed that within certain ranges of temperature and oxygen pressure discrete oxide crystals, "nuclei", were formed on large grained iron samples. The number and shape of nuclei were functions of crystallographic orientations. Similar observations have been made on the oxidation of nickel at 1000°, by Martius[5]. Thus an oxide grows on a metallic surface under distinct orientation relationships between its different crystallographic faces and that of the underlying metal. There are several theories[6,7] attempting to explain epitaxial growth on the basis of the misfit between the lattices or to the relations of close packed direction in the metal and in the growing oxide.

These relationships of orientation are very important; for example, rate of diffusion through oxide will depend on the oxide orientation if the oxide is crystallographically anisotropic. Even an oxide which is normally isotropic can show anisotropic growth on a metal due to the presence of line and surface defects. Such behaviour is found with nickel oxide[8,9,10].

Concerning the simple kinetic laws of oxidation on the one hand and the very complicated "real situation" existant during oxidation on the other hand due to chemical and crystallographic factors a survey of experimental oxidation results is the most appropriate approach to realize the development of our understanding on oxidation mechanisms. Following the very early investigations in which the elementary ideas of kinetics, structural and topographical aspects of oxidation were proposed, a period followed in which investigations on the kinetic were predominant, reaching a considerable degree of sophistication. In recent years, the limitations of a simple kinetics approach have been appreciated by many workers in the field. The kinetic measurements are now accompanied by careful investigations on oxide structures, preferred orientations of growing scales, defect structures of the formed oxides and mechanical properties of the metal and oxide systems. As will be illustrated in the following section, the oxidation properties of nickel is a good example of this kind of historical development.

## II.3 LITERATURE REVIEW ON NICKEL OXIDE PROPERTIES AND ON NICKEL OXIDATION

### II.3.1 Thermodynamic, Electronic and Transport Properties of Nickel Oxide

Oxidation kinetics are determined by the reaction mechanisms. The reaction mechanisms, in turn, are determined by the properties of nickel oxide, the reaction product of the nickel-oxygen system. It is possible, therefore, to predict the oxidation kinetics from the appropriate properties of nickel oxide or conversely to determine these properties from the kinetic behaviour of nickel during the oxidation under different conditions. It is therefore important to complete a review of the physical and chemical properties of nickel oxide.

(a) Lattice properties of nickel oxide. Nickel oxide has a NaCl type of structure, with a lattice parameter a = 4.1769 Å. This means that the oxygen ions are cubic closed packed and the cations occupy the octahedral holes.

(b) Thermodynamics of nickel oxide. The simplicity of the system nickel-oxygen is in a major part due to the fact that during the oxidation of nickel only one oxide is formed: NiO. The deviation from stoichiometry (nonstoichiometry) of nickel oxide has made the subject of several investigations

because the concept of nonstoichiometry is directly related to that of point defects.

Deviations from stoichiometry in nickel oxide equilibrated under various conditions have been studied by Mitoff[11], Schmalzried[12], Tretyakov and Rapp[13], Tripp and Tallan[14]. These authors have used experimental techniques based on thermogravity and coulometric titrations. Measuring the weight changes at pressures varying between $10^{-1}$ and $10^{-4}$ atm $O_2$, Tripp and Tallan[14] found that nonstoichiometry was proportional to $p_{O_2}^{1/5}$. All measurements illustrated that nickel vacancies are the predominant point defects in nickel oxide but these defects may exist in singly or doubly charged states.

The defect equilibria involving singly and doubly charged nickel vacancies and positive holes can be represented by the following equations:

$$[V'_{Ni}]p = K_{V'_{Ni}} p_{O_2}^{1/2} \qquad \text{[II.3.1-1}$$

$$[V''_{Ni}]p^2 = K_{V''_{Ni}} p_{O_2}^{1/2} \qquad \text{[II.3.1-2}$$

$$\text{if } [V'_{Ni}] >> [V''_{Ni}] \text{ then } p = [V'_{Ni}] = k_{V'_{Ni}}^{1/2} p_{O_2}^{1/4} \qquad \text{[II.3.1-3}$$

$$\text{if } [V''_{Ni}] >> [V'_{Ni}] \text{ then } p = \frac{[V''_{Ni}]}{2} = [\tfrac{1}{4} K_{V''_{Ni}}]^{1/3} p_{O_2}^{1/6} \qquad \text{[II.3.1-4}$$

In these expressions, $K_{V'_{Ni}}$ and $K_{V''_{Ni}}$ are the equilibrium constants for the respective defect equilibrium.

Results of Tripp and Tallan[14] measured the variations of the weight change of nickel oxide samples as a function of oxygen pressure. Depending on temperature the values $\frac{1}{n}$ vary

from $\frac{1}{4}$ to $\frac{1}{6}$. It is difficult to assign an exact charge to the nickel vacancies because the pressure dependence of nonstoichiometry does not follow an exact $p_{O_2}^{1/4}$ or $p_{O_2}^{1/6}$ dependence. Results of nonstoichiometry measurements must be correlated with the transport properties in order to define the defect structure of nickel oxide.

(c) Electrical conductivity of nickel oxide

The dependence of electrical conductivity on temperature is determined by both concentration and mobility terms. However, at high temperatures, the concentration term is by far the most important and the activation energy of the electrical conductivity reflects that of heat of formation of the electronic defect. The electrical conductivity of nickel oxide increases with partial pressure of oxygen but there is no general agreement as to the exact dependence. The experimental results may be divided into two main groups in which the conductivity is alternatively found to be proportional to approximately $p_{O_2}^{1/4}$ or to about $p_{O_2}^{1/6}$. Correspondingly the nickel vacancies are interpreted to be single or doubly charged[15].

(d) Diffusion in nickel oxide

The self-diffusion coefficient of nickel in nickel oxide has been studied by means of the tracer technique by Lindner and Akerström[16], Shim and Moore[17], Choi and Moore[18], Volpe and Reddy[19]. Klotsman et al[20] have estimated the self-diffusion coefficient from tracer distribution studies in growing oxide scales and Fueki and Wagner[21] from studies of parabolic oxidation of nickel. All these results are summarized

in fig. II.3.1-1.

These values of the diffusion coefficient differ by a factor of ten and the activation energy varies from 43.5 to 60.8 kcal/mole.

Diffusion of $^{18}O$ in a nickel oxide single crystal between 1100° and 1500° and a $p_{O_2}$ = 50 Torr has been determined by O'Keefe and Moore[22]. They found the following value: $Do = 6.2 \times 10^{-4} \exp(-57{,}500/kT)$.

At temperatures below $\frac{T_{melting}}{2}$ of a solid, diffusion cannot be arbitrarily regarded as proceeding by a point defect mechanism. Structural defects such as dislocations and grain boundaries act as preferred paths for diffusion and hence serve as an important mode of transport. Therefore these kinds of defects play an important role in the oxidation of nickel at intermediate temperature. These considerations have been demonstrated for nickel oxide growth on polycrystalline nickel[23] and nickel single crystals[24].

Hart[25] has discussed the possible role of dislocations in solid diffusion and derived for the measured diffusion coefficient the equation:

$$D_{meas} = D_{disl.} \cdot f + D_{\ell}(1-f) \qquad \text{(II.3.1-5)}$$

where f is the fraction of time which an atom spends in dislocations and $D_{disl}$ is the dislocation diffusion coefficient, and $D_{\ell}$ is the lattice diffusion coefficient.

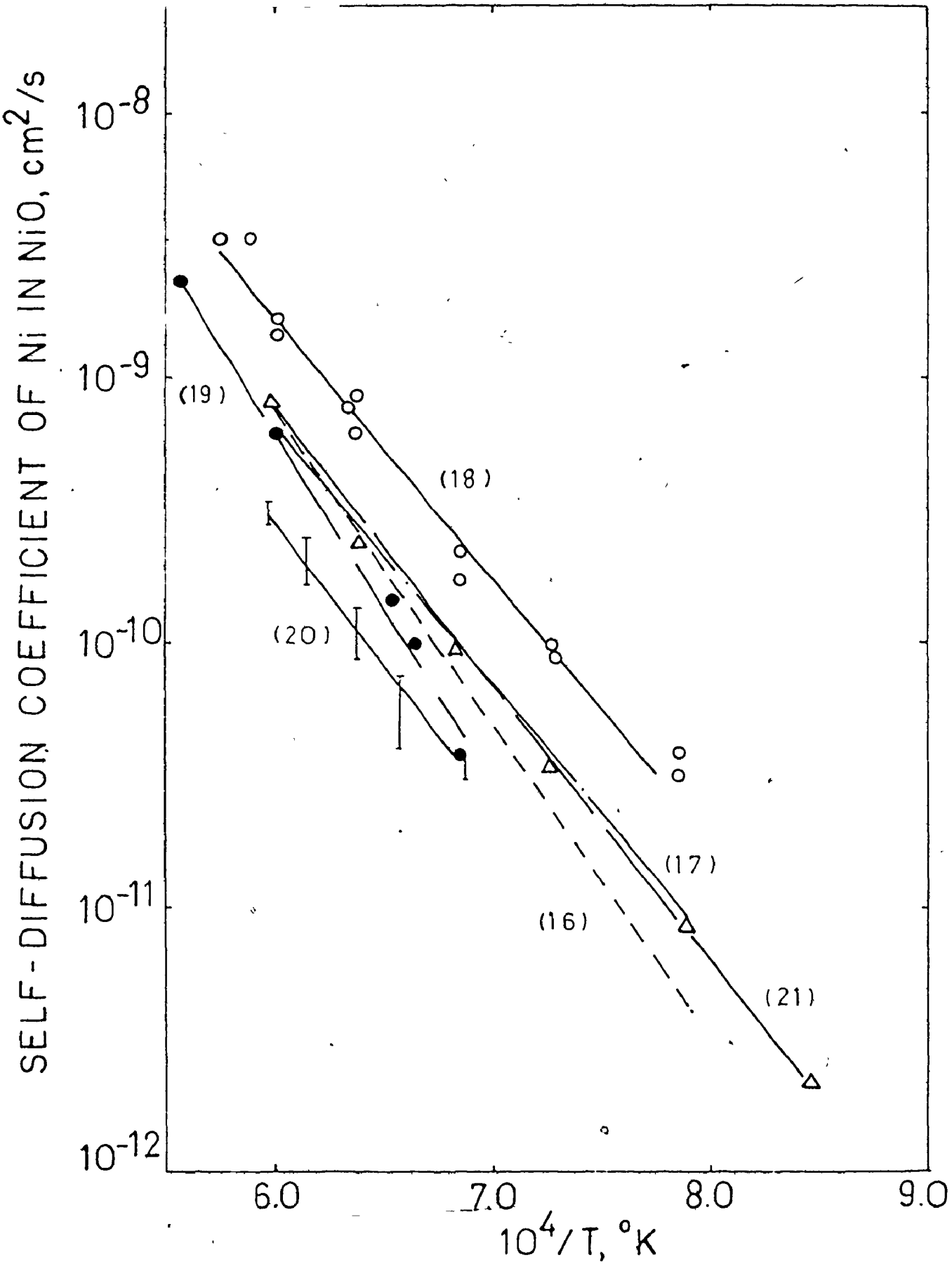


Fig. II.3.1-1 Reported value of self-diffusion coefficient of Ni in NiO [16] [17] [18] [19] [20] [21]. (After Kofstad[3]).

II.3.2 Literature Review on Nickel Oxidation

The system Ni-$O_2$ was chosen for investigation because of its simplicity. Only the one oxide, NiO, forms on nickel. Moreover the thermal expansion coefficient of oxide and metal differ only by .05% from room temperature to 1000°. Accordingly the microstructure of the scales formed under different exposure conditions will not change upon cooling specimens to room temperature. Presently available results demonstrate that the nickel oxide scale formed during oxidation can be considered as compact exhibiting good adherence to the metal. In spite of controversial experimental evidence, as shown in the preceding section, nickel oxide can be considered as a p-type semiconductor in which the prevalent defects are nickel vacancies, existing predominantly in the doubly charged state. In this simple case nickel diffuses through the nickel oxide scale to react with oxygen at the external scale surface.

The oxidation mechanism of nickel is not so simple and it is therefore appropriate to delineate oxidation results obtained at low temperature, $T < 200°C$, at intermediate temperature, $200° < T < 1000°C$, and at high temperature, $T > 1000°C$. The interaction of nickel with oxygen starts at very low temperatures, at small time of exposure and low pressure of oxygen. The process of interaction begins with the formation of a chemisorbed oxygen layer on a nickel surface followed by the fixation of molecular oxygen on the top of the chemisorbed film and the beginning of oxidation. For each

crystallographic surface it is possible to find a structural NiO configuration. These intermediate structures formed on nickel in many aspects have characteristics of a three-dimensional compound. These intermediate compounds have their own characteristics:- a - mode of oxygen adsorption, b - sticking probability of oxygen, c - degree of coverage, and d - a degradation temperature associated with it. Each structure is formed on the surface of its predecessors. This means that when nickel oxide is grown on a nickel substrate at room temperature, the nickel substrate is separated from the oxide by distinct states representing increasing oxygen activity until nickel oxide is formed. The oxidation kinetics of nickel have been studied over a wide range of temperature and pressure on polycrystalline and single crystal specimens.

(a) Kinetics and reaction mechanisms of nickel oxidation

At intermediate temperatures there have been attempts to establish a comprenensive mechanism for nickel oxidation but none of the proposed mechanisms have received general acceptance. Uhlig and collaborators[26] investigating the oxidation of nickel at temperatures within 307-442°C, found that the metal oxidized logarithmically. There is a discontinuity in the oxidation curve at the Curie temperature, the processes fitting to a two-stage logarithmic law. This transition in

the oxidation curve was interpreted as due to a change in the electron work function. The mechanism postulated by the authors involved the transfer of electrons from metal to oxide as the rate controlling reaction step.

Engel and coworkers[27], studying the oxidation of nickel at 400°C and 500°C, have found that the first period of oxidation may be represented by a logarithmic rate law (for approximately 5 hours). At longer periods of time, the oxidation was explained by a quartic rate law. The step determining the rate for this latter law was considered as the diffusion of nickel ions under the presence of a negative space charge caused by the distribution of nickel vacancies in the growing oxide. Different investigators have found at intermediate temperatures a cubic law for nickel oxidation. Thus Hauffe and coworkers[28] derived a model for explaining the cubic oxidation law at 400°C by assuming that the rate determining process was the migration of cations in the oxide phase under the influence of an electrical charge layer governed by local equilibrium at both the Ni/NiO and NiO/gas interfaces.

Starting from the investigation of Boreskov[29] on isotopic exchange of oxygen on nickel films, Wagner[30] derived a model for the oxidation results obtained at 250°C in which it is assumed that the process of dissociation of oxygen molecules played an important role. Perhaps at this stage it is useful to take into consideration the investigation of

Ritchie [31]. This author considers that kinetic measurements alone are insufficient for deciding the mechanisms of oxidation. He studied the influence of an applied electric field across the growing scale on the oxidation rate. The measured resistance across the growing nickel oxide implied that nickel oxide grew at the oxygen/oxide interface. Moreover, void formation at the oxide-metal interface which might be expected to lead at an appreciable increase in resistance, could be discounted.

None of these mechanisms have found general applications. Recently Graham and Cohen [32] have completed a detailed study of nickel oxidation from 24° to 450° at oxygen pressures ranging from $5\times10^{-3}$ to $6\times10^{-1}$ Torr using a manometric method. They found that initial rapid oxygen adsorption on nickel was followed by slower oxidation, obeying a logarithmic rate law over the thickness range 8-30 Å. In growth of thicker films, nickel transport through the oxide occurred predominantly via easy boundary diffusion paths.

From 500° to 1400°C nickel oxidizes at long times by a parabolic relationship. When this type of oxidation occurs by the ambipolar diffusion of nickel through nickel oxide by cation vacancies, the classical expression derived by Wagner [33] for the rational parabolic rate constant may be applied.

$$k_r(\text{eq/cm sec}) = \bar{C}_{eq} \int_{a_o'}^{a_o''} D^*_{Ni}\, d\ell n a_o. \qquad \text{(II.3.2-1)}$$

In this expression, $\bar{C}_{eq}$ is the average nickel content in equivalents, $D_{Ni}$ is the self-diffusion coefficient of nickel and $a_o$ is the oxygen activity which is integrated from outer to inner interface as designated by the primes. Khoi[10] has recently demonstrated that these principles apply to the oxidation of nickel at temperatures exceeding 900°C. This is illustrated by plotting the parabolic rate constants in Arrhenius form as shown in Fig. (II.3.2-1)[34][38]. The full lines represent the temperature coefficient of the rate constants estimated from nickel tracer diffusion in nickel oxide crystals. Values obtained by graphical integration of eqn. (II.3.2-1) were determined from the diffusivities obtained at different oxygen pressures. Since the atom fraction of vacancies in nickel oxide is extremely small and assuming that they are divalent eqn. (II.3.2-1) reduces to $k_r = 3\bar{C}_{eq} D_{Ni}^*$. This formula was also used to calculate $k_r$. The plots demonstrate that the calculated values by both methods are consistent with those obtained experimentally above 900°C. The causes for the much larger experimentally determined parabolic oxidation constants at lower temperatures result from nickel transport in the oxide scales being more rapid than assumed by this vacancy diffusion mechanism.

Gulbransen and Andrew[35], studying the nickel oxidation between 400 and 750° have found that at 400 and 550° the initial oxidation rate was nonparabolic. Two possible explanations for this non-Wagnerian behaviour were advanced

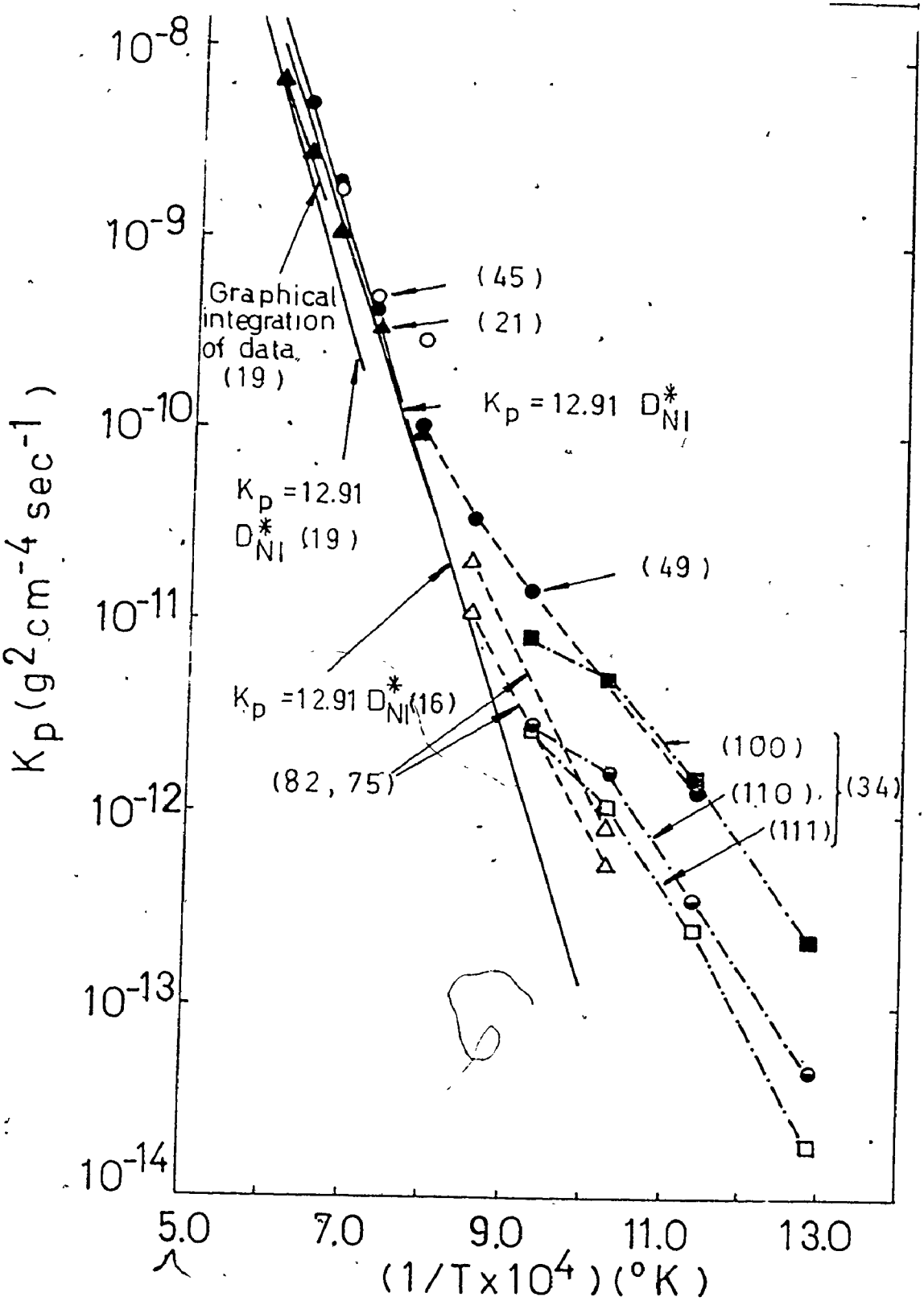


Fig.II.3.2-1 Reported and calculated value of temperature coefficient of the parabolic oxidation constants for nickel oxide growth on polycrystalline and single crystals nickel[16] (19) (21) (34) (45) (49) (75) (82) (After Khoi et al.)[38]

by the authors: (a) a decrease in the number of nickel vacancies available for nickel ion diffusion caused a corresponding decrease in the rate of oxidation, and (b) an increasing oxide grain size as the film thickened, decreased the contribution of boundary diffusion in the overall reaction.

To explain this behaviour Perrow et al[23], working on polycrystalline nickel, advanced a model for the oxidation mechanism taking into account short circuit diffusion. The effective diffusion coefficient for movement of atoms in a solid ionic matrix containing a random array of short circuit paths can be expressed as a function of the coefficients for lattice and boundary diffusion as

$$D_{eff} = D_L(1-f) + D_B(f) \quad . \qquad \text{(II.3.2-2)}$$

The rate of oxidation under ambipolar diffusion conditions can then be expressed as:

$$\frac{dx}{dt} = \Omega D_{eff} \frac{\Delta c}{\Delta x} \quad . \qquad \text{(II.3.2-3)}$$

In these expressions, $D_L$ is coefficient for lattice diffusion, $D_B$ is the coefficient for boundary diffusion, and $\Omega$ is the volume of oxide/Ni ion.

The degree of short circuit diffusion will depend on processes such as recrystallization and grain growth which govern the increase in crystalite sizes. If the fraction of

diffusion sties at boundaries is not time dependent, integration of equation (II.3.2-3) yields

$$x^2 = 2\ \Omega\ D_{eff}\ \Delta ct = K_p(eff)t. \qquad \text{(II.3.2-4)}$$

From structural investigations the authors found that the fraction of surface area associated with boundaries was constant during the initial stages of the reaction. In these conditions, the initial reaction may be defined by a parabolic relationship in which the effective parabolic constant contains terms for lattice diffusion, boundary diffusion and a constant fraction of sites within low resistance paths. That is,

$$D_{eff} = D_L(1-f^\circ) + D_b f^\circ = \simeq D_L + D_B f^\circ\ , \qquad \text{(II.3.2-5)}$$

where $f^\circ$ is the constant fraction of sites in boundaries during the incubation period before onset of oxide recrystallization.

To determine the fraction of sites in short circuit paths per unit area at time t, the authors made two assumptions: (a) the crystallite growth, during the rapid increase in crystal size due to recrystallization, was well represented by the standard grain growth equation, and (b) the fraction of surface covered by boundaries would be the number of boundaries per unit area of film surface multiplied by the boundary width. The equation obtained for the fraction of sites in the short

circuit path was

$$f(t) = \frac{2d}{D_t} , \qquad \text{(II.3.2-6)}$$

where d is the boundary width and $D_t$ is the crystallite size at time t. The standard equation for grain growth during recrystallization is:

$$D_t^2 - D_o^2 = Kt. \qquad \text{(II.3.2-7)}$$

Equation (II.3.2-6) becomes after substitution:

$$f(t) = \frac{2d}{(D_o^2 + Kt)^{1/2}} \qquad \text{(II.3.2-8)}$$

and finally the authors obtained for the growth of oxide films determined by both short-circuit diffusion and lattice diffusion of the reactants through a film the equation:

$$x^2 = 2\Omega D_L \Delta c t\{1 + D_B/D_L \frac{2d}{k} \frac{2(D_o^2+Kt)^{1/2}}{t}\} \qquad \text{(II.3.2-9)}$$

This model was used to explain results for the oxidation kinetics of polycrystalline nickel at intermediate temperature.

Working with annealed and cold worked nickel, Graham Caplan and Cohen[36] have interpreted the apparent parabolic rate constant as made up of two components: a normal lattice diffusion term plus a contribution from leakage paths. For cold-worked nickel, the contribution from leakage paths was greatest at short times and temperatures < 700°, but remained

appreciable at higher temperature. The cold worked nickel developed finer-grained oxide and oxidized most rapidly. The autnors concluded that the experimental data fitted to a model based on a decreasing number of leakage paths for nickel at nickel oxide grain boundaries by a first order reaction.

Herchl et al[34], in an extensive investigation on the oxidation properties of nickel single crystals of (100), (111) and (110) orientations at temperatures in the range 500°-800° correlated the oxidation kinetics with structure and texture of the oxide films. A marked anisotropy in the reaction rate and oxidation behaviour of the metal orientations investigated was observed. The (100) crystal exhibited the largest oxidation rate at all the temperatures. All kinetic curves indicated a continuously decreasing rate with exposure time. This behaviour was explained by the previously given model for short-circuit diffusion of nickel through lattice defects and along low resistant boundary paths in nickel oxide. Equation (II.3.2-9) can be placed in the form

$$\frac{dx^2}{dt} = 2\ \Omega\ \Delta c D_L + 2\ \Omega\ \Delta c\ D_B f(t) \qquad \text{(II.3.2-10)}$$

in which $2\ \Omega\ \Delta C D_L$ is the parabolic rate constant for lattice diffusion and $2\ \Omega\ \Delta c\ D_B\ f(t)$ is the line defect contribution to the overall transport of the reactant. Accordingly, the effective time dependent parabolic oxidation constant can be

expressed as

$$k_p(t) = k_L + k_B f(t) \quad . \qquad \text{(II.3.2-11)}$$

Upon testing different models for f(t), the authors found that the general grain growth equation, eqn. (II.3.2-8) gave a first approximation to the decay of diffusion sites at the oxide grain boundaries. Eqn. (II.3.2-9) was placed in the following form for analysis of the kinetic curves,

$$\frac{1}{\left(\frac{dx^2}{at} - k_L\right)^2} = \frac{k_3}{4k_B^2 d^2} t + \frac{D_o^2}{4k_B^2 d^2} \qquad \text{(II.3.2-12)}$$

Plots of $\frac{1}{\left(\frac{dx^2}{at} - k_L\right)^2}$ versus t were linear for the (100) and (111) faces. Also, estimates of the relative values of boundary to lattice diffusion of nickel in nickel oxide were of the correct order of magnitude.

A more sophisticated approach to short-circuit diffusion behaviour in oxide films at intermediate temperature has been proposed by Matsunaga and Homma[37]. In a recent investigation, the authors considered not only the influence of the decay of short circuit diffusion paths in a growing oxide film, but also the influence of the type and the width of the grain boundaries. Because the films considered are generally of a bi-layer structure, effective diffusion coefficients, $D^I_{eff}$ and $D^{II}_{eff}$ were assigned to the inner and outer oxide layers respectively. Thus an effective diffusion coefficient for each layer

can be defined as,

$$D^i_{eff} = D_L(1-f_i) + D_B f_i \quad . \qquad \text{(II.3.2-13)}$$

To find an expression for $f_i$, they considered a square shape for the grain with a certain width. Thus

$$f_i = \frac{\sum_{j=1}^{N} \left( \sum_{k=1}^{4} d^i_{jk} \right) B^i_j}{2 \left( \sum_{j=1}^{N} B^{i\,2}_j \right)} \qquad \text{(II.3.2-14)}$$

where $B^i_j$ is the grain diameter on the j grain in the i layer and $d^i_{jk}$ is the kth boundary width of the j grain in the i layer. This square grain is represented in the figure

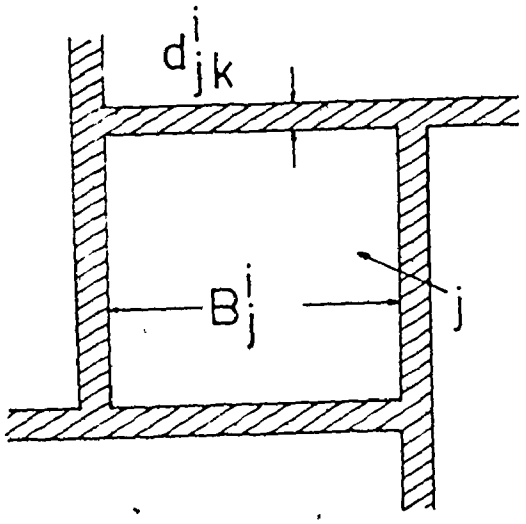


Fig. II.3.2-2 A model of the j-th grain in the i-th scale layer [25]

The time dependence on the average grain diameter was considered to obey a general grain growth equation of the form

$$(E^i_t)^n - (E^n_o) = G^i(t-t_1) \qquad \text{(II.3.2-15)}$$

where n is an integer, $E_t^i$ is the average grain diameter in layer i at time t and $E_o$ the initial average grain diameter. This modified treatment for short-circuit diffusion of metal in an oxide film undergoing recrystallization and grain growth was employed to interpret the growth kinetics of cuprous oxide on copper and nickel oxide on the (110) nickel face which could not be interpreted by the simplified model utilized by Khoi et al[38].

(b) The structure of thin nickel oxide films

All the data reported in the literature on thin films indicates a strong anisotropy of the oxidation rate with orientation of the nickel face (L. E. Collins[39], Otter[40], Lawless and coworkers[8] Mitchell and coworkers[41] and Khoi[10] The results are different in some respects and depend very much on the preparation and characterization of surface prior to oxidation. These authors agree that (100)Ni oxidizes more rapidly, followed by (110) and (111) faces. Also the oxide films formed on (100) and (111)Ni are characterized by parallel orientations with the nickel substrate. The film on (110)Ni is exhibited both on (110) and (100) planes. Some results also indicate that (111)NiO grows on a less perfectly prepared (100)Ni face. Pu and coworkers[42] suggest that the number of orientations of an overgrowth phase existent on each orientation of the substrate is related to the number of the directions of maximum atomic density existent in the respective surface. For example the (100) face has two close-packed

directions; there will be less restriction for the oxide to grow and the perfection of the nickel substrate will influence the oxide orientation. The (111) face of nickel is characterized by three close packed directions which define a plane uniquely and then always the parallel orientation has been found. On the (110) plane of nickel there is only one close packed direction and the oxide can grow in any radial direction around the <110> film axis.

At this point it is worthy to take into account the most recent investigation of Mitchell et al[41], regarding the thin film formation on (100)Ni. The authors attempted to correlate the oxidation kinetics and crystallographic structure of the developing film in order to understand the mechanism of the formation of a protective oxide film. Based on the kinetic measurements and the structural observations, they have suggested the following model for oxidation of (100)Ni. Oxygen is first chemisorbed with little or no activation energy to form a dissociatively bound oxygen c(2×2) structure. Before this structure completely fills the geometrically available c(2×2) sites, nickel oxide nucleates in two different orientations at a fixed number of sites dependent on temperature but independent of pressure. These nuclei are growing laterally by the interaction at their periphery with oxygen gas. Oxidation at low temperature virtually ceases when all the surface has been covered by oxide. The authors also conclude that the most probable mechanism involves a fixed number of nucleation sites on the metal surface. The nickel oxide nuclei, in turn, grow above the critical size by receiving

reactants by diffusion over the completed c(2×2) chemisorbed structure and in addition oxygen by direct impingement from the gas phase. When the oxide was developed, it was detected in two discrete morphologies:

(1) A parallel or (001) epitaxy: Ni(001)//NiO(001), Ni[110]//NiO[110] and

(2) A (111) oxide with two equivalent orientations Ni(001)//NiO(111), Ni[$\bar{1}$10]//NiO[$\bar{1}$10], Ni[1$\bar{1}$0]//NiO[$\bar{1}$10].

(c) Epitaxy of nickel oxide formed on polycrystalline nickel

The early stage oxidation in the $H_2/H_2O$ atmosphere at 1100°C was studied by Martius[5]. This author studied the influence of the metal grain orientation on the number, size and shape of the oxide nuclei and also the influence of the grain boundaries of the metal on nucleation. Perrow and coworkers[23] have investigated the structure of oxide films formed at 500 and 600° on mechanically polished polycrystalline nickel. The films consisted of small crystallites 200-800 Å in size; the oxide thickness and orientation depended on metal grain orientation. Two important investigations on the epitaxy of nickel oxide are those by Gulbransen[43] and Gulbransen and Hickman[44]. They have determined and characterized the orientation of the oxide in thin films, the texture of thick scales using transmission electron microscopy and x-ray techniques. The size of the NiO crystallites in the films varied from 300 to 800 Å at 400° and from 300 to 2000 Å at 550°C depending on the exposure time. They observed

that nickel oxide is formed layer by layer, the size and the shape of the crystal depending on the rate of formation of the nuclei and on the rate of growth of the oxide crystals. The nuclei formed not only on the very initial oxide film but between the different crystals or oxide.

The preferred orientations of thick NiO scales, as as confirmed by Douglass[45], is the (001)NiO plane lying parallel to the metal surface. In studies effectuated by Goswami[46], the oxide initially has its fiber texture parallel to the metal which later becomes randomly oriented and finally after longer exposures exhibits a preferred orientation determined by the oxidation conditions.

Baur and coworkers[47], investigating the oxidation of very pure nickel between 850° and 1200° and at oxygen pressures from $6.5\times10^{-3}$ to 20.4 atm. have observed the development of a preferred orientation of nickel oxide. The authors found that with increasing temperature the {111}, {220}, {331} and {421} peaks disappeared whereas the (200) and (400) peaks increased in intensities until the (200) peak predominated. This latter orientation provides the densest possible nickel atom packing parallel to the metal surface.

(d) The microstructure of the nickel oxide scales formed in different conditions of oxidation of nickel

A fascinating aspect of nickel oxidation is associated with the microstructures of the scales. Oxidation of nickel, believed one of the simplest metal oxidation processes, is actually very complicated, especially because of the bilayer structure of nickel oxide scale formed. The formation of a single or a double scale during the oxidation process has been subjected to many controversial theoretical interpretations. The actual situation is still more complicated, because the experimental data reported by different workers on the scale structure is characterized by disagreements. To illustrate the challenge of a systematic investigation on scale microstructures, a review is presented of the experimental results on this subject.

Thus Berry and Paidassi[48,49] found that the oxidation of polycrystalline nickel at temperatures equal to,or below 900° and for periods of time up to 100 hours led to the formation of a single layer scale. Oxidation at temperatures higher than 900°, however, resulted in the formation of a double layer oxide consisting of a compact outer layer surmounted on a fine porous inner layer. Both of these layers grew parabolically; the ratio of their thickness (outer/inner) varied from 0.4 at 1000° to 0.2 at 1200°C. The presence of the two layers was suggested to be associated with the purity

of nickel specimens; a single layer scale was formed on nickel of 99.98% purity while bilayer scales were found on nickel of 99.95% purity.

Hales[50], working with a very pure nickel, 99.999% purity, at 1000° and for long periods of oxidation until 98% of the nickel was transformed in oxide, always found a single layer scale. The metallographic cross section obtained by Douglass[45] from an oxide scale obtained by the oxidation of nickel of 99.97% purity during 30 hours of oxidation also indicated a single layer scale consisting of columnar crystals, fig. (II.3.2-3).

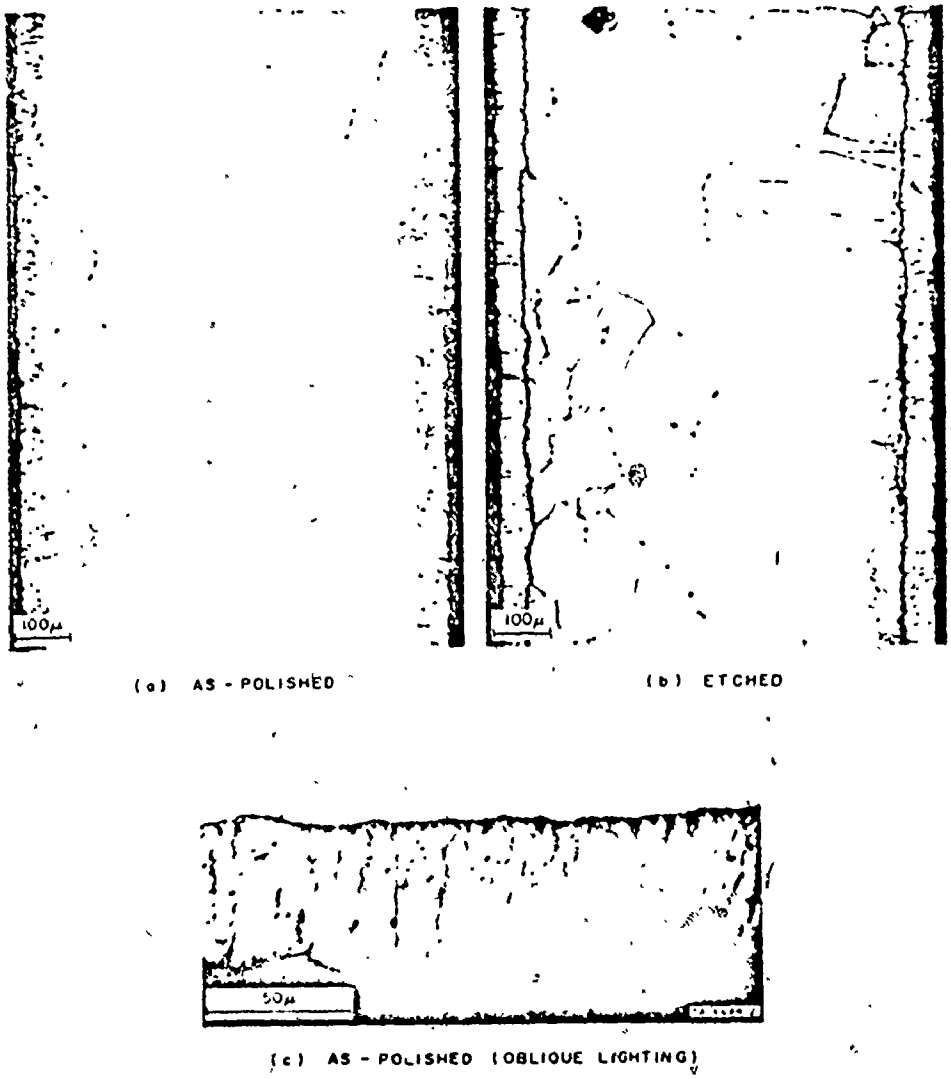


Fig. II.3.2-3 Structure of NiO formed during oxidation of pure Ni for 30h at 1000° in air.

Khoi and coworkers[38] investigated the oxidation of (100), (110) and (111)Ni single crystals of 99.999% purity in the temperature range 500-800°C. They found in all cases a scale consisting of two layers except for the (110)Ni orientation on which both single and duplex scales were found. The ratio outer/inner layer for the majority of the situations increased with time and temperature. It was also established that the grain size increased in the outer layer, in time. Caplan and coworkers[51] have demonstrated from an investigation on the oxidation of cold worked and annealed nickel at 700°, 900°, 1100° and 1270° for 20 hours, that nickel oxide grows as a bilayer scale at 700° and 900°C while at 1100° and 1270° a single layer scale is formed independent of the surface condition of the nickel specimens. The preparation of nickel prior to oxidation (cold worked or annealed), however, influenced the size of the oxide grains and the thickness of the inner layer. To illustrate these conclusions some of Caplan and coworkers'[51] micrographs are reproduced in figs.II.3.2-4 to II.3.2-7. Ilschner and Pfeiffer[52] have established that during the oxidation of > 99.5% pure nickel a scale consisting of two easily distinguishable zones is found. Inert platinum markers used by the authors were always located within the scale, implying that both anion and cation diffusion is involved in the growth of the oxide.

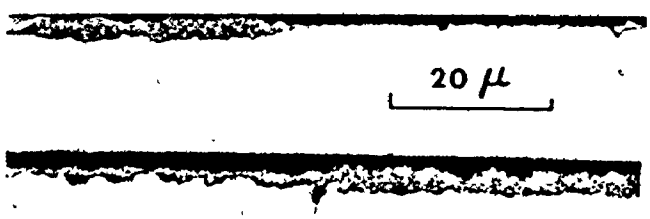


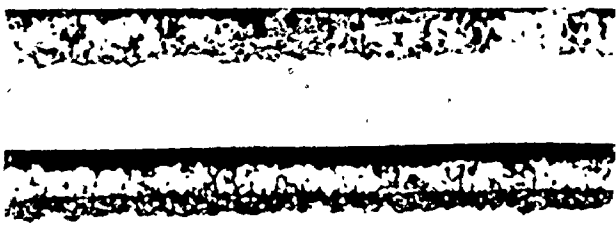








Fig. II.3.2-4 Oxide structures formed on Z.R. Ni in 20 hours at 700°: (a) and (b) for annealed nickel and (c), (d) and (e) for cold worked nickel. (a) and (c) are nonetched micro-sections; (b) has the metal etched, (d) has the oxide etched and (e) is a fractured sample. × 5000.


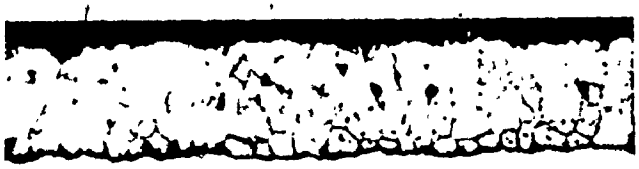

Fig. II.3.2-5 Nickel oxide scale formed on cold worked C.P. nickel at 900° in 20 h. The oxide is etched. × 750

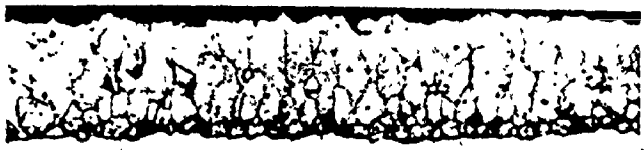

Fig. II.3.2-6 Oxide structure formed on Z.R. nickel in 20 h at 900° (cold worked nickel). × 75

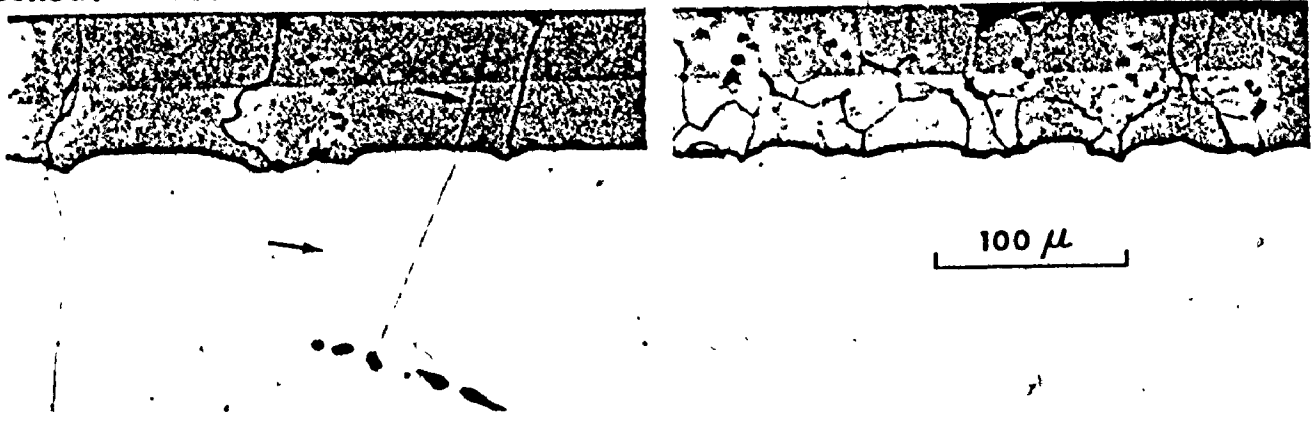


Fig. II.3.2-7 Oxide formed on C.P. nickel in 20 h at 1270°. (a) the nickel was annealed (b) the nickel was cold worked × 250

Sartell and Li[53] working with spectrographically pure nickel oxidized at temperatures ranging from 950° to 1200°C and exposures up to 140 hours have found that the isothermal kinetic data fitted two consecutive parabolic relationships, for earlier and for later periods of oxidation. Inert markers (platinum wires 0.00025 cm in diameter) were also found to be located within the oxide scale composed of an outer black layer of coarse columnar grains and a light green inner layer of fine equiaxed grains. X-ray examination of both layers indicated different values for the lattice parameters of NiO; the structure of the inner layer was slightly expanded while that of the outer was slightly contracted with respect to bulk crystalline oxide. The authors also measured the rate of increase in thickness of the two layers and of the total layer and parabolic dependences approximately represented the results. These similar results for the outer layer and total scale growth and the location of the inert markers at the boundary between the oxide layers indicated that growth of the outer layer and the total scale are mainly controlled by diffusion of the cations.

Working on nickel of 99.95% purity at 1000°C, Rhines and Wolf[54] have correlated the development of the bilayer scale with accumulation of stress. It was found that the "undergrowth" inner layer of nickel oxide was less developed upon oxidation of cylindrical specimens.

Several workers have attempted to directly correlate the formation of the bilayer scale to the presence of the impurities in the nickel specimens. On this line, Terao[55] studied the structure of nickel oxide formed on nickel of 99%, 99.3% and 99.98% purity at 1100° for periods up to 100 hours. The scales formed on less pure nickel consisted of three layers. The outermost layer was black, the intermediate layer was grey and the innermost one was green in colour. The scale formed on very pure nickel indicated the presence of only one layer of bright green colour. The growth of the two inner layers followed a parabolic law and the outer layer (I) increased at a faster rate than parabolically, observations similar with those of Sartell and Li[53]. Electron microprobe analysis of the nickel and oxygen distributions in the different oxide layers were determined. The author related the difference in the morphological structure of the three layers to the different nickel-oxygen contents and the physical conditions under which the layers formed.

In contrast to the above results, Ueno[56,57,58,59] observed that multilayer scales form independent of the purity of nickel. On impure nickel, the scale obtained after 29 hours of oxidation at 1170° consisted of black outer and green inner layers. Also this layer could be subdivided into two differently oriented sublayers. Two major types of grain orientation, (100) or (311)NiO parallel to the metal surface, were found in the outer oxide layers of different specimens. The author designated these scales as $R_1$ and $T_1$. On

high purity nickel two types of scales formed differing in the orientation of the grains: outer layer of a $R_2$ scale consists of grains oriented with {100} planes parallel to the surface and $T_2$ scales exhibit {311} oriented grains. The inner layer of the $R_2$ scale is randomly oriented while the inner layer of the $T_2$ structure had a slight tendency toward a {111} orientation.

These scale structures were influenced by the surface treatment of nickel prior to oxidation such as mechanical polishing by different grades of abrasives and electropolishing. However, definite conclusions could not be formulated on the effect of these variables. The ratio of thicknesses black/green layer in the type $R_2$ scale varied depending on the temperature and time of annealing. To correlate the scale microstructures with the stresses developed in the scale during oxidation the author used the flexure technique. The flexure was independent of temperature and on the difference in thickness between the type $R_2$ and $T_2$ scales but it was proportional to the thickness of the green layer. The deflection of the black/green bilayer scale having the same thickness as that of the black outer layer reversed upon decreasing the thickness of the green layer. This behaviour suggests that the deflection is caused principally by a stress gradient existing predominantly in the green layer.

The total scale and the individual layers of the type $R_2$ scale grew according to parabolic kinetics. In the case of the type $T_2$ scale, the inner layer is initially formed before subsequent development of the outer layer. Parabolic kinetics were obeyed in both stages but the rate of oxidation of the earlier stages was higher than those of the latter stage.

The number of oxide grains per $mm^2$ as a function of time at different temperatures for $T_2$ and $R_2$ types of scales was determined. In the initial growth stage of type $T_2$ scale, the growth rate of grain size is highest. Electrical conductivity measurements coupled with the colours of the different types of oxides were interpreted by assuming that the green inner zone of the type $R_1$, $T_1$ and $R_2$ scales consisted of stoichiometric nickel oxide, while the black oxide in the four types of scales contained an excess of oxygen.

(e) The mechanism of formation of bilayer scale

Despite the lack of correlation between the experimental results reported in the literature on the microstructures of nickel oxide scales, it is possible to conclude that the following factors influence the single and bilayer scale characteristics: a) range of temperature, (b) purity of the nickel specimen and type of impurities, (c) heat treatment of nickel specimens, (d) surface preparation of the metal, (e) specimen geometrical shape, (f) mechanical properties of the nickel oxide scales formed during oxidation and (g) time of exposure of nickel specimens to the oxidizing

atmosphere. Therefore the discrepancies observed in the experimental data arise from the fact that different authors considered the influence of an insufficient number of these factors on the morphological development of scales and, also, to the lack of different types and systematic observations of the development of the scale in time for a well characterized nickel specimen under precisely defined experimental conditions. In view of the diverse observations the attempts of explaining the formation of the bilayer structure of nickel oxide have resulted in a number of oxidation mechanisms but to the present a unique understanding of the mechanism has not been advanced.

Dravnicks and McDonald[60] made the first attempt to explain the process for formation of a bilayer oxide scale. They analyzed the oxidation process starting at the atomic scale up to the formation of a scale consisting of up to three layers of different structured oxide. A columnar layer was considered to initially form. Due to the consumption of the metal a so-called "zone of metal consumption" was then assumed to be filled with another structured oxide. This assumption implied that the scale must grow in its interior and not only by transfer of metal atoms for reaction at the oxide/gas interface. The authors proposed three possible mechanisms responsible for oxygen supply to the metal consumption zone:

a) diffusion of oxygen through cracks of the scale;

b) dissociation of the scale at the inner interface,

c) regular ion or atomic diffusion of oxygen through the scale.

All the mechanisms proposed by different workers to explain the formation of a bilayer scale can be classified as follows:

1) The models based on the postulate that the first formed layer is columnar which transforms in its inner region to an equiaxed layer. Depending on the transport process for oxygen required to form the inner layer, three types of mechanism were developed. a) Birks and Rickert[61] considered that oxygen results from dissociation of the columnar nickel oxide scale at the oxide/metal interface. As defined in fig. II.3.2-8 oxygen reacts with nickel metal forming new oxide and the nickel resulting from dissociation diffuses to react with oxygen at its outer surface. b) This above mechanism was expanded by Mrowec[62] who considered that oxygen is supplied from the atmosphere through grain boundaries in the columnar layer, which in time could develop into fine vertical microchannels and permit inward gaseous diffusion of oxygen. Oxygen migration in the inner equiaxed layer was assumed to occur predominantly by grain boundaries. (c) Pfeiffer and Ilschner[52], and Sartell and Li[53] adopted a mechanism by which oxygen diffusion via lattice anionic point defects in the scale is the rate determining process irrespective of the oxide structure. (d) Rhines and coworkers[54] have

postulated that nickel diffuses outward through NiO lattice and that oxygen diffuses inward along grain boundaries and new oxide forms at grain boundaries. The process leads to oxide recrystallization at the metal/oxide interface and development of the inner equiaxed layer.

2) The second principal model for growth of a bilayer scale is based on the postulate that the inner layer is formed first on the nickel specimen and that the columnar layer subsequently grows as a textured overgrowth as a result of recrystallization and grain growth processes. This type of growth suggested by Perrow's[63] and Khoi's[10] results is also a characteristic of some of the data reported in the literature by Caplan[51], Ueno[57] and Homma[37]. This mechanism at low and intermediate temperatures leads to short-circuit diffusion of nickel in the scale as the rate determining oxidation step previously outlined in section II.3.2 .

Model (1), based on the postulate that the first formed oxide layer is columnar has been used by many investigators[61,62] to interpret the formation of bilayer thick scales while different workers[38,63] investigating formation of relatively thin oxide films at lower temperatures have favored model (2) involving recrystallization and grain growth leading to development of a columnar oxide layer.

Due to the wide application of mechanism (1-a) a detailed review is given in the following of the oxide dissociative mechanism and also of a recent model by which columnar oxide growth involves both metal and oxygen transport leading to formation of oxide within the scale (1-d).

Oxide dissociative mechanism: Growth of the initial columnar oxide layer is assumed to grow by a Wagnerian diffusion process of nickel by cation vacancies in the oxide characterized by local equilibrium at the M/MO and $MO/O_2$ interfaces. As oxidation proceeds, the scale thickness exceeds a critical value at which further consumption of the metal cannot be compensated by the plastic flow of the scale. Therefore a crack develops between scale and metal and the transport of the metal to the scale decreases. This drop in the chemical potential of the metal is associated with an increase in the potential of oxygen and this means also an increase in concentration of the vacancies in a p-type oxide at the crack-scale boundary. This increase of oxygen pressure in the crack above its equilibrium value creates a concentration gradient in the crack leading to the possibility of secondary oxide formation in the crack. Loss of the oxidant in the crack is followed by the dissociation of columnar oxide to provide oxygen for reaction and the resulting metal will diffuse to the outer surface of oxide to react with oxygen. This mechanism is illustrated

in fig. (II.3.2-8).

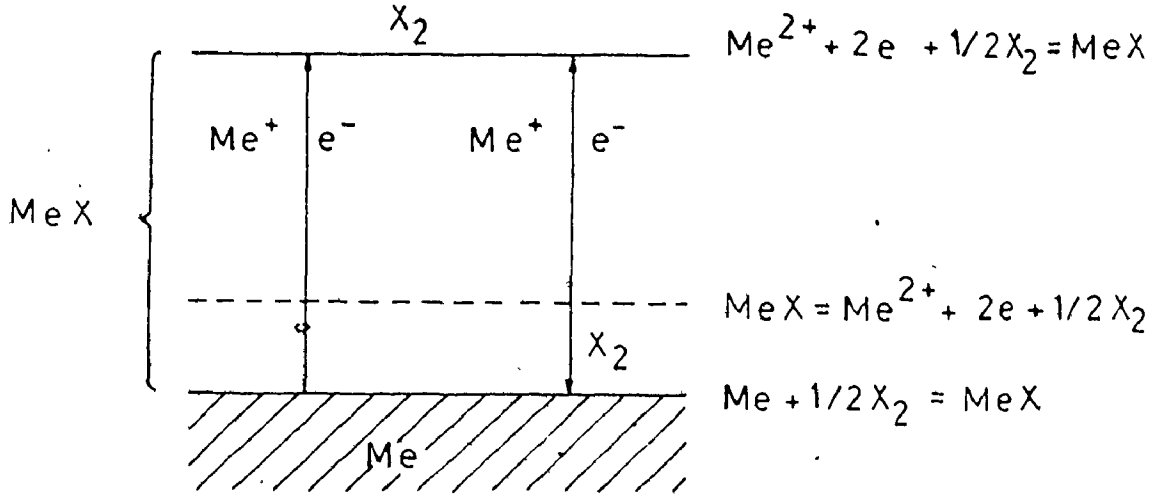


Fig. II.3.2-8 Scheme of the processes occuring during formation of the duplex layer scale. (After Mrowec [62]).

Dissociation of the columnar oxide can be anisotropic in character because the highest rate of solid decomposition usually occurs at grain boundaries. This process must therefore lead to the formation of marked irregularities at the inner surface of the outer layer, i.e. the formation of an intermediate layer. This model is represented in fig. (II.3.2-9).

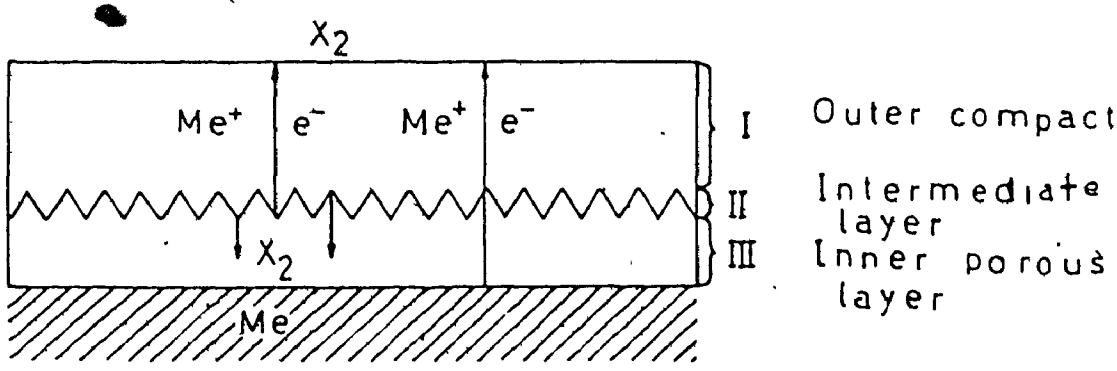


Fig. II.3.2-9 Scheme of the formation of the triple layer scale on metals. (after Mrowec [62]).

This secondary oxidation process led, on the one hand, to the formation of a porous layer (II) and, on the other hand, to the gradual destruction of the compactness of the oxide columnar layer by formation of fissures at the grain boundaries especially around the edges of plate specimens. Accordingly oxygen of the environment can directly contribute to the reaction as in fig. (II.3.2-10).

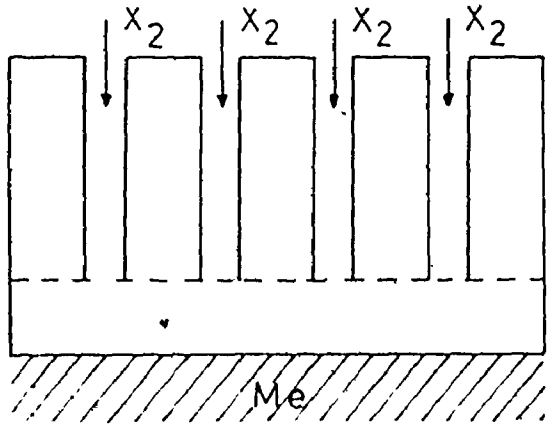


Fig. II.3.2-1o Scheme of the destruction of the compactness of the oxide columnar scale by formation of the fissures. (After Mrowec [62]).

Mechanim for oxide formation within the scale: Rhines and Wolf[54] have advanced a model for nickel oxidation under conditions in which the scale develops initially as a columnar, void free structure characterized by parabolic growth kinetics. At longer time of reaction, an inner layer appears, producing a decreasing oxidation rate and hence slower thickening of the scale. The authors consider that nickel ions act as the mobile species in the oxide lattice whilst oxygen has the ability to diffuse through the oxide grain boundaries. New

oxide is formed at the grain boundaries when nickel diffusing across the oxide grains and oxygen from the atmosphere diffusing through grain boundaries meet and react. This creates a lateral compressive stress, a so called "grain boundary pressure" in the oxide scale. This stress leads to recrystallization of the oxide especially at the high stress regions in the vicinity of the metal surface. Thus, recrystallization of the oxide near the metal-oxide interface promotes formation of the "undergrowth" layer of equiaxed oxide. This undergrowth, in turn, forms a barrier to the transport of nickel to the external surface of the scale; accordingly the site of the reaction shifts from the gas-columnar oxide interface to the undergrowth-columnar interface. At this stage, nickel reaches this site by volume diffusion and meets the oxygen delivered again through the grain boundary sections of the scale. This model is represented schematically in fig. (II.3.2-11)

The authors have also correlated the mechanical properties associated with the formation of a duplex structured nickel oxide scale. The bilayer structure forms when the deformation rate of the dense, coarse-grained external layer of nickel oxide is less than the rate of void formation in the inside of the metal depletion zone. Thus the inner layer of this bilayer structure consists of fine grains and coarse porosity; its mechanical properties are similar to those of bulk nickel oxide which exhibits only a limited ductibility at temperature below 1000°C. The compressive

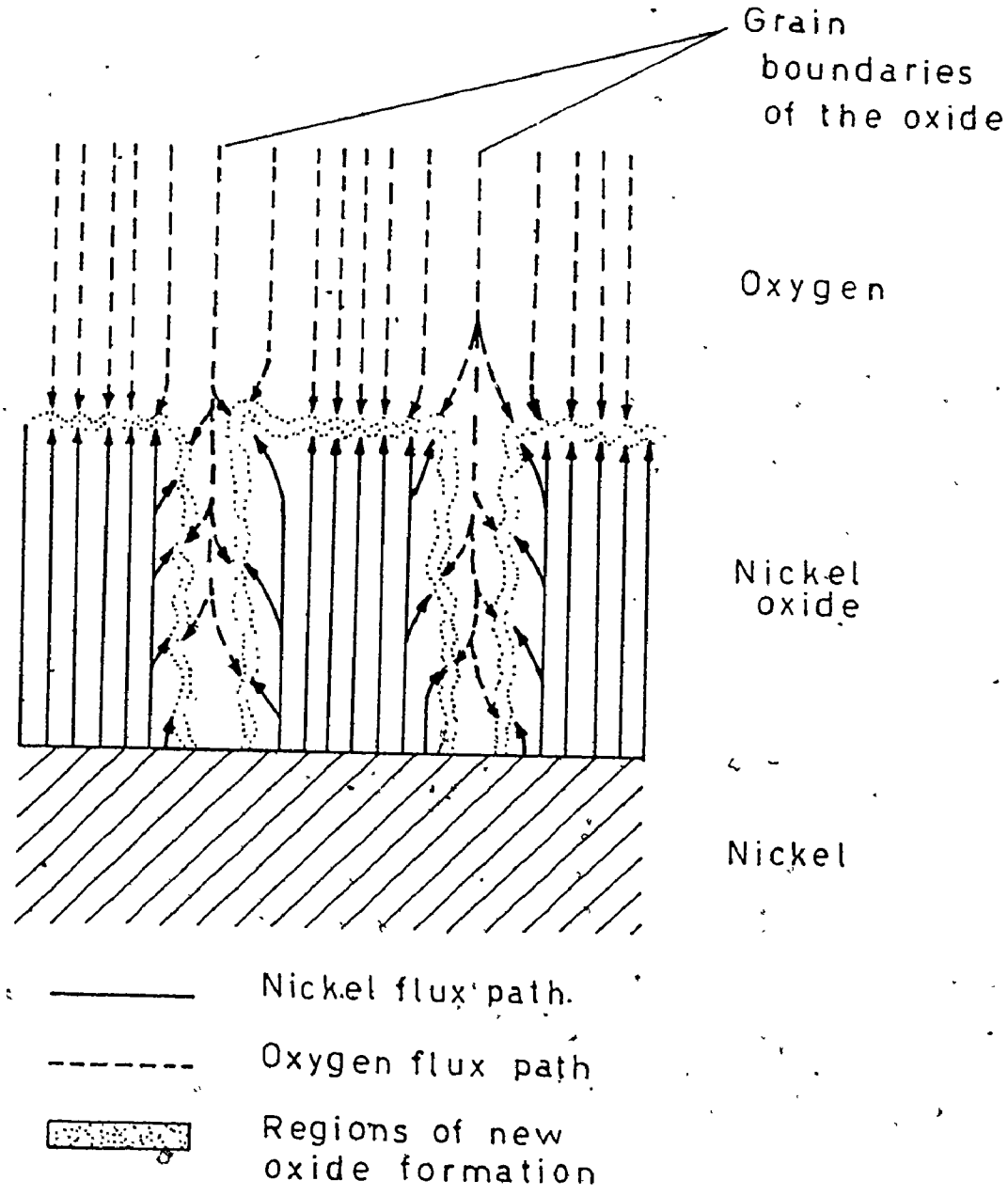


Fig. II.3.2-11 Scheme of the model leading to the mechanism for the oxide formation within the scale (After Rhines and Wolf(54).)

stresses generated in the porous layer cannot be fully relieved by plastic flow and therefore the layer will fracture. This ultimately leads to exfoliation primarily from the positions in the film where the geometry accounts for rapid formation of the columnar outer layer into a porous layer by a dissociation/vacancies condensate mechanism.

To explain the decrease in the parabolic rate constant of oxidation in time ageing experiments would be useful.

The idea of the ageing of the oxide during oxidation processes is a very old one. We have shown previously that in spite of a simple chemical representation of oxidation, the process is very complicated and influenced by several factors. In considering oxidation mechanisms, investigators take into account the influence of factors such as pressure, temperature, the purities of the metal and atmospheres, and preparation of the specimen surface. The "time" variable is generally not taken into consideration. "Time" is only used to express the period of oxidation in an oxidant atmosphere. There is another aspect of the "time"; that is, the transformation that may occur in an oxide grown on a metal, in time, which is dependent only on temperature. Thus we wish to know how annealing of the oxide scale during its growth influenced the oxidation mechanism.

There is the possibility that the "permeability" of the oxide, formed after the first moments of exposure, for the diffusing particles is greater when it is fresh and decreases with its age. Such an ageing process will accelerate

with increasing temperature, thus opposing the normal temperature dependence of the rate of oxidation. Such effects may be expected for the metals that do not obey the parabolic law of oxidation. Such a result was found by Smeltzer[88] on studying aluminum oxidation. For example oxidation after 5 hours at 500° was larger as indicated by weight gain than during the same time at 600°.

One of the first indications existent in the literature about the ageing effect may be that of Dunn[64], in 1931, observed in a study of the oxidation of some copper zinc alloys. Studying the oxidation of some Cu alloys with different amounts of zinc they concluded that the nonparabolic behaviour of some alloys was due to the change in permeability of zinc oxide. This assumption was confirmed by comparing the amount of oxygen consumed during continuous oxidation and the oxygen uptake for an equal period of oxidation interrupted by a period of annealing. The author suggested that the oxygen is transferred mainly across intercrystalline surfaces in the oxide and that during the interruption period the number of these "avenues" for oxygen penetration was materially diminished.

More recently Meijering[65] has reported direct ageing experiments on the oxidation of $Cu_2O$ to CuO. They stopped oxidation temporarily by replacing the air by a neutral atmosphere. After a certain time they switched

to air again. The oxidation after this interruption proceeded slower than in the normal condition. The authors assumed that the effect was due to the removal of the supernumerary lattice vacancies in CuO.

Van Den Broek and coworkers[66] have studied the oxidation of nickel by indirect ageing experiments. Indirect ageing experiment signifies changing the temperature to a higher or lower value at a certain moment during the oxidation and observing the effect of this temperature change on the reaction rate. The authors interpreted the results obtained as due to an ageing effect in the oxide layer and at the temperatures above 950°C to the formation of a second oxide layer under the first formed layer. Yamashina and Nagamatsuya[67] have also effectuated similar ageing experiments on the scale formed on nickel at 800°C. Attempts were not made to explain the ageing of nickel oxide other than to assume that some structural changes must take place. One can therefore conclude that direct observations on the structure of nickel oxide scales after ageing could yield important information for explaining the anomalies occurring during nickel oxidation.

# CHAPTER III

# EXPERIMENTAL PROCEDURE

## III.1 INTRODUCTION

Two types of experimental technique have been systematically used to understand the growth and the development of the microstructures of nickel oxide scales: 1) a method for determining the oxidation kinetics and 2) methods for examining the specimens before and after oxidation. The rate of oxidation was followed by the thermogravimetric technique employing a vacuum microbalance to measure the weight increase of the nickel specimen. The oxidation conditions and the experimental procedure were chosen so that the results could be compared with previous results obtained in our laboratory on oxidation of nickel single crystals of different orientations. To characterize the metal and especially the oxide scales obtained in different conditions, different experimental techniques were used depending on the compatability between the advantages and disadvantages of the respective technique with the characteristics of the oxide scales formed and the types of information required. The most important techniques employed were scanning electron microscopy using secondary and back scattered electrons for topographic information and observations of the microstructures by cross sections and fractured scales; optical microscopy to characterize

the adherence of the oxide scale to metal, and X-ray diffraction to characterize the texture of the metals and the preferred orientation of the oxide scales.

## III.2 SAMPLE PREPARATION

The material for the first investigations was nickel sheet of approximately 99.97% purity purchased from Falconbridge Nickel Mines Limited. The chemical analysis of this nickel is given in Table III.2-1. Nickel sheet, 99.999% pure and 0.02" thickness was purchased from Gallard-Schlessinger Chemical Corporation and this was used to obtain results representative of ultra-pure nickel.

Metal plate specimens of 2-3 $cm^2$ area were cut on a precision shear and a suspension hole was drilled in each specimen. The importance of surface preparation of nickel has been emphasized in the literature review. The chosen method was that used by Khoi[10] for nickel single crystals. The cut sample was mounted on bakelite and polished on 240, 320, 400 and 600 grit silicone carbide papers using water as the lubricant. The final polishing was done on 6μ and 1μm diamond paste lubricated with kerosene. The deformed layer usually produced by mechanical polishing was removed by electropolishing in a 60% sulfuric aqueous solution with a current density of 0.6 amps/$cm^2$. During electropolishing the solution was vigorously agitated and the bath temperature was kept near 0°C. After electropolishing the samples

Table III.2-1

Chemical analysis of polycrystalline Falcombridge Ni < 10 ppm

| Elements | Fe | Co | Cu | Si | Ti | Pb | Ca | Al | Cr | Mg | Mn | Ag |
|---|---|---|---|---|---|---|---|---|---|---|---|---|
| Contents in ppm (of impurities) | 108 | 77 | 15 | 7 | 7 | 5 | 4 | 4 | <0.7 | 1 | <0.9 | <0.4 |

were washed for 30 minutes in distilled water and acetone and after this transferred to a high vacuum ($4\times10^{-6}$ Torr) apparatus for annealing. The specimens were annealed for 18 hours at 800°C. After this they were weighted to ± 2 μg on a Mettler microbalance and placed in the oxidation apparatus.

## III.3 OXIDATION APPARATUS AND OXIDATION PROCEDURE

The assembly for determining weight changes of the specimens during oxidation consists of a Cahn R.G. electrobalance, a glass vacuum unit containing a quartz reaction tube and an electrical furnace. This balance unit could sustain a vacuum of $10^{-5}$ Torr. High purity research grade oxygen was used as oxidizing atmosphere, the total impurity content being less than 25 ppm. The pressure was 400 Torr as controlled by a mercury manometer. During the oxidation the temperature was controlled to ± 2°, by a Pyrovane temperature regulator. The control thermocouple and a measuring thermocouple were both placed at the center of the hot zone of the furnace. The furnace had the possibility of being raised or moved down under the reaction tube. Each specimen was oxidized immediately after annealing to prevent any further contamination due to the handling. Each specimen was oxidized for different periods of time ranging from 10 minutes to 3 hours after which the oxygen was pumped out and the oxidized sample was annealed in a $5\times10^{-3}$ Torr

vacuum, measured with Edwards high vacuum Pirani gauges. The oxidized specimens were kept in vacuum at the same temperature as during the oxidation or at 900° for determined periods of time. At a certain moment the oxygen was introduced again and the reoxidation was continued. During an exposure period, the weight variations were continuously recorded by the Cahn microbalance connected to a Texas instrument recorder. All the specimens were oxidized for different periods of time to a maximum of 240 hours.

### III.4 EXAMINATION OF SAMPLES BY SCANNING ELECTRON MICROSCOPY AND X-RAY DIFFRACTION.

#### III.4.1 Scanning Electron Microscopy

To understand the apparition and morphological development of the bilayer scale, the structural characteristics must be followed from the early oxidation stage to long exposure time. The principal characteristics of the electron scanning microscope as a major instrument in our investigation are: 1) the high resolution that can be obtained up to a magnification of 30,000 x, 2) the three dimensional appearance of the specimen which is a direct result of the depth of focus and 3) the possibility of observations on thick samples with a minimum of preparation. This instrument was used to obtain two types of information: 1) topographical development of the oxide scale obtained by continuous oxidation and during oxidation interrupted by vacuum anneals from the stage of oxide nucleation and to scale growth at very long time, 2) to follow the development of the bilayer scale in time by

observation of microsectioned oxidized samples or of the fractured oxidized samples. The Cambridge Stereoscan used for these measurements gave the possibility of observation of the microstructure over magnification practically varying from 20 to 26000 times and at a depth of field hundreds of times greater than that of the optical microscope. The Ultraphot II Carl Zeiss optical microscope was used only for observations on thick scales in the unetched state to determine adherence of scales to the metal.

Sample preparation for observation with scanning electron microscope. The topography of an oxidized specimen could be examined without any special preparation. To obtain information on the internal structure of the oxide scale from cross sections, the oxidized specimen was mounted in a cold setting resin with two strips of stainless steel arranged parallel to the oxide surface for better retention of the oxide edges. Polishing was carried out through the usual sequence of silicon carbide papers using kerosene as lubricant followed by lapping on wax containing a suspension of 40 μm alumina. The final polishing was done as usually on 6 μ and 1 μm diamond paste. The structure of the duplex scale with its characteristics (porosity, interface between the inner and outer layer, aspect of the grains of the oxide) was revealed by electroetching in 1:1:4 solution of hydrofloric acid, glacial acetic acid and water using a potential of 3-5 volts applied across the electrodes for 1 to 5 minutes, depending on the thickness of scale and temperature of oxidation. To avoid the difficulties

encountered, due to the chemical attack of the mounting resin used to obtain the cross sections by this strong etching medium, the Metset Resin FT as a cold mounting was used. After electroetching the specimens were washed in water and acetone and shadowed with gold-palladium alloy by vapor deposition to avoid electrical charging effects, and used for scanning electron microscopy observations. Cross sections were also obtained by mechanical fracture and observed under scanning electron microscope at different tilting angles.

III.4.2. X-Ray Studies of the Oxide Scales. It has been shown in the previous chapter[45,47] that even in the case of polycrystalline nickel oxidation resulted in a textured oxide scale. Therefore, to understand the structural development of the scale, the examination of the preferred orientation and of the changes in preferred orientation with oxidation time could be very important. The oxidation conditions, a temperature equal to 800° and a pressure of 400 Torr, used in this investigation, indicates that at very short times of oxidation, as 10 minutes, a thick oxide scale will form. Transmission electron microscopy cannot be used for oxide exceeding 5000 Å in thickness due to absorption effects. But for oxide scales thicker than 1 μ the preferred orientation can be readily studied by x-ray diffraction. For this reason the inverse pole figure technique developed by Harris[68] and applied by Khoi[10] to the oxidation of single crystals of nickel

was used. This method consists of comparing the integrated intensities of diffracted x-rays by a textured specimen to those diffracted from a random specimen. The integrated intensity was measured by counting the pulses at the peak maximum for a fixed time and subtracting the background counts. To compensate for the surface irregularities a special device was adjusted to allow the rotation of the specimens during measurements. The counter was provided with a LiF monochromater and the X-rays were produced by a copper tube.

# CHAPTER IV

# EXPERIMENTAL RESULTS

## IV.1 INTRODUCTION

As was shown in Chapter II, the structural changes in the oxide scale formed during oxidation could explain the nonparabolic oxidation behaviour of nickel. A correct understanding of these structural changes of the oxide, perhaps due to the annihilation of some defects giving rise to a change in "permeability" of the oxide, could also explain the duplex aspect of the nickel oxide scales.

The present research has involved the following stages:

1. The oxidation kinetic behaviour of nickel at 800° and $P_{O_2}$ = 400 Torr.
2. The effects of annealing of the nickel oxide scale in different conditions, on the oxidation kinetic behaviour of nickel.
3. Comparison between the topographical development of the nickel oxide scales obtained at different periods of oxidation, during continuous oxidation with those obtained during oxidation interrupted by vacuum anneals.
4. Determination of a preferential oriented growth of nickel oxide scale obtained during oxidation under different conditions.

5. Following the development of the duplex layer of nickel oxide in time by observations of the different microsections and of fractured samples by scanning electron microscopy.
6. To transform, if possible, the duplex layer structure into a single layer structure.
7. To determine the influence of the metal grain orientation and structure on the anisotropy of oxide nucleation and growth.
8. To interpret all experimental evidence relating the kinetic behaviour, oriented preferential growth, topographical and microstructural development of nickel oxide scales, in relation to the nickel transport mechanism and defect structure of the oxide in order to obtain a model to explain the present controversial arguments on the development of bilayer nickel oxide scales.

Following these objectives the general scheme of the investigation was to produce samples of oxidized nickel under chosen conditions and to analyze them from kinetics, metallographic and preferred orientation points of view. Practically all the experimental work can be systematized as in Table (IV.1-1).

Table IV.1-1 Design of experiments

| Type of Nickel | 99.97% | 99.999% |
|---|---|---|
| Type of experiments | continuous oxidation<br>oxidation with anneals | continuous oxidation<br>oxidation with anneals |
| Type of information | kinetics of oxidation<br>oxide grain growth<br>preferred orientation of metal and oxide<br>topography of the oxide scale cross section. | kinetics of oxidation<br>oxide grain growth<br>preferred orientation of metal and oxide<br>topography of the oxide scale cross section. |

## IV.2 THE CHARACTERIZATION OF POLYCRYSTALLINE NICKEL SPECIMENS

Two types of polycrystalline nickel were used in this investigation, a nickel of 99.97% purity and a nickel of 99.999% purity. The main impurities in the less pure nickel were shown in table (III.2-1. Since the rate of oxidation is known to vary markedly with crystal face, a kinetic study involving the weight gain of a polycrystalline material will give an average value for the different crystal faces concerned. For this reason it was thought that in the case of nickel, which manifests a strong anisotropy in the rate of the oxidation the metal grain preferred orientation could play a very important role. Generally in many polycrystalline materials the constituent crystals are arranged at random. In others there is a tendency for a particular axis or plane to become similarly oriented. The nature and the degree of preferred oxidation in a specimen may be determined by allowing a parallel X-ray beam to fall on the sample and measuring the variation of the intensity of the diffracted rays. The type of preferred orientation is obtained by comparing the integrated intensity of a (hkℓ) plane of the specimen with the intensity of a similar plane of a random sample. The degree of orientation could be expressed by the texture coefficient defined by Harris[68] as:

$$P_{(hk\ell)} = \frac{\frac{I_{hk\ell}}{I_{r,hk\ell}}}{\frac{1}{n}\sum \frac{I_{hk\ell}}{I_{r,hk\ell}}} \qquad \text{(IV.2-1)}$$

where $P_{hk\ell}$ is the texture coefficient of the (hkℓ) plane, $I_{hk\ell}$ is the integrated intensity of the textured sample, $I_{r,hk\ell}$ is the integrated intensity of a random sample given by ASTM and n is the number of peaks investigated. Thus in Figures (IV.2-1) and (IV.2-2) are represented the first part of the recordings obtained for polycrystalline nickel, purity 99.97% and polycrystalline nickel, purity 99.999%, respectively. Table (IV.2-1) represents the principal intensities for nickel taken from the ASTM card index. From these two recordings it is possible to see that there is a strong difference between these two types of nickel. The calculation of texture coefficient, $P_{hk\ell}$, using the formula (Iv.2-1) gives the results indicated in Table (IV.2-2) for the two relfections (200) and (111). This method can also be used for polycrystalline nickel oxide.

From these recordings and from Table (IV.2-2) it is possible to remark that the nickel of 99.97% purity has a preferred orientation on the {111} planes; on the other hand, nickel of 99.9999% purity has a fairly strong preferred orientation on the {100} planes. From this it is possible to conclude that some of the differences found in the literature on the same metal oxidized in equivalent conditions are not only due to the difference in purity but due to the different orientations (and this especially for the metal that exhibits an anisotropy of the reaction rates). Thus, each study of a metal oxidation must have the preferred orientation determined

Table IV.2-1

A.S.T.M. card for nickel [69]

| d spacing | $I/I_o$ | hkl |
|---|---|---|
| 2.034 | 100 | 111 |
| 1.762 | 42 | 200 |
| 1.246 | 21 | 220 |
| 1.062 | 20 | 311 |
| 1.0172 | 7 | 222 |
| 0.8810 | 4 | 400 |
| 0.808 | 14 | 331 |

Table IV.2-2

Texture coefficients for polycrystalline nickel samples

| Type of nickel | Texture coefficients | | | | | | |
|---|---|---|---|---|---|---|---|
| | $P_{111}$ | $P_{200}$ | $P_{220}$ | $P_{311}$ | $P_{222}$ | $P_{331}$ | $P_{400}$ |
| $Ni_{99.97\%}$ | 2.7 | | | | 2.13 | 0.9 | |
| $Ni_{99.999\%}$ | | 2.02 | | 1.17 | | | 1.73 |

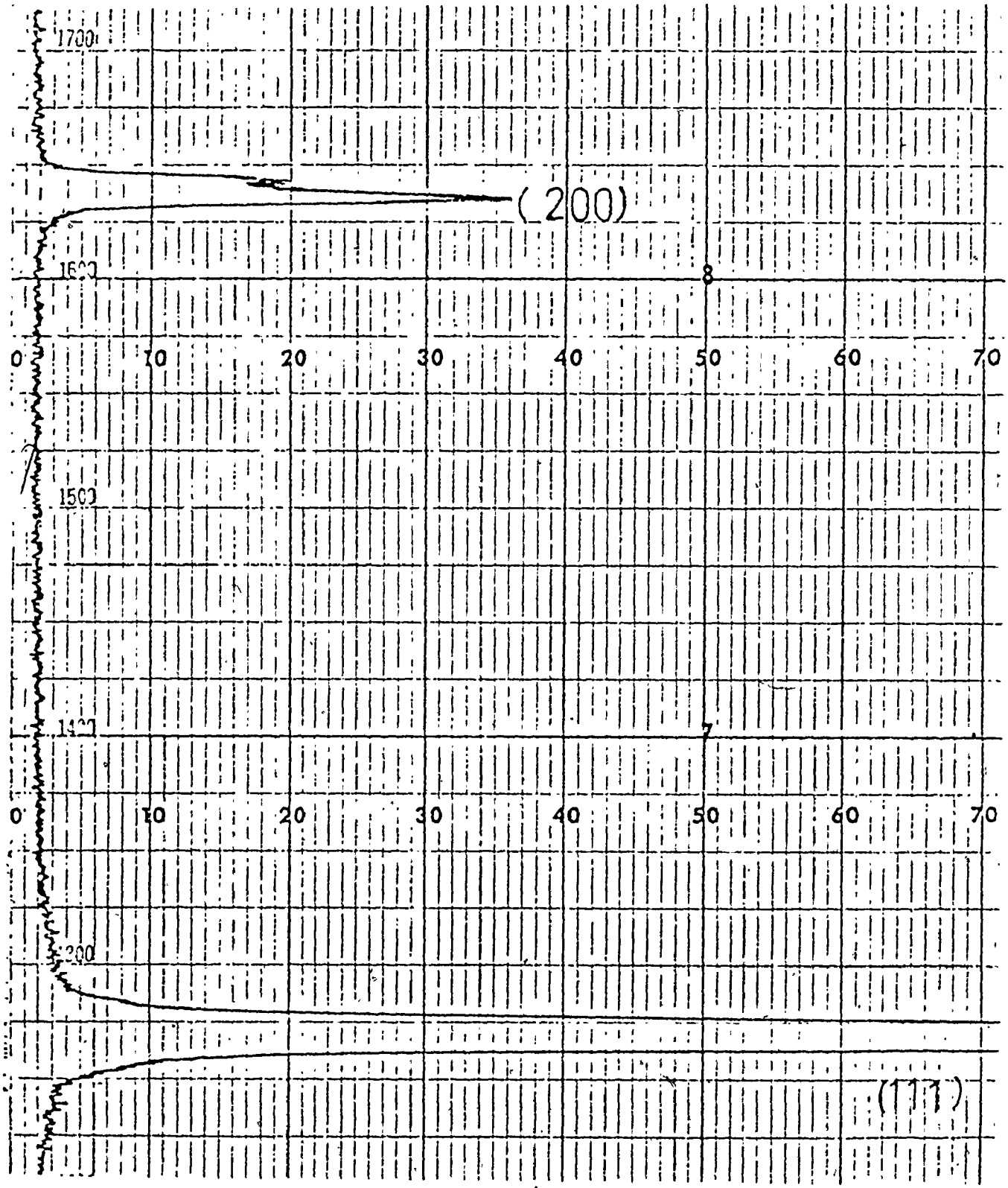


Fig.IV.2-1 Diffractometer tracing for the nickel of 99.97% purity.

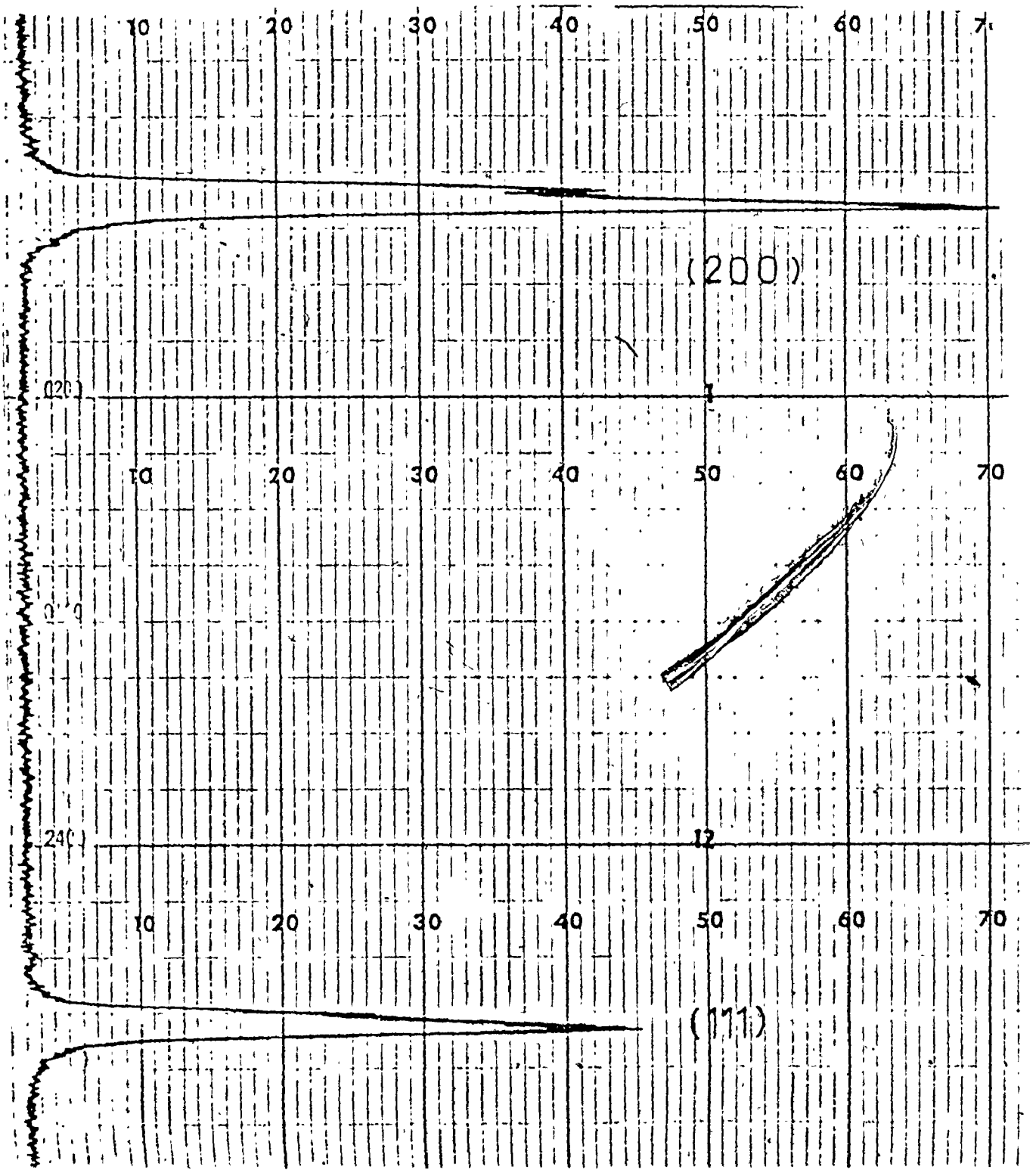


Fig.IV.2-2 Diffractometer tracing for the nickel of 99.999% purity.

for the respective metal. To compare also the two types of nickel used during this investigation the grain size was measured using the Fernet diameter. The average grain size for the less pure nickel was approximately 50 μm while for the pure nickel the average grain size was 100 μm as represented in fig. (IV.2-3 a,b,c).

## IV.3 KINETIC MEASUREMENTS

Kinetic measurements were carried out to establish the oxidation behaviour of nickel of 99.97% and 99.999% purity during continuous oxidation and during oxidation interrupted by vacuum anneals. Different investigators have generally found that nickel oxidizes parabolically. Recent results obtained in this laboratory[10] as well as those of Cohen and coworkers[32], Berry and Paidassi[48] demonstrate that this type of parabolic behaviour is only an approximation since the values of the effective parabolic oxidation constant decreases with increasing exposure when the oxidation is carried out for periods of several hours. Also the oxidation of nickel below 900° gives much larger experimentally determined parabolic oxidation rate constants than those calculated by the Wagner model. As previously discussed in the literature review, a few experiments have been performed on nickel[66,67] at 800° using annealing method of oxidation to understand the change in "permeability" of nickel oxide during an oxidation process. Taking into account these considerations and previous work on oxidation of nickel single crystals, the reaction temperature and oxygen pressure for investigation were chosen as 800°C and

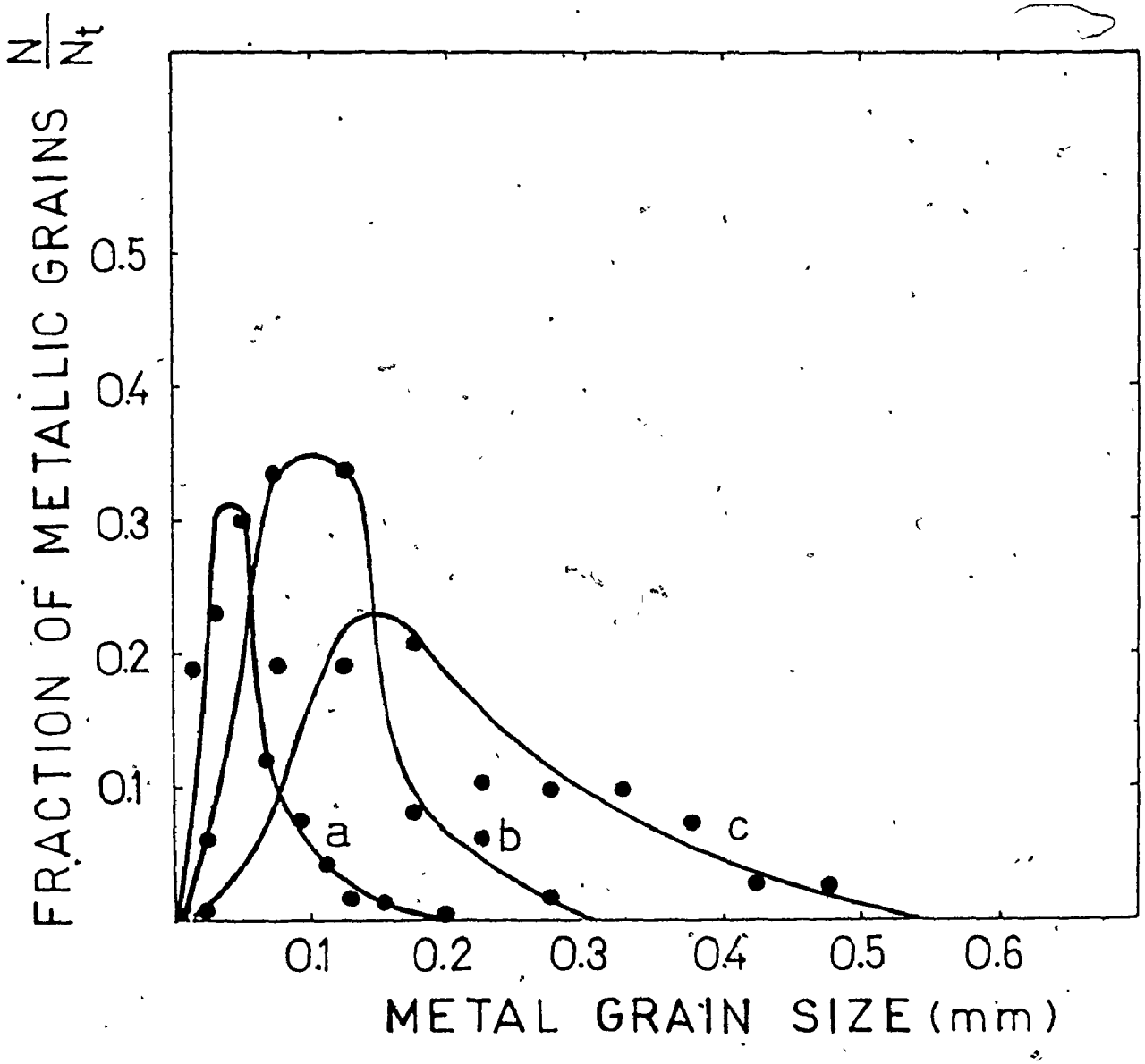


Fig. IV.2-3 Metal Grain size distribution
a. less pure nickel annealed at 800°
b. pure nickel annealed at 800°
c. pure nickel annealed at 1000°

400 Torr, respectively.

To illustrate the oxidation behaviour of the impure and high purity nickel, plots are given in fig. (IV.3-1) of the weight gains of the respective specimens at 400 Torr and 800° plotted versus time. It is immediately evident upon examination of these curves that pure nickel is oxidized faster than the less pure nickel. These oxidation curves are represented in Fig. (IV.3-2) according to the parabolic relation:

$$(\frac{\Delta w}{A})^2 = k_p t + c \qquad \text{(IV.3-1)}$$

where $\Delta w/A$ is the change in weight per unit area, $k_p$ is the parabolic rate constant, t is the time and C a constant. These plots demonstrate that the two types of polycrystalline nickel do not obey the parabolic law. No improvement was obtained by representing the results in parabolic form as $\Delta w/A$ function of $t^{1/2}$. The results were also plotted on a logarithmic scale to conform to the relation

$$(\frac{\Delta w}{A})^m = k_m t \qquad \text{(IV.3-2)}$$

where the symbols have the same significance as in formula (IV.3-1). Figures (IV.3-3) a and b illustrate the results obtained for the two types of nickel represented or this double logarithmic scale. From all these representations, it was obvious that a straight line representing parabolic oxidation behaviour was valid only for the very early periods of time and that this rate continuously decreased from parabolic oxidation when the exposures were

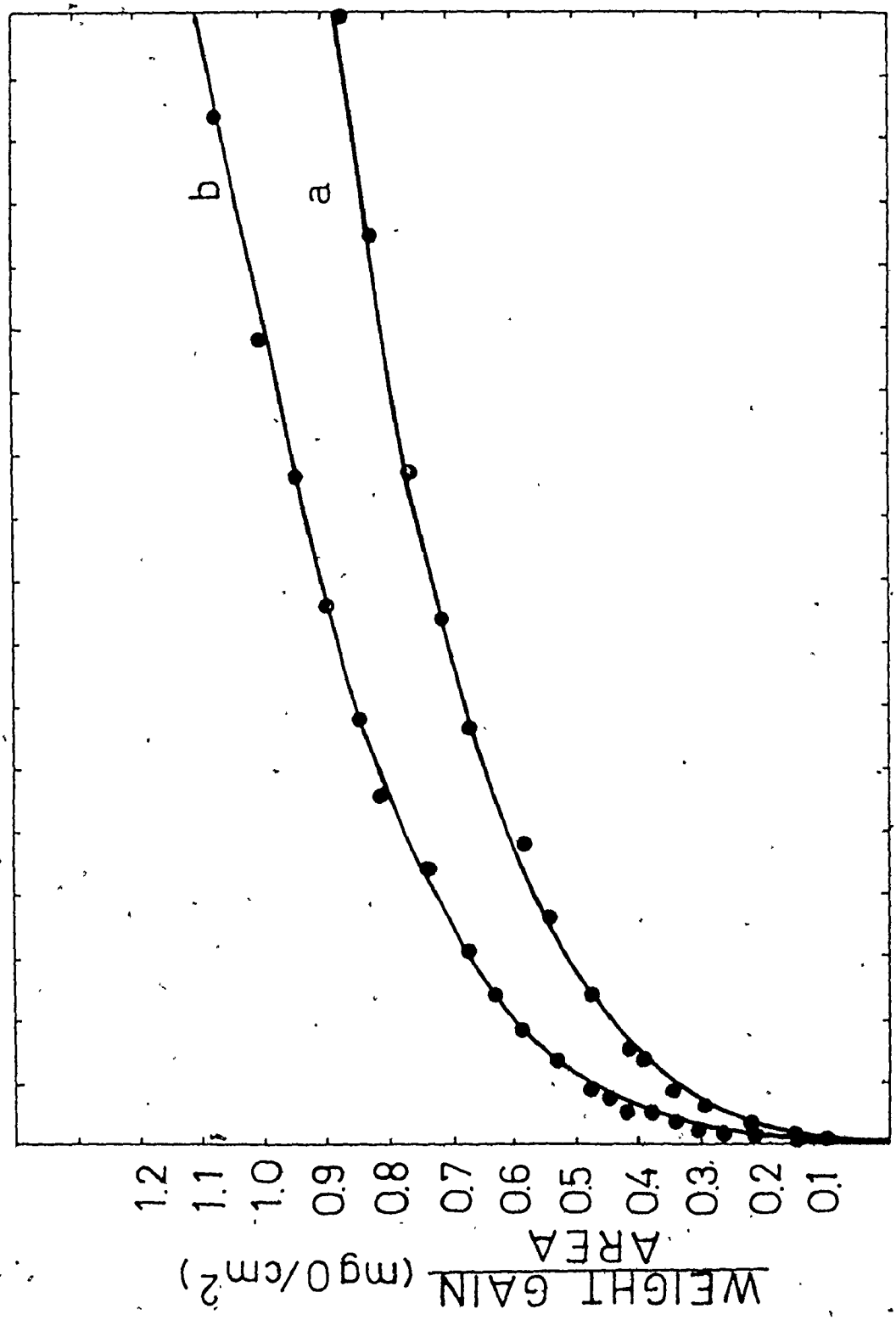


Fig.IV.3-1 Oxidation kinetics of polycrystalline nickel at 800°:
a. less pure nickel
b. pure nickel

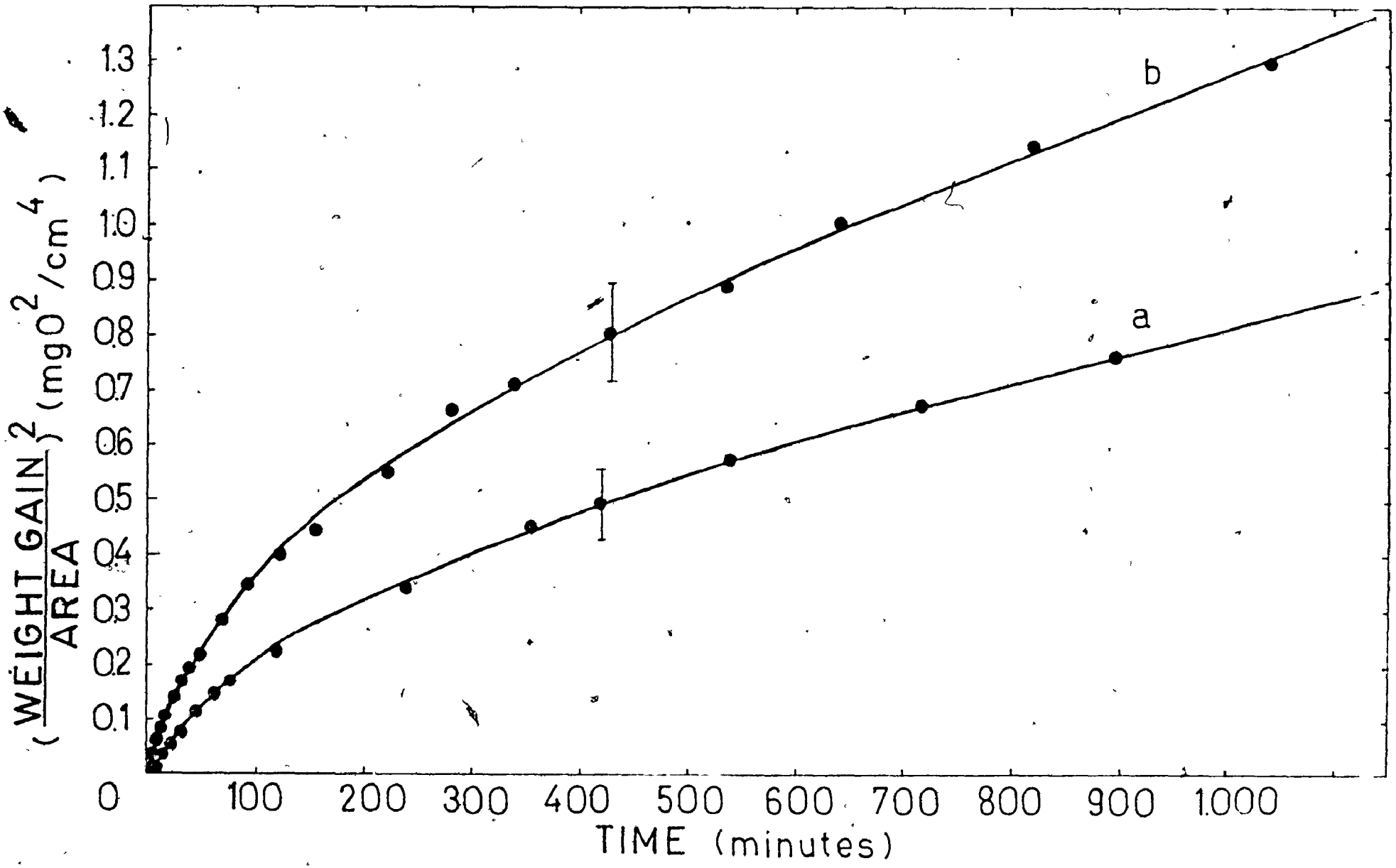


Fig. IV.3-2 Oxidation kinetics of polycrystalline nickel in parabolic form.
a. less pure nickel b. pure nickel.

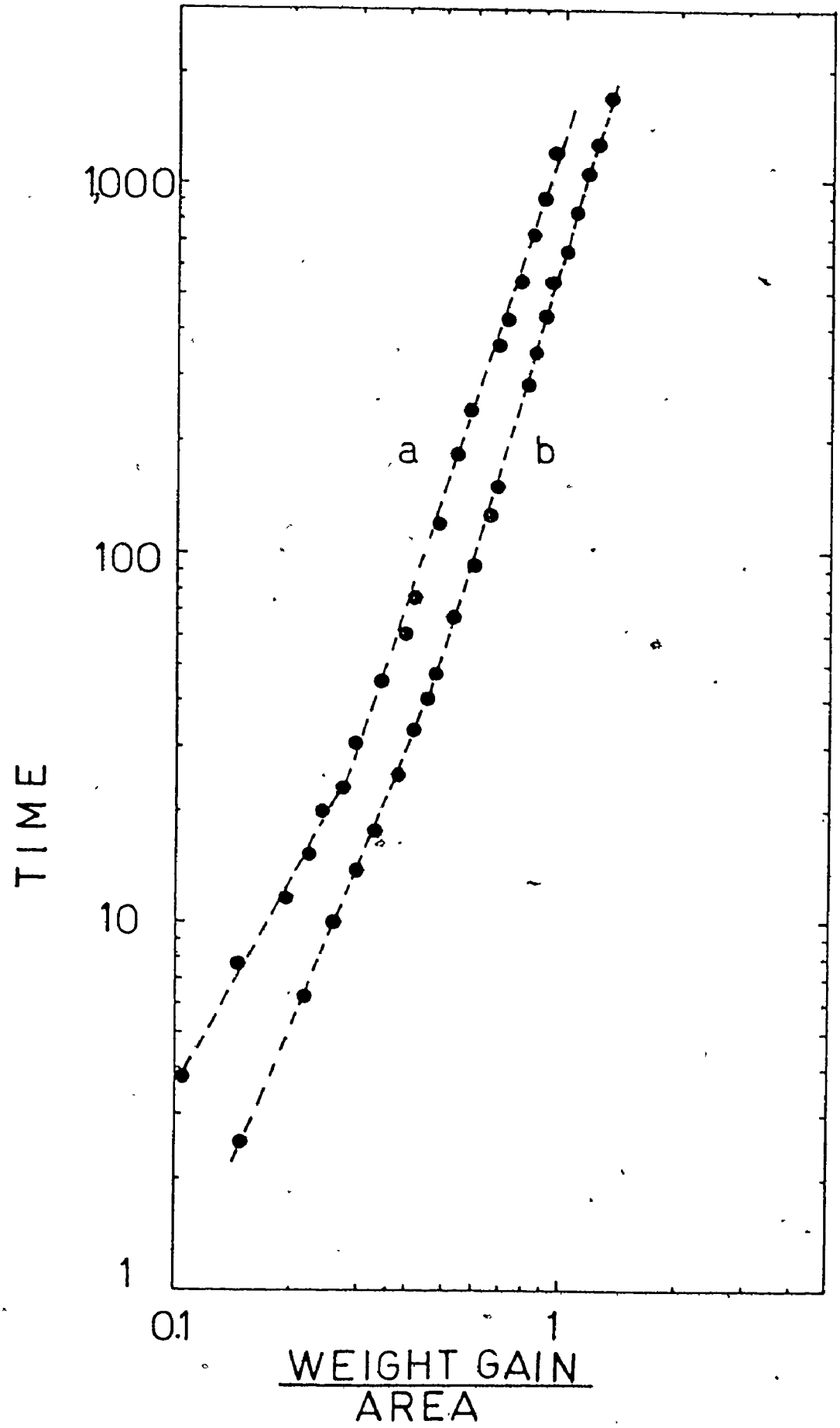


Fig. IV.3-3 Double logarithmic plot of weight gain versus time during oxidation at 800°
a. less pure nickel
b.

carried out for several hours. Eventually this decreasing rate when represented according to the parabolic relationship became approximately constant at very long times of exposure.

Some oxidation experiments interrupted by vacuum anneals were carried out under different conditions of time and temperature in order to understand the structural changes that may take place in the oxide scale formed during oxidation. Under the experimental conditions, these kinetic measurements effectuated with specimens of less pure nickel can be divided as follows: a) those obtained after different periods of initial oxidation, b) those kinetics obtained for different temperatures of annealing and c) the kinetics obtained after different periods of annealing. For easier understanding, these types of experiments are described in tables (IV.3-1) to (IV.3-3).

In the case of pure nickel only two types of oxidation kinetics and annealing experiments were carried out, as illustrated in Table IV.3-4.

Table IV.3-1

Kinetic variable used during the experiments: initial period of oxidation (less pure nickel)

| Steps of experiments | Time | Temperature |
|---|---|---|
| Initial period of oxidation | 3 hours<br>1 hour<br>20 minutes<br>10 minutes | 800° |
| Annealing | 1 hour | 800° |
| Reoxidation | Minimum 2 hours | 800° |

Table IV.3-2

Kinetic variable used during the experiment: temperature of vacuum annealing (less pure nickel)

| Steps of experiments | Time | Temperature |
|---|---|---|
| Initial period of oxidation | 20 minutes | 800° |
| | 1 hour | 800° |
| Annealing | 1 hour | 900° |
| | | 900° |
| Reoxidation | Minimum 2 hours | 800° |
| | | 800° |

Table IV.3-3

Kinetic variable used during the experiments: time of vacuum annealing (less pure nickel)

| Steps of experiments | Time | Temperature |
|---|---|---|
| Initial period of oxidation | 20 minutes | 800° |
| | 1 hour | |
| Annealing | 2 hours | 800° |
| | 20 hours | |
| Reoxidation | Minimum 2 hours | 800° |

Table IV.3-4

Kinetic variable used during the experiments: temperature of annealing (pure nickel)

| | | |
|---|---|---|
| Initial period | 20 minutes | 800° |
| Annealing | 1 hour | 800° |
| Reoxidation | Minimum 2 hours | 800° |
| Initial period | 20 minutes | 800° |
| Annealing | 1 hour | 900° |
| Reoxidation | Minimum 2 hours | 800° |

Results from these kinetic curves represented in the parabolic form as square of weight change versus time are illustrated in figs. (IV.3-4), (IV.3-5), (IV.3-6), and (IV.3-7). These curves show the oxidation behaviour of nickel in the initial period of exposure to oxygen, the oxidation kinetics after annealing the oxidized specimens for different times at 800° and 900°C. To have the possibility to compare the effects of annealing conditions and also to relate these effects to the continuous oxidation of nickel, the effective parabolic rates of oxidation were determined as $k_1$ (effective parabolic rate constant for the initial period of approximately 20 minutes), $k_2$ (effective parabolic rate constant of reoxidation after annealing. Constants $k_1$ and $k_2$ were calculated from the tangents to the curves representing the square of weight changes versus time.

These effective parabolic rate constants and their ratios are given in tables (IV.3-5) and (IV.3-6) for less pure and pure nickel respectively. It is possible to observe from all curves represented in figs. (IV.3-4) to (IV.3-7) that they are composed of two linear sections with one exception, that for the run where the initial period of oxidation was of 10 minutes. The curves indicate parabolic kinetics for the initial period of approximately 20 minutes of oxidation as well as for the oxidation periods after the process was interrupted by vacuum anneal. It is possible to observe from the oxidation curves and the tabulated values of

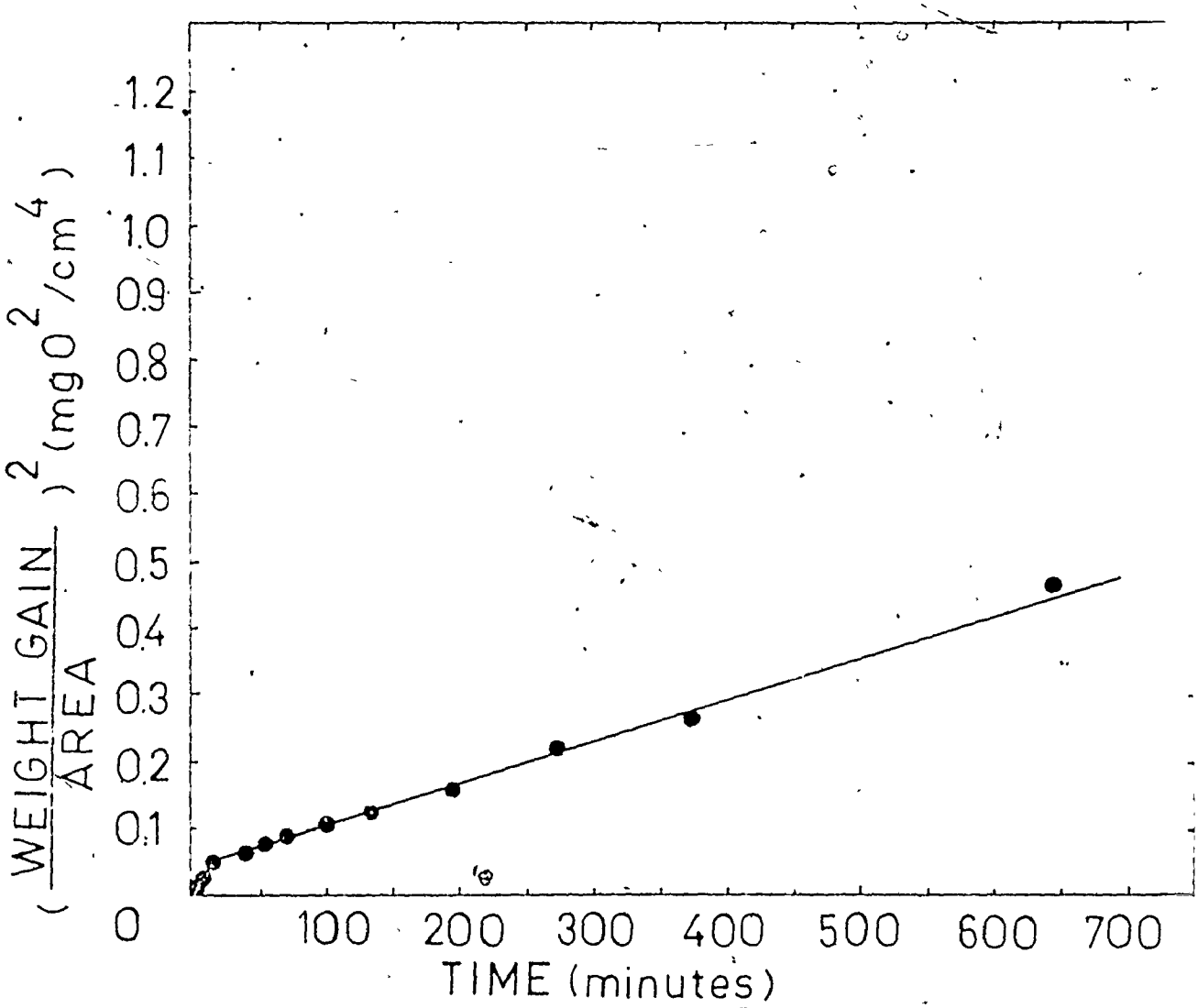


Fig. IV.3-4 Oxidation kinetics of less pure nickel at 800° represented in parabolic form:
20 minutes oxidation at 800°
1 hour annealing at 900°
Reoxidation.

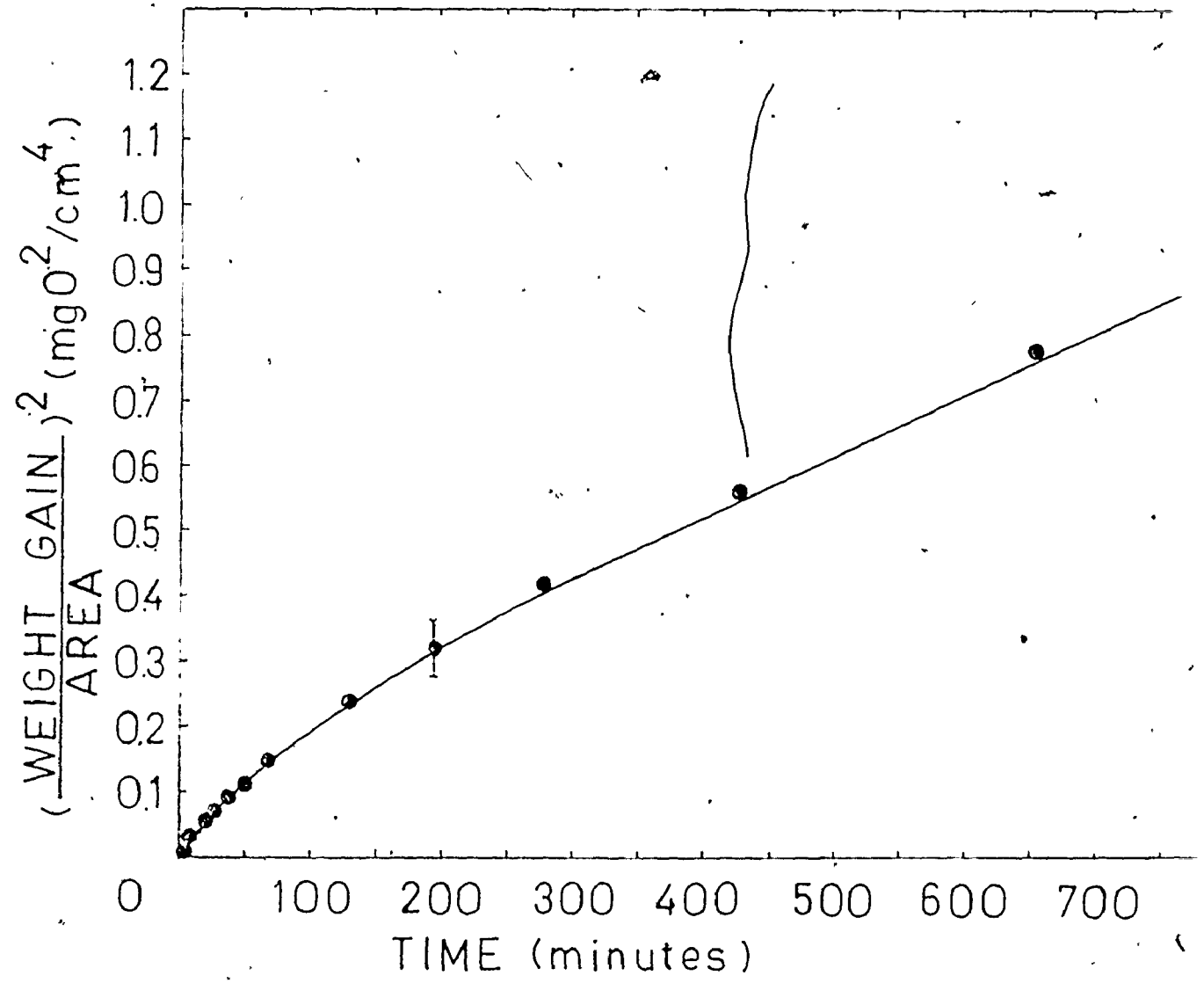


Fig. IV.3-5 Oxidation kinetics of less pure nickel in parabolic form:
10 minutes oxidation
1 hour annealing at 800°
Reoxidation

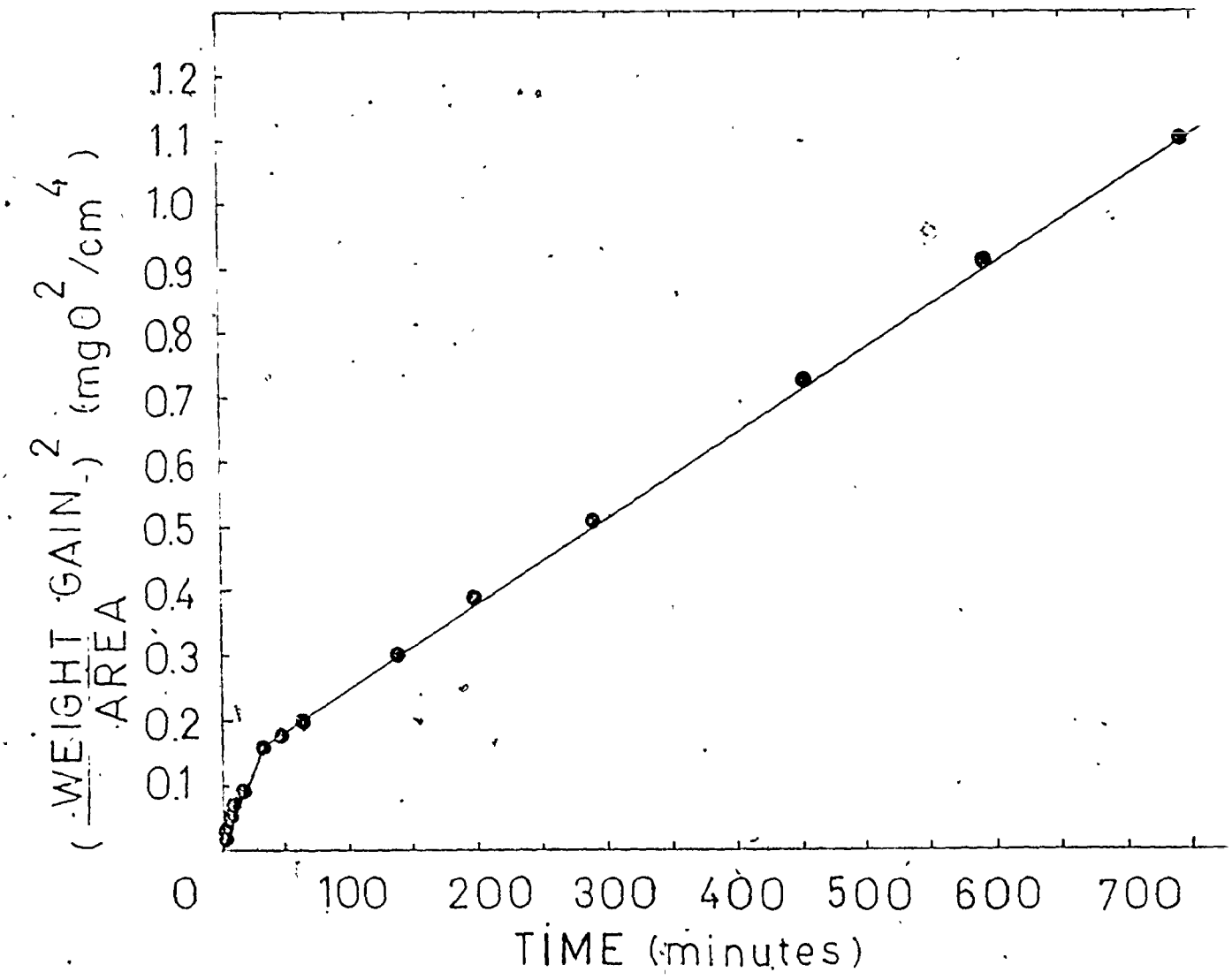


Fig. IV.3-6 Oxidation kinetics of less pure nickel at 800° plotted in the parabolic form:
20 minutes oxidation
2 hours annealing
Reoxidation.

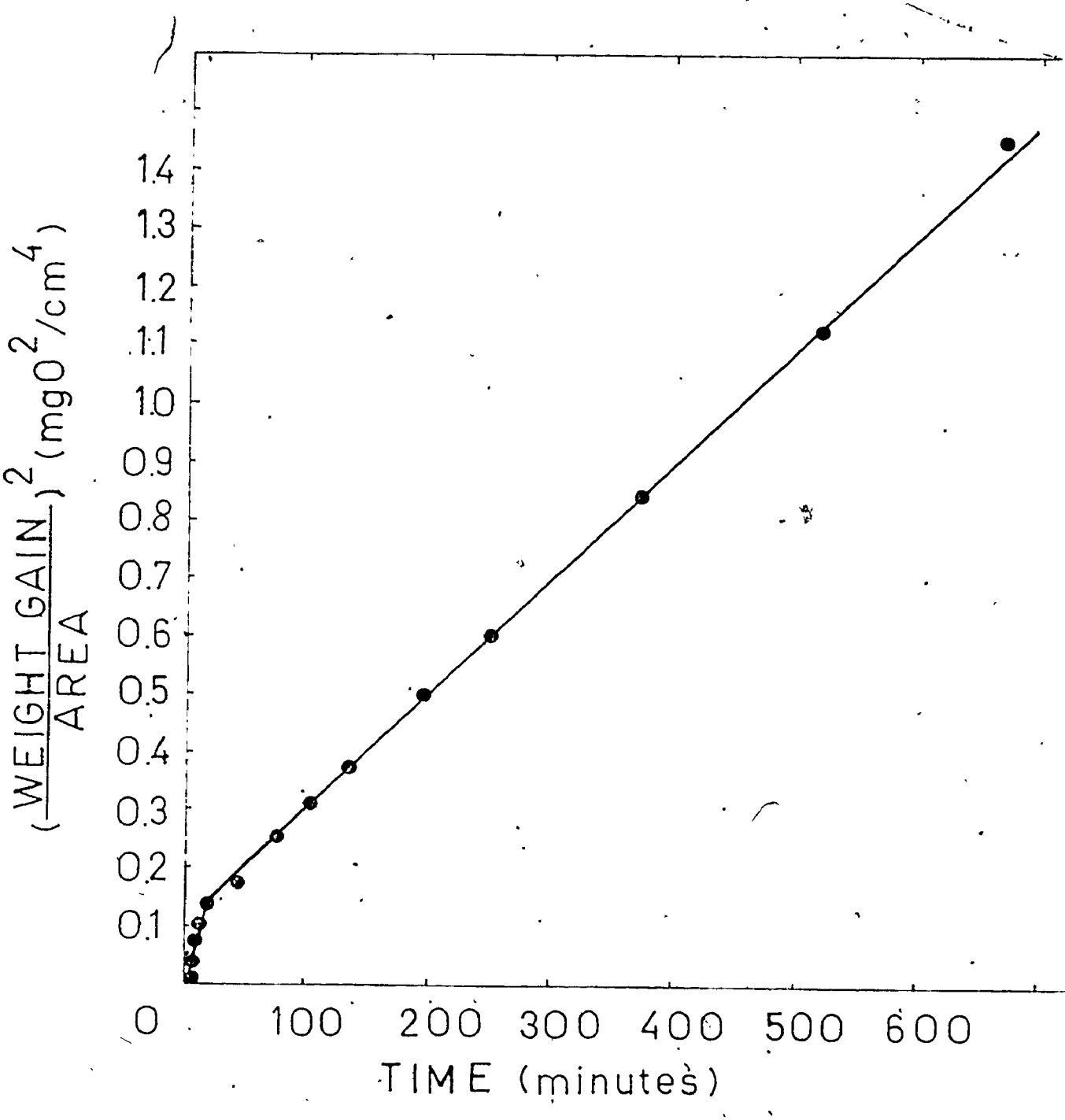


Fig. IV.3-7 Oxidation kinetics of pure nickel:
20 minutes oxidation at 800°
1 hour annealing at 900°
Reoxidation

Table IV.3-5

Relative rate constant of oxidation for less pure nickel

| Type of experiment | $k_1 \times 10^{+3}$ ($mg^2/cm^4 \cdot min$) | $k_2 \times 10^{+3}$ ($mg^2/cm^4 \cdot min$) | $\frac{k_1}{k_2} \pm 28\%$ |
|---|---|---|---|
| (continuous oxidation) | 4.0 | | |
| 20 min. oxidation at 800° | | | |
| After 20 min. oxidation | | 2.5 | 1.6 |
| 1 hour oxidation at 800° | 4.9 | | |
| 1 hour annealing at 800° | | | |
| Reoxidation at 800° | | 2.0 | 2.45 |
| 1 hour oxidation at 800° | 4.8 | | |
| 20 hour annealing at 800° | | | |
| Reoxidation | | 0.7 | 6.8 |
| 1 hour oxidation at 800° | 4.8 | | |
| 1 hour annealing at 900° | | | |
| Reoxidation | | 0.9 | 5.2 |
| 10 min. oxidation at 800° | 4.7 | | |
| 1 hour annealing at 800° | | | |
| Reoxidation | | 2.0 | 2.3 |
| 3 hours oxidation at 800° | 5.0 | | |
| 1 hour annealing at 800° | | | |
| Reoxidation | | No effect | |

(continued next page)

Table IV.3-5 (continued)

Relative rate constant of oxidation for less pure nickel

| Type of experiment | $k_1 \times 10^{+3}$ ($mg^2/cm^4.min$) | $k_2 \times 10^{+3}$ ($mg^2/cm^4.min$) | $\frac{k_1}{k_2} \pm 28\%$ |
|---|---|---|---|
| 20 min. oxidation at 800° | 4.5 | | |
| 1 hour annealing at 800° | | | |
| Reoxidation | | 1.3 | 3.45 |
| 20 min. oxidation | 4.3 | | |
| 1 hour annealing at 900° | | | |
| Reoxidation | | 0.6 | 7.2 |
| 20 min. oxidation at 800° | 5.0 | | |
| 2 hours annealing at 800° | | | |
| Reoxidation | | 1.2 | 4.2 |

Table IV.3-6

Relative rate constant of oxidation for pure nickel

| Type of experiment | $k_1 \times 10^{+3}$ ($mg^2/cm^4.min$) | $k_2 \times 10^{+3}$ ($mg^2/cm^4.min$) | $\frac{k_1}{k_2} \pm 22\%$ |
|---|---|---|---|
| continuous oxidation | 7.0 | | |
| 20 minutes oxidation at 800° | | | |
| After 20 minutes | | 3.1 | 2.2 |
| 20 minutes oxidation at 800° | 6.0 | | |
| 1 hour annealing at 800° | | | |
| Reoxidation | | 2.0 | 3.0 |
| 20 minutes oxidation at 800° | 7.7 | | |
| 1 hour annealing at 900° | | | |
| Reoxidation | | 1.8 | 4.2 |

the effective parabolic oxidation rate constants that depending on the initial time of oxidation, temperature and time of annealing, the relative rate constant of oxidation varies. In fig. (IV.3-8) the relative rate constants of oxidation for different oxidation runs in which the initial periods of oxidation were changed are compared. Because the rate constants of oxidation are effective constants which in time changed during the continuous oxidation of nickel at 800°, the ratios $\frac{k_1}{k_2}$ for these experiments with annealing should be compared those corresponding to continuous oxidation. The influence of the time of annealing on the oxidation rate is illustrated in fig. (IV.3-9) in the same representation as for fig. (IV.3-8). In the case of pure nickel, as illustrated in table (IV.3-6), the effect of annealing is less important than in the case of less pure nickel.

## IV-4 X-RAY DIFFRACTION RESULTS FOR NICKEL OXIDE SCALES

As the working temperature was 800°, the thicknesses of the nickel oxide scales formed during oxidation were greater than 0.5 μm, the limit for using transmission electron microscopy. Accordingly, the structural development of oxide in the scale was followed by X-ray diffraction. This technique is very suitable for the study of these oxide scales because of large penetrating power (an X-ray beam penetrates 20 μm of scale), and of the large cross section of the oxide sampled by the beam. The actual diffraction techniques permit also

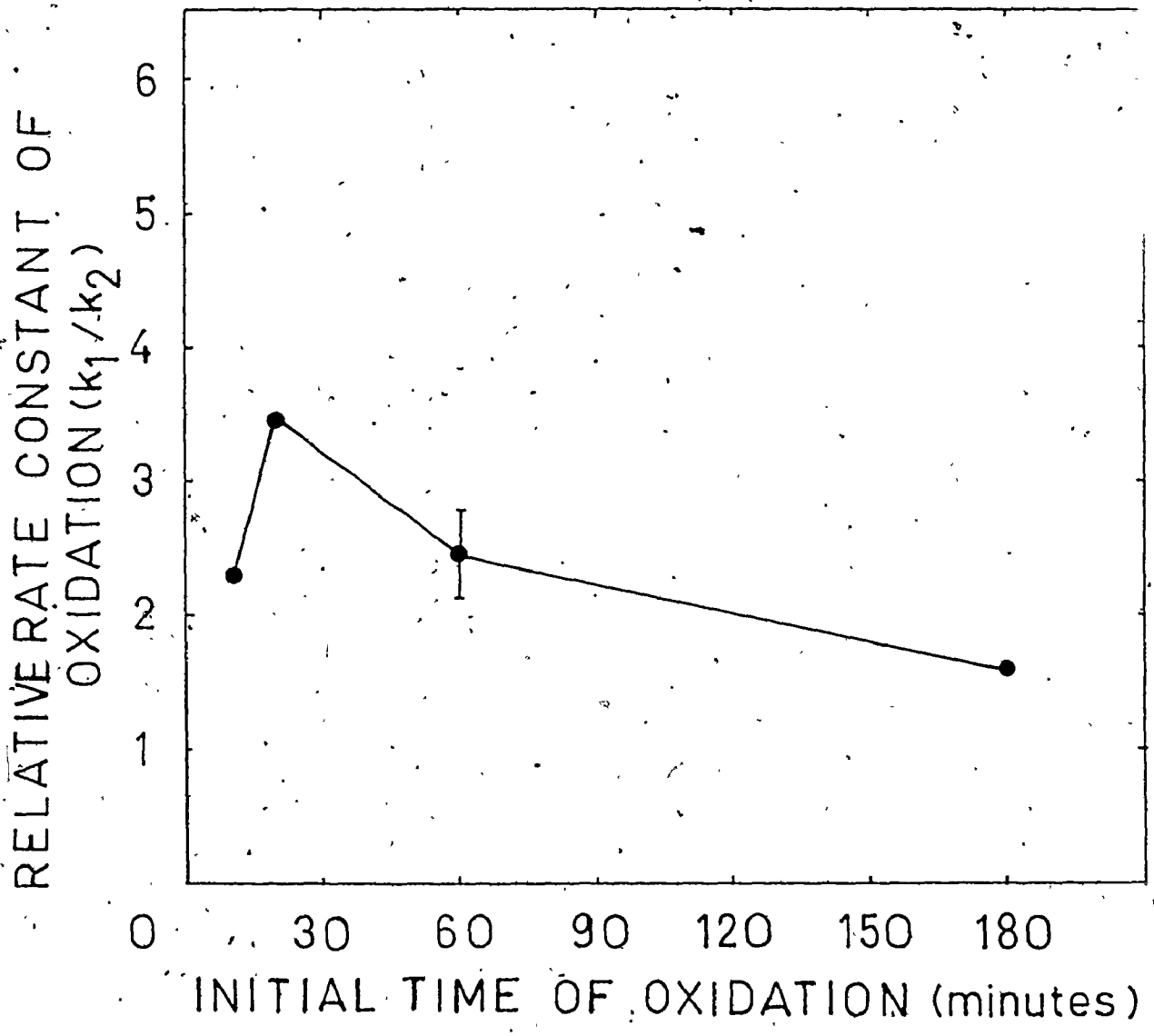


Fig. IV.3-8 Influence of the initial period of oxidation on the relative rate constant of oxidation on less pure nickel.

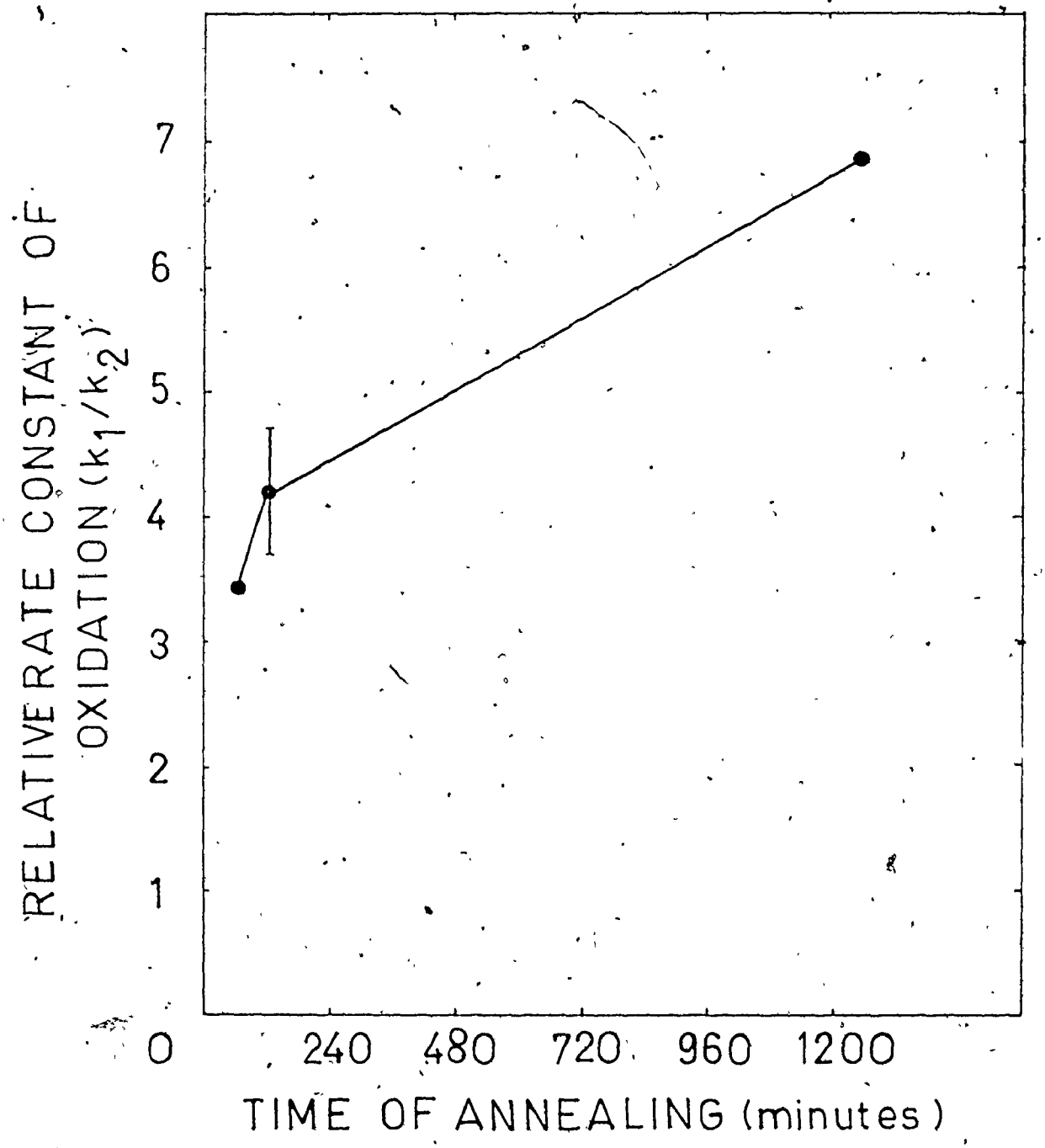


Fig. IV.3-9 Influence of the annealing time on the relative rate constant of oxidation of less pure nickel.

accurate measurements of the diffracted beam intensities.

The primary interest in X-ray diffraction was to determine the parallel orientation of oxide planes with the metal surface. The Harris texture coefficient, eqn. (IV.2-1) was used to determine the preferred orientation of the nickel oxide scale obtained under different conditions of oxidation for different periods of exposure. A parallel orientation can be obtained from the diffractometer measurements, since the conditions are set up so that only the planes parallel to the surface satisfy the Bragg condition for diffraction. Because some of the diffracted planes may not be parallel to the surface, the specimens were continuously rotated during the measurements. To follow the development of the preferred orientation of the nickel oxide scales during the oxidation, the texture coefficients were plotted versus time of oxidation for a specific type of experiment. All the points belonging to the same (hkl) plane are joined by the lines. In figs. (IV.4-1) to (IV.4-4) the obtained results are shown. It is possible to conclude from fig. (IV.4-1) that the nickel oxide scale on the less pure nickel developed a preferred {111} orientation characterized by an increased value for $P_{\{111\}}$ with time of exposure. Fig. (IV.4-2) indicates that during oxidation interrupted by vacuum anneals the same {111} orientation of nickel oxide develops. There are also preserved some other orientations,

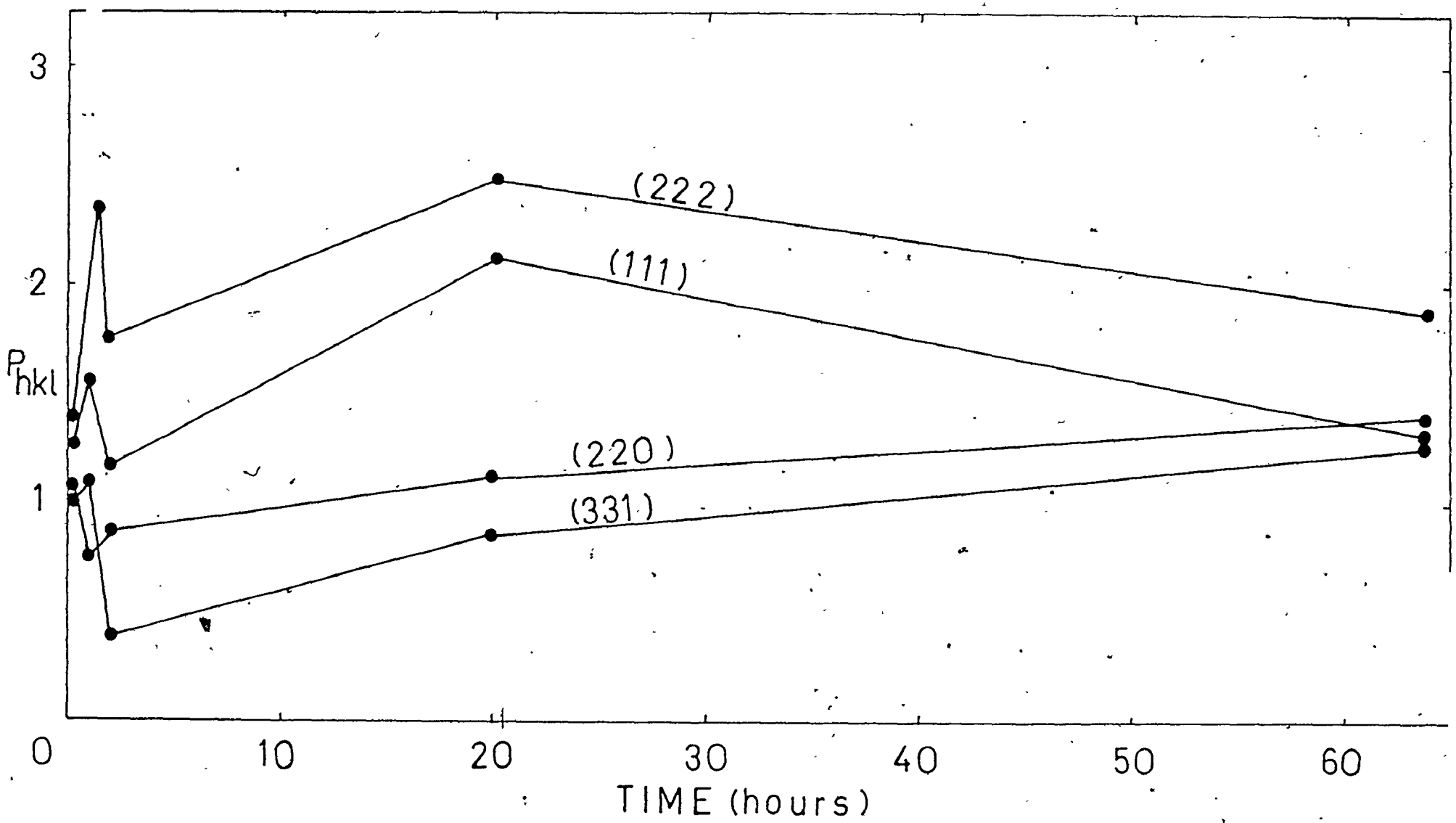


Fig. IV.4-1 Texture coefficients plotted versus time for continuous oxidation of less pure nickel.

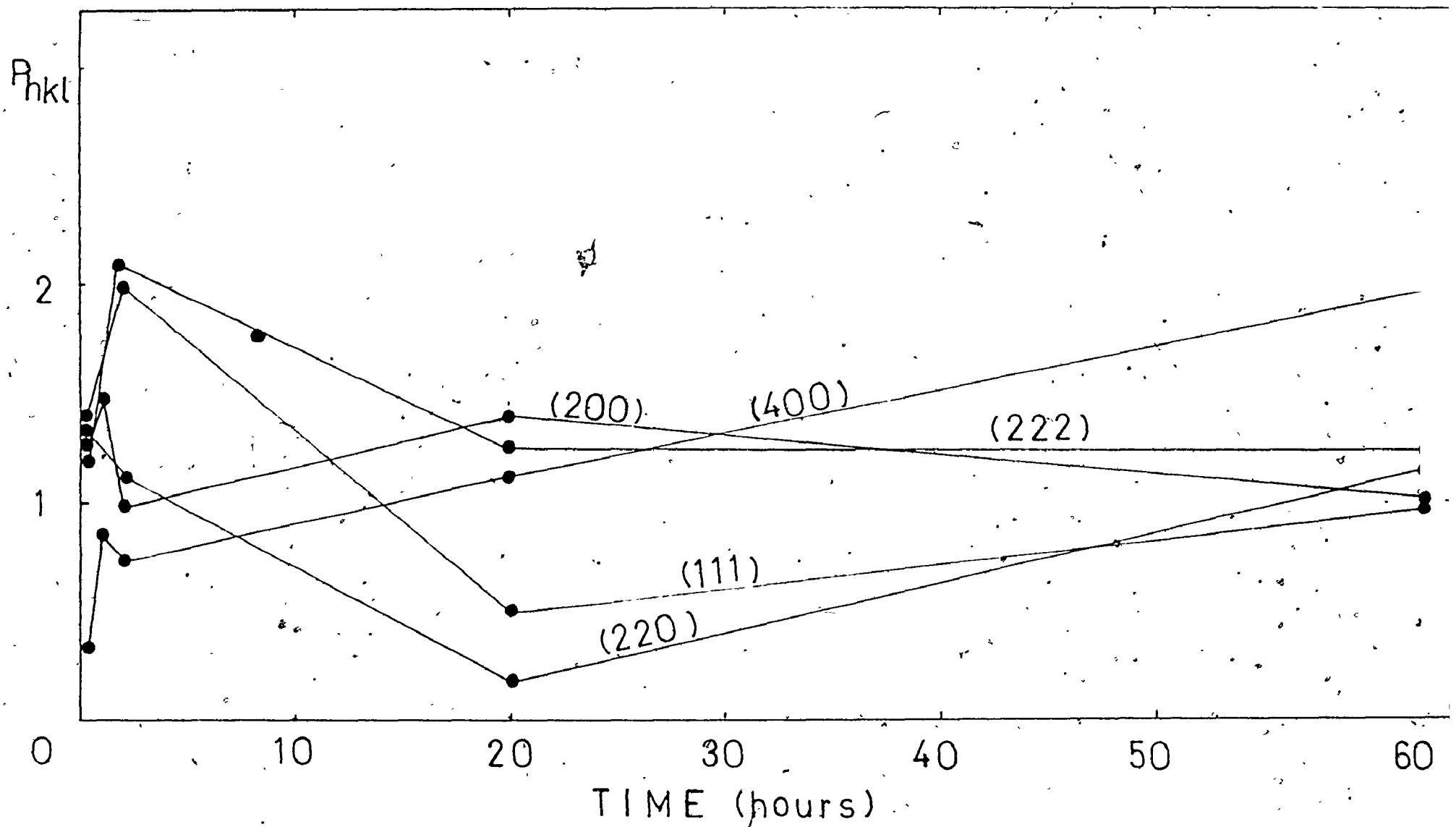


Fig. IV.4-2 Texture coefficients versus time for oxidation interrupted by vacuum anneals of less pure nickel.

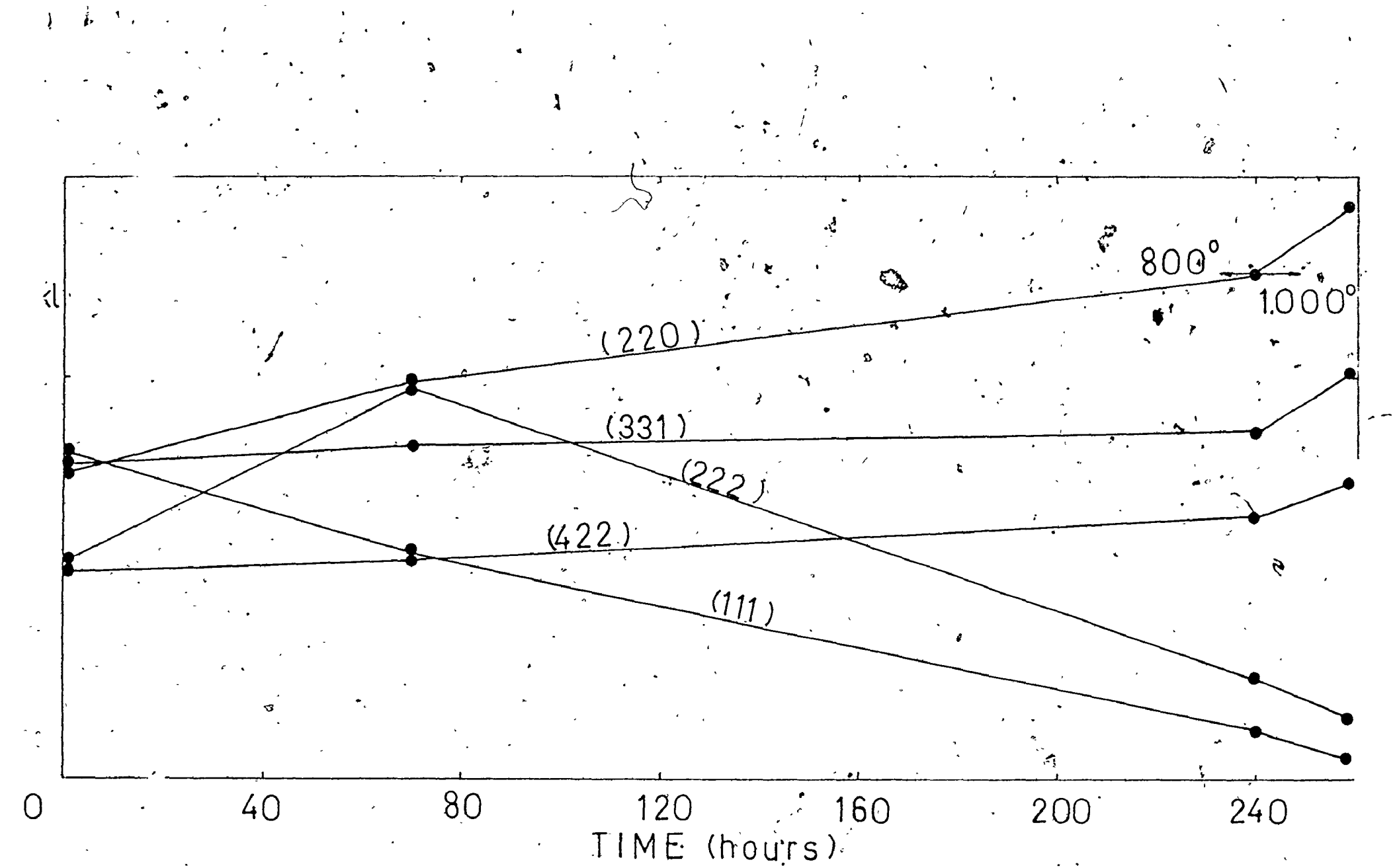


Fig. IV.4-3 Texture coefficients plotted versus time for continuous oxidation of pure nickel.

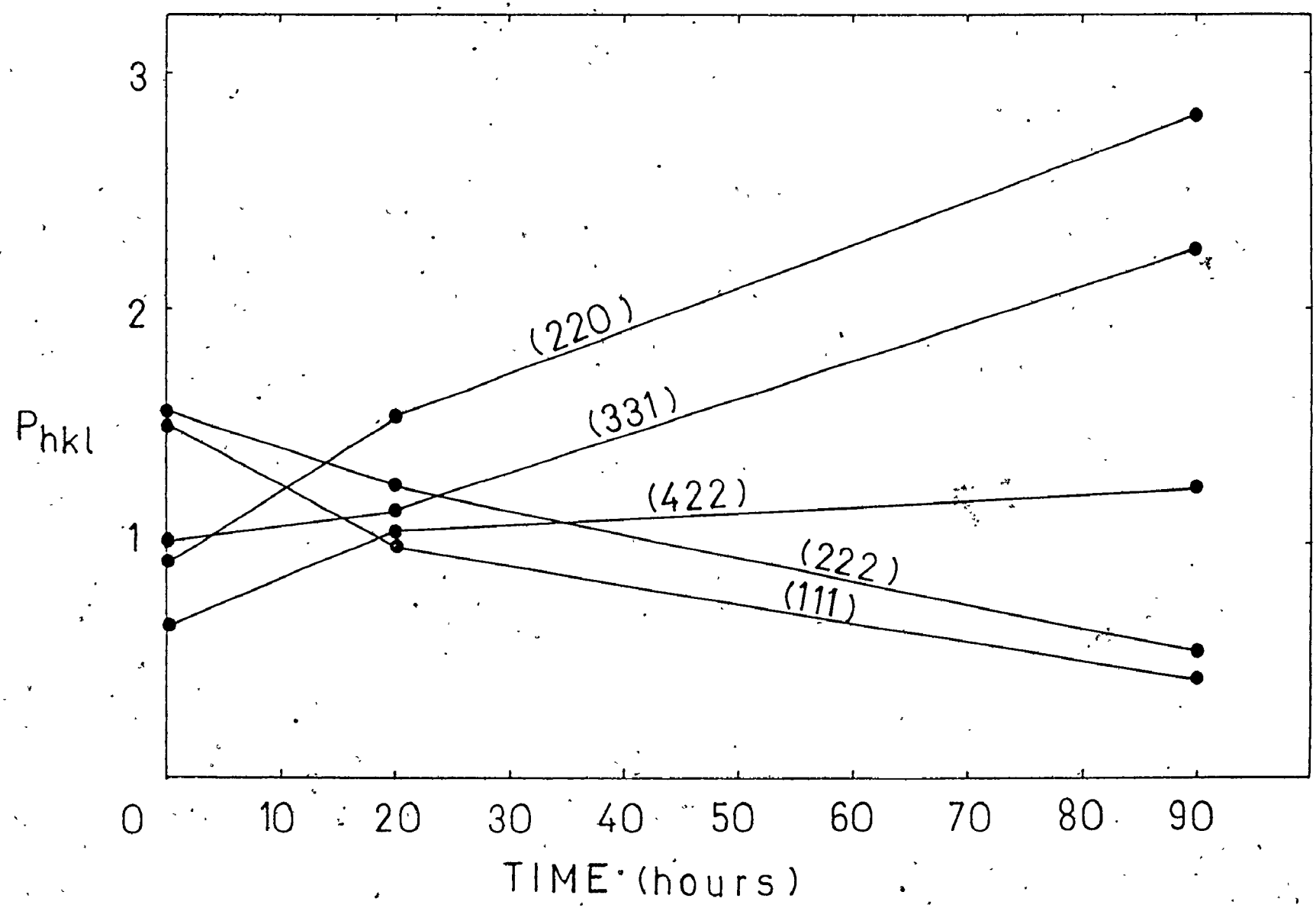


Fig.IV.4-4 Texture coefficients versus time for the oxidation interrupted by vacuum anneals of pure nickel.

especially (331) and (200). During the continuous oxidation of pure nickel, the oxide scale develops a texture characterized by an increasing texture coefficient for (220) and (331) planes. There is also a decrease in the $P_{111}$ texture coefficient of {111} plane with oxidation time. As illustrated in fig. (IV.4-3) changing the temperature from 800° to 1000° increases the (220) and (331) texture coefficients. From fig. (IV.4-4), it is readily concluded that the annealing of the oxide obtained in 20 minutes initial oxidation and reoxidation after annealing more substantially increases the (220) and (331) texture coefficients than does more extended continuous oxidation to longer exposures.

## IV.5 SCANNING ELECTRON MICROSCOPY OBSERVATIONS: TOPOGRAPHIES

Scanning electron microscopy observations were made on all the oxidized samples. They are a complement to X-ray texture measurements. The advantages of using this technique consist in having a complete description of the oxide scale structure: shape and size of the grains, grain size distribution and scale microstructure. This technique has also the advantage of a combined high resolution with a depth of field. To determine the morphological development of the oxide scales in time two types of observations were made using this technique: surface topography and microstructure of the oxide scale. For

topographical observation of the outer surface of the scale the sample does not require any special treatment. For the microstructure of the scale two types of methods were used to obtain observations: 1. mounting the sample in a room - setting plastic and revealing the structure by polishing and etching and 2. fracturing the samples of oxide. These observations will be presented as follows: a) topographical aspect of the nickel specimens oxidized at 1,000° and 800° and low pressure of oxygen, b) topographical aspects of the nickel specimens in the early stage of oxidation, c) topographical aspects of the outer surfaces of less pure nickel and pure nickel oxidized continuously and by oxidation interrupted by vacuum anneal, for different periods of time, d) topographical aspect of the sample oxidized at 800° for a certain period and compared with the aspect of the same specimens but reoxidized for long time at 1000° , e) morphological development of the microstructure of the oxide scales formed during different periods of continuous oxidation or during oxidation interrupted by vacuum anneals by examining fractured samples and metallographically prepared cross sections.

IV.5,1 Results on Early Stage of Oxidation.

To understand the morphological development of the oxide scale, experiments were carried out on nickel of 99.999% purity at 800° and 1000° and at low oxygen pressure of $5 \times 10^{-3}$ Torr. To follow the morphological development of the nickel oxide scales it was considered that all the experiments should be completed

under the same conditions in order to make possible a correlation of the observations.

(a) Nickel oxide formation and growth at 1000°

The sample of nickel of 99.999% was prepared as described in Chapter III, except that it was deformed by bending approximately two degrees after the regular annealing, was oxidized for 2 hours at 1000° and at $p_{O_2} = 5 \times 10^{-5}$ Torr . This temperature was chosen because several nickel oxide scales obtained at 800° by continuous oxidation for a number of hours were reoxidized for 20-30 hours at 1000°. Some of the most important features of this sample are represented in figs. (IV.5-1a) to (IV.5-1 j). The first four micrographs indicate the general aspects of the samples. It is possible to observe striations on the majority of the metallic grains. By examining the (IV.5-1 a,b,d,h) micrographs, it is seen that the direction of the striations varies from grain to grain, depending on the metal grain orientation. Some of the metallic grains are quite free of oxide nuclei as in micrographs (IV.5-1h). The shape; the number and the orientations of the nuclei related to the bases metal vary from metal grain to metal grain , depending on their orientation. On the same metallic grain, ~~the~~ oxide nuclei have the same orientation relative to the metal as illustrated by micrographs (IV.5-1c), (IV.5-1d) and (IV.5-1e). Some of the nuclei form at the metal grain boundaries but these do not appear as being necessarily preferred sites because oxide nuclei are formed within grains as

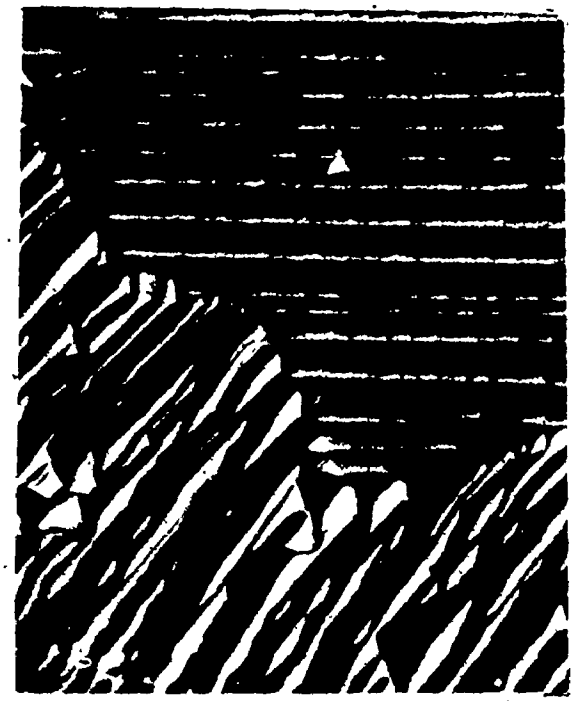

(x 1,600)

a

(x 800)

b

(x 4,000)

c

(x 800)

d

Fig. IV.5.1-1 a,b,c,d,e,f,g,h,i,j : Topographical aspect of pure nickel oxidized 2 hours at 1000° and $p_{O_2}$ $5 \times 10^{-5}$ Torr..

22° (x 2,100)

e

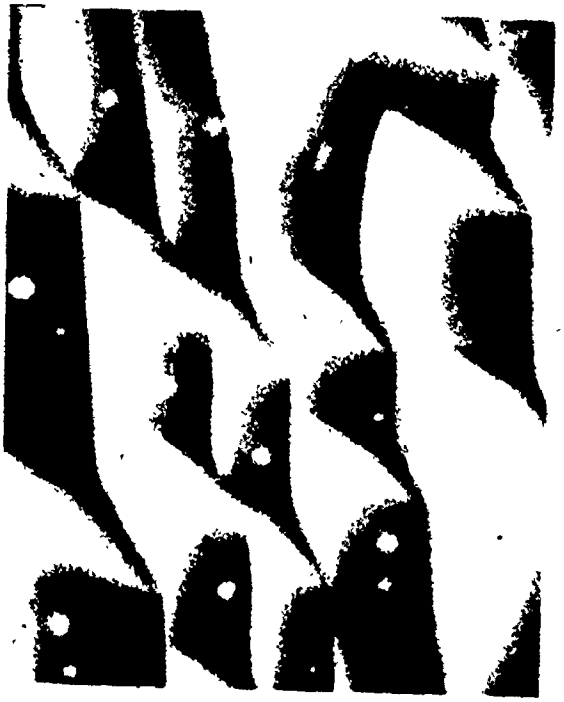

(x 8,000)

f

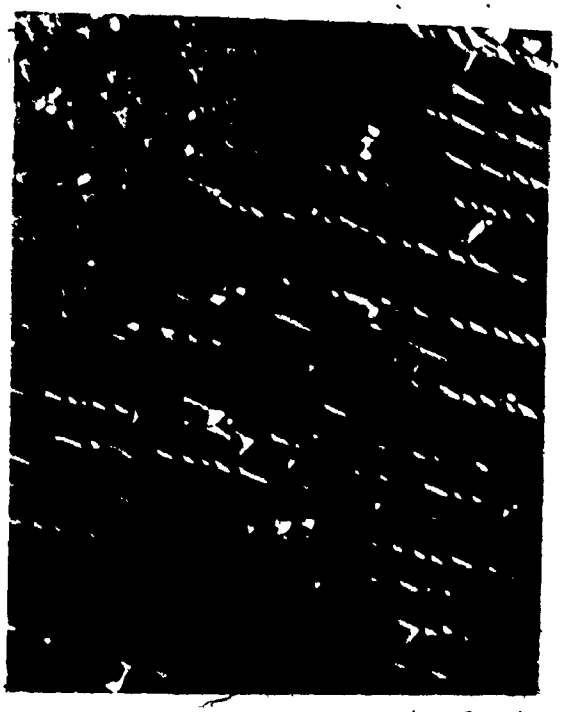

(x 800)

g

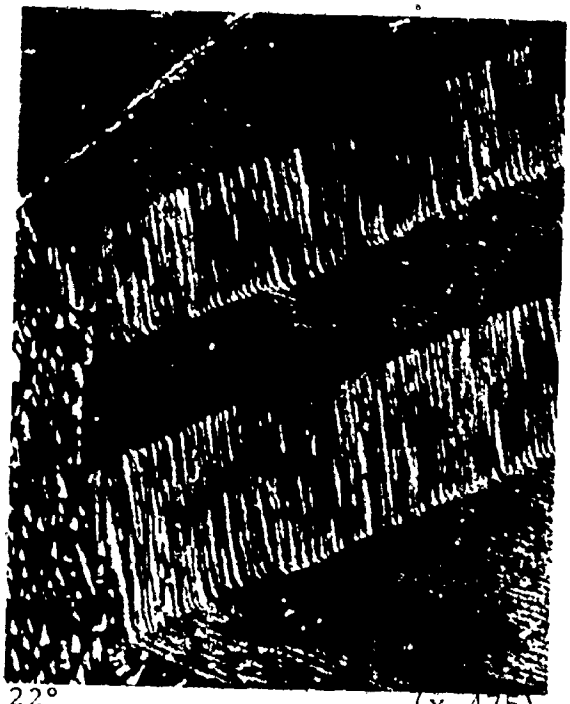

22° (x 475)

h

22° (x lo,ooo)

22° (x lo,ooo)

is obvious from micrograph (IV.5-1d). From micrograph (IV.5-1h) it is evident that oxide formation did not take place at the metal twin grain boundaries. Micrographs (IV.5-1i) and (IV.5-1j) illustrate a magnified aspect of two different crystallites exhibiting tetrahedral and octahedral shapes. The height of the striations (or steps) from these micrographs is approximately between 1-2 μm depending on the metal grain; the nuclei form on the surfaces of different striations and meet each other both on the same striation and on different striations.

(b). Nickel oxide formation and growth at 800° and $pO_2=5\times10^{-5}$ Torr.

Experiments were carried out on samples oxidized at 800° and $5\times10^{-5}$ Torr oxygen pressures for 18 hours and 45 minutes at an oxygen pressure of $5\times10^{-3}$ Torr. Topographical aspects of pure nickel oxidized at 800° and $p_{O_2} = 5\times10^{-5}$ Torr are represented in the next micrographs, (IV.5.1-2 a,b,c,d,e, f and g). Micrograph (IV.5.1-2a) illustrates the general aspect of the oxidized sample. Some metallic grains are completely free of the oxide; the amount of oxide and the shape and texture of the oxide nuclei are dependent upon the orientations of the metal grains. This micrograph as well as micrographs (IV.5.1-2b) indicate that at 800° the grain boundaries of the metal are preferred sites for oxide formation whereas this type of phenomenon did not occur upon oxidation at 1000°. Also the aspect of striations of the nickel surface appears

22°

(x 200)

a

(x 2,000)

b

(x1,000)

c

(x 5,000)

d

Fig. IV.5.1-2 a,b,c,d,e,f,g : Topographical aspects of pure nickel oxidized 18 hours at 800° and $p_{O_2} = 5 \times 10^{-5}$ Torr.

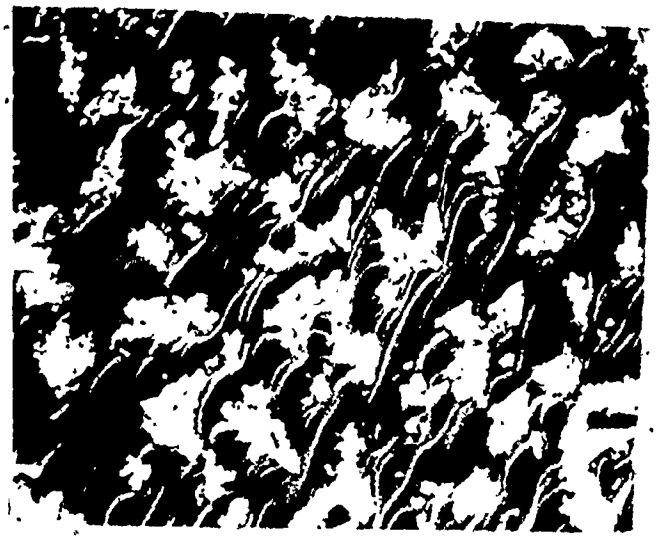

(x 1,000)

e

(x 2,000)

f

(x 5,000)

g

completely different than at 1000°. These micrographs illustrate at different magnifications several aspects of the oxide nucleated on different metallic grains.

The micrographs in figs. (IV.5-1.2 c and d) indicate a high rate of oxide formation. The oxide crystallites form on the valley between the metallic striations at different sites. The oxide formed on the exhibited grains shows a fast nucleation rate and a slow lateral growth rate. In general this type of metal surface exhibited a high oxidation rate.

The micrographs in figs. (IV.5.1-2 f and g) indicate that on this specific grain the rate of formation is slower than on the surrounding grains, but that the crystallites grow faster and are well developed. They continually grow in height and spread laterally at a slower rate to impinge on each other. The nuclei are also differently oriented within the same metallic grain in comparison to the behaviour at 1000°.

The micrograph in fig. (IV.5.1-2e) represent a completely different situation compared with previous micrographs. The crystallites are also characterized by different shape and different orientation related to the respective metallic grain. It appears that the crystallites form at a high localized density of sites on the grain surface leaving the rest of the grain surface free of oxide localized growths. The rate of formation appears to be low and some crystallites grow preferentiall before meeting one another. The crystallites are also different-

ly oriented relative to the metal, their heights ranging from 0.2 μ and 2 μm.

(c) Oxidation at 800° and $p_{O_2} = 5 \times 10^{-3}$ Torr.

Topographies of a pure nickel specimen oxidized for 45 minutes are illustrated by the micrographs in figs. (IV.5.1-3 a, b, c, d and e. All these micrographs indicate again that the oxidation rate depends on the orientation of the metal grain on which the oxide grows. The micrograph (IV.5.1-3a) illustrates again that the grain boundaries of the metal are preferred sites for formation of the oxide. It appears that the oxide crystals are growing in height before they spread laterally. The crystallites differ in shape and size. The distribution of the size of these oxide crystals on different metal grains is represented in fig. (IV.5.1-4) by relative frequency curves. The graph represents $f = \frac{N}{N_t}$ as a function of size of the crystals in which N represent the total number of crystallites counted on a metal grain and $N_t$ is the number of the crystallites having their diameter in a certain class of sizes. It is possible to observe on all metal grains used for calculations that the average size of the oxide crystallites is around r = 1.0 ± 0.2 μm but that the maximum crystal size differs from grain to grain and in one case is equal to 2.3 μm.

The micrographs (IV.5.1-3 b and c) illustrate the difference in size and shape of the oxide crystallites. The majority of the crystallites are rectangular but some exhibit a

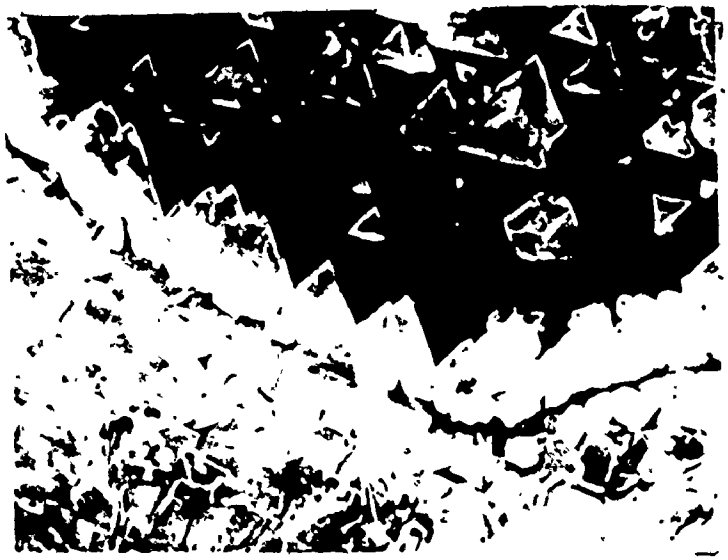

22° (x 4,000)

a

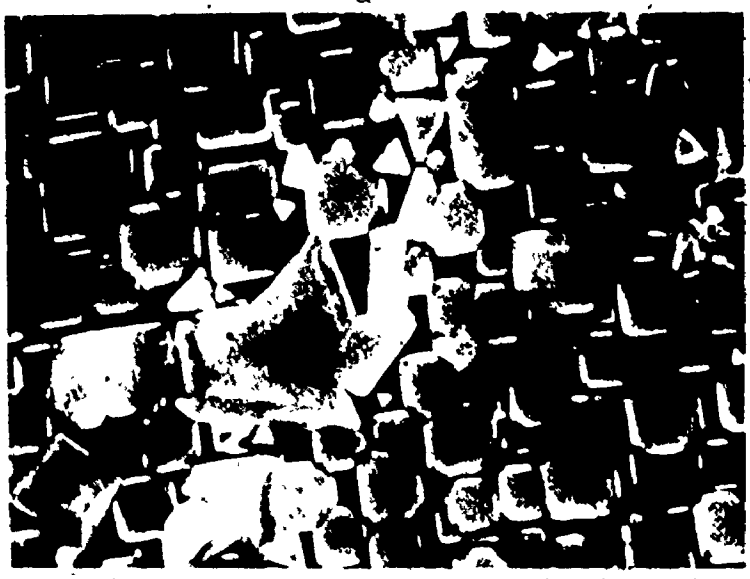

(x 8,000)

b

(x 8,000)

Fig. IV.5.1-3 a,b,c d,e. Topographical aspect of pure nickel oxidized for 45 minutes at 800° and $P_{O_2} = 5 \times 10^{-3}$ Torr.

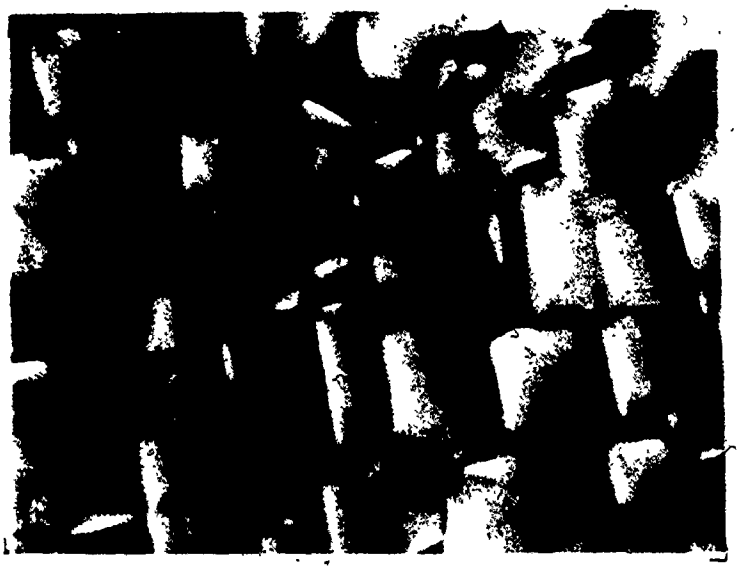

(x 16,000)

d

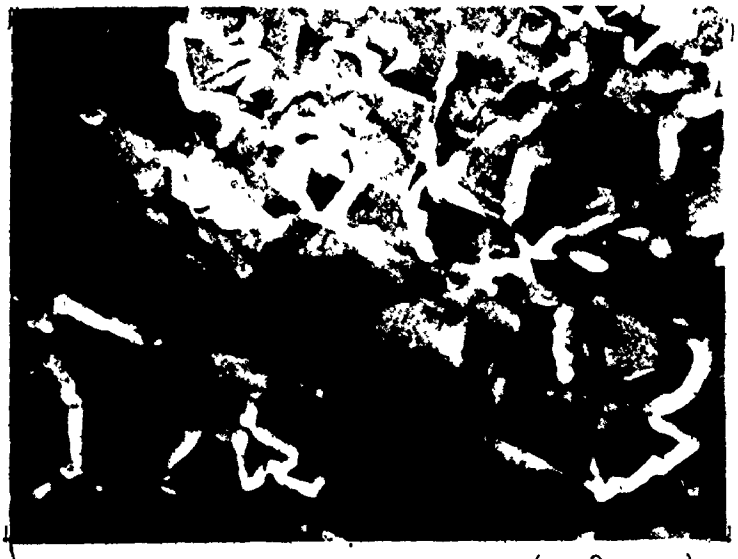

(x 8,000)

e

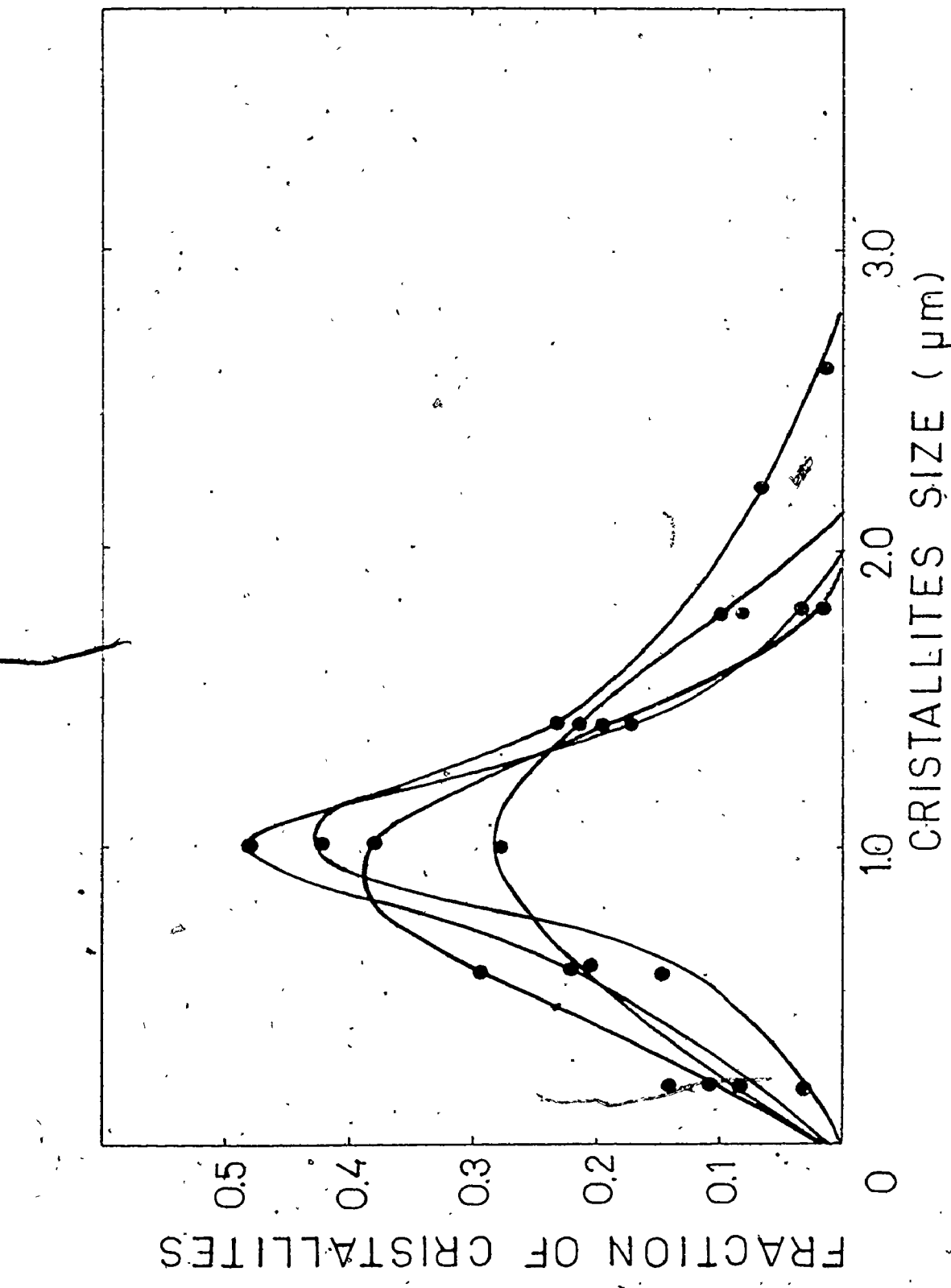


Fig. IV.5.1-4 Crystallite size distribution for oxide film formed on four different metallic grains by oxidation of pure nickel at 800° and $p_{O_2} = 5 \times 10^{-3}$ Torr.

triangular shape. One of the advantages of working with polycrystalline nickel consists in the fact that due to the anisotropy of oxidation, the reaction is at different stages of development on the same sample. Thus it is easy to observe on Fig. (IV.5.1-3 b,c,d, and e) different stages of formation of crystallites and of their growth. The oxide crystallites cover the surface; they grow in height and also laterally. Small crystallites form in the space between the larger crystallites while some of the larger crystallites spread on top of others. It appears that these latter crystallites could be considered as leading to formation of polycrystalline oxide. When these larger crystallites meet each other they preferentially commence thickening at their grain boundaries. Development of these crystals with this thickening of the oxide at the grain boundaries is specifically illustrated by the micrographs in Figs. (IV.5.1-3 c and e). This aspect can be considered as the beginning of the formation of the "cellular structure", a structure very characteristic for formation of nickel oxide scales reported in the literature by almost all investigators[51,54].

IV.5.2 Initial Oxidation Stages for Less Pure Nickel and Pure Nickel by Continuous Oxidation and Oxidation Interrupted by Anneals: Topography.

Different specimens of the two types of nickel were oxidized at 800° and $p_{O_2}$ = 400 Torr in the continuous mode up to two hours or in this mode interrupted by vacuum anneals for one hour. The topographical aspects of these specimens are

illustrated by the micrographs in Figs. (IV.5.2-1), (IV.5.2-2), (IV.5.2.-3) and (IV.5.2.-4). Micrographs (IV.5.2-1 a) (back reflection and (IV.5.2-1 b and c) illustrate the general surface appearance of nickel oxide obtained during 5 minutes, 1 hour and 2 hours continuous oxidation. All these micrographs show that the scale thickness varies from grain to grain, which indicates that at these periods of oxidation the metal structure influences oxide development. The micrographs (IV.5.2-2a) representing a magnified view of a pure nickel specimen oxidized for 5 minutes, as well as micrograph (IV.5.2-2 b) representing the pure nickel samples oxidized for 1 hour, demonstrate the development of the cellular oxide structure. Fig. (IV.5.2-2 c) is a magnified picture of the cellular oxide growth on a less pure nickel specimen oxidized for 2 hours.

The micrographs in fig. (IV.5.2-3) represents the topographical view of a pure nickel specimen oxidized for 5 minutes and annealed for 4 hours; the micrographs in fig. (IV.5.2-4 a, b and c) represent the surface aspects of four less pure nickel specimens obtained under different conditions of oxidation at 800° a) 1 hour continuous oxidation at 800°, b) 1 hour oxidation and 20 hours annealing at 800°, c) 1 hour oxidation and 1 hour annealing at 900°.

These micrographs illustrate the cellular aspect of the outer oxide scale. Annealing accentuates the cellular aspect of the oxide and the oxide seems more laterally spread.

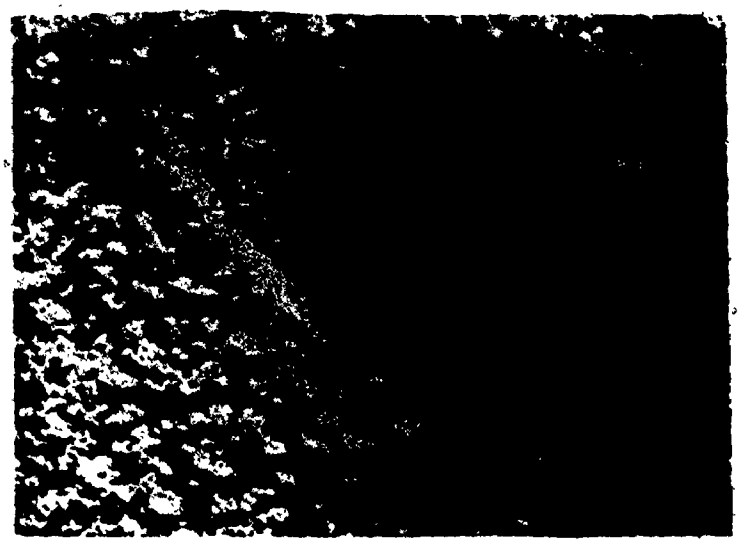

(Back reflection) (x 1,950)

a

(x 200)

b

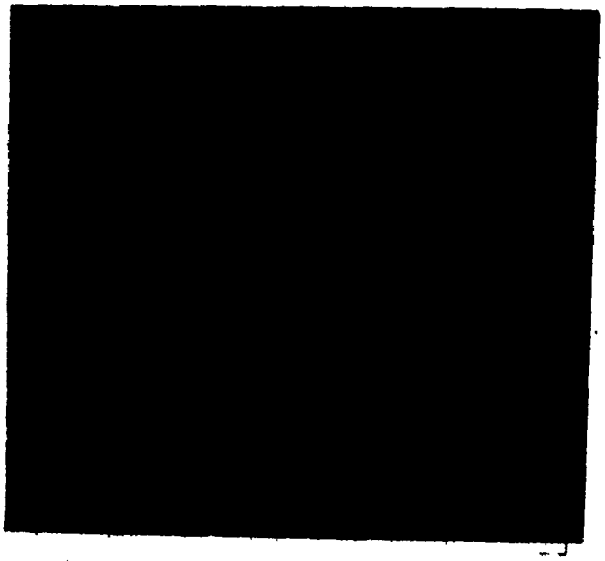

(x 200)

c

Fig. IV.5.2-1 a,b,c General aspect of nickel oxide surface obtained in the initial stages of oxidation at 800° and $p_{O_2}$ = 400 Torr.

a. pure nickel oxidized for 5 minutes

b. pure nickel oxidized for 1 hour

c. pure nickel oxidized for 2 hours.

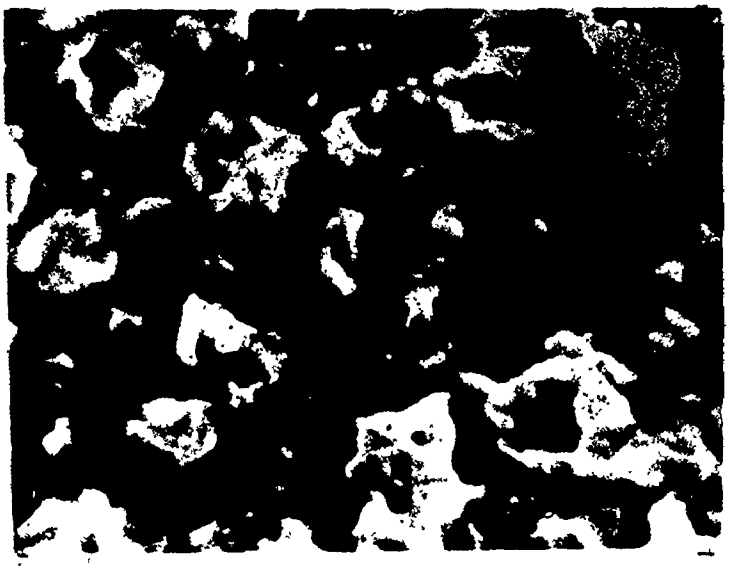

(x lo,ooo)

a

Fig. IV.5.2-2a,b,c "Cellular" structure of the outer surface layer of nickel oxide at 800° and $p_{O_2}$ = 400 Torr

a. pure nickel oxidized for 5 minutes.

b. pure nickel oxidized for 1 hour

c) less pure nickel oxidized for 2 hours.

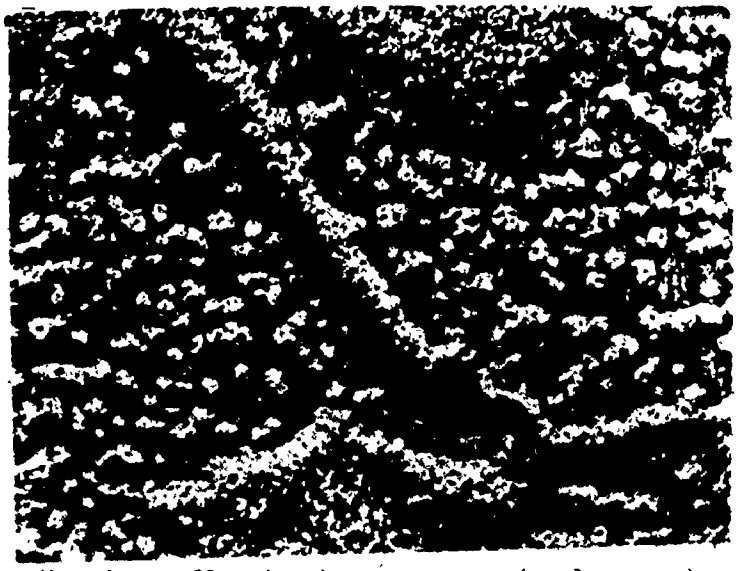

(back reflexion) (x lo,ooo)

b

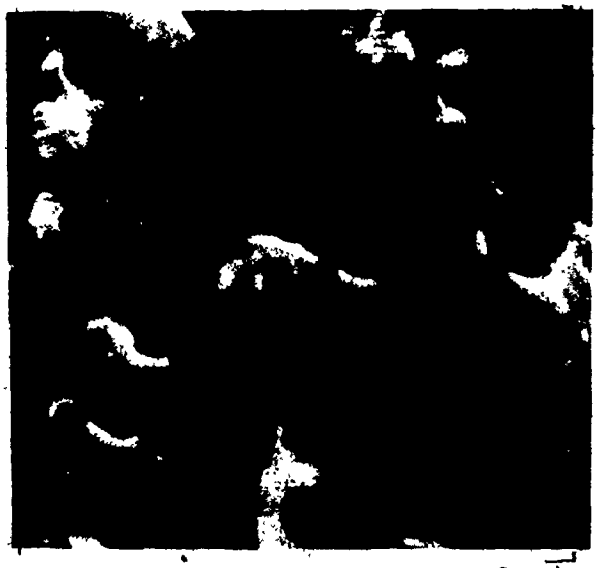

(x 13,3oo)

c

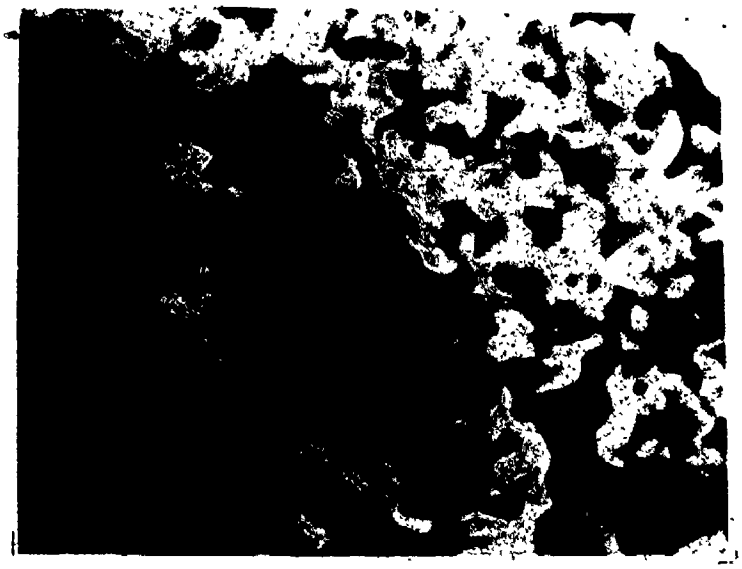

(x 10,000)

a

(x 10,000)

b

Fig. IV.5.2-3 a,b Topographical aspect of pure nickel oxidized for 5 minutes at 800° and annealed for 4 hours at 800°.

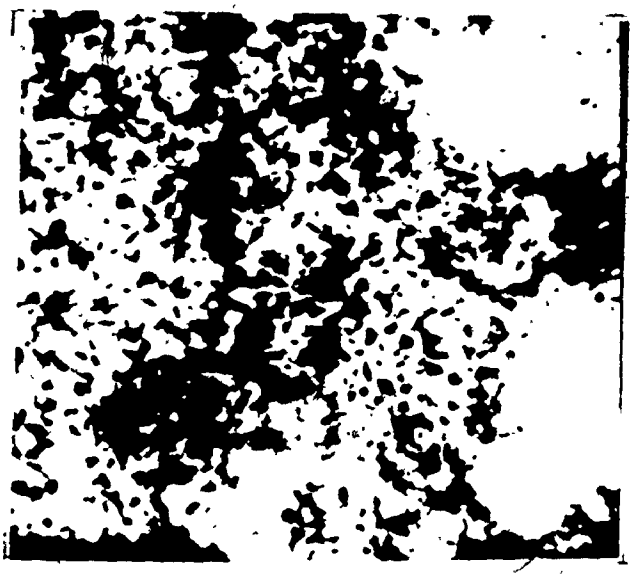

(x 3,5oo)

a

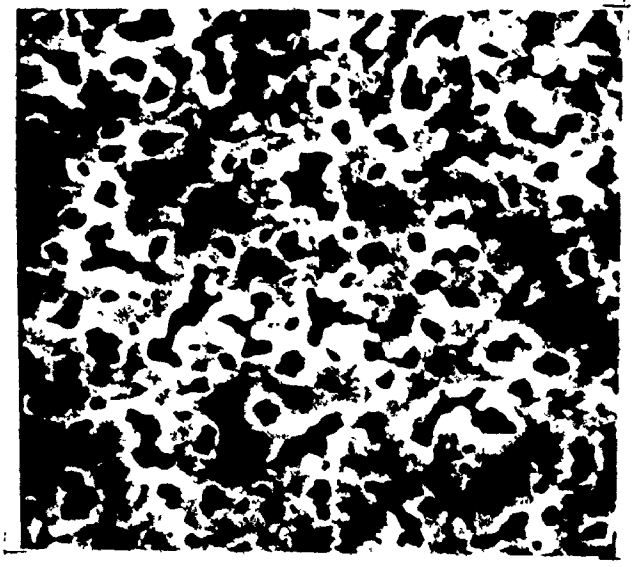

(x 3,45o)

b

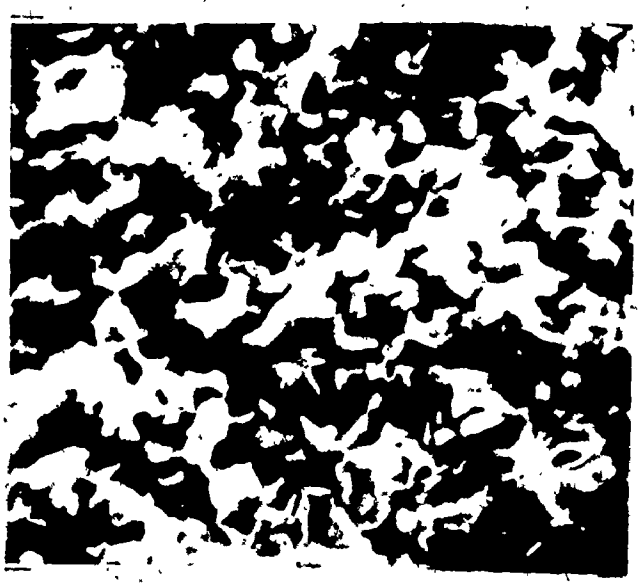

(x 6,3oo)

c

Fig. IV.5.2-4 a,b,c , Topographical aspect of less pure nickel oxidized in different conditions at 800°.
a. 1 hour continuous oxidation, b. 1 hour oxidation and 20 hours annealing at 800°, c. 1 hour oxidation and 1 hour annealing at 900°

The micrographs in figs. (IV.5.2-5 a,b,c,d,) represent less pure nickel specimens oxidized under different conditions: a) 2 hours continuous oxidation, b) 1 hour oxidation, 1 hour annealing at 800° and 1 hour reoxidation, c) 20 minutes oxidation, 1 hour annealing at 800° and 1 hour 40 minutes reoxidation and d) 20 minutes oxidation, 1 hour annealing at 900° and 1 hour and 40 minutes reoxidation at 800°. The cellular oxide structure as shown in the picture (IV.5.2-5 a) is well developed on the nickel sample oxidized continuously for two hours. However, the specimens oxidized also for 2 hours but by oxidation interrupted by anneals as in picture b and c exhibits a less cellular aspect and especially on the (IV.5.2-5 d) micrograph it is obvious that the surface is characterized by well developed oxide grains of regular geometrical shape.

IV.5.3. Topography of the Oxide Scales Formed at the Intermediate and Long Exposure Periods

To follow the topographical development, specimens of less pure and pure nickel were oxidized for periods ranging from 20 up to 240 hours in continuous oxidation experiments and oxidations interrupted by anneals. In this respect, the micrographs in fig. (IV.5.3-1) represent oxide scales obtained on less pure nickel (a,b,c) and pure nickel (d) after 20 hours of oxidation. The nickel specimen oxidized for 20 hours in a continuous experiment is characterized still by some cellular oxide structure and also by the presence of very fine grains

(x 3,450)

a

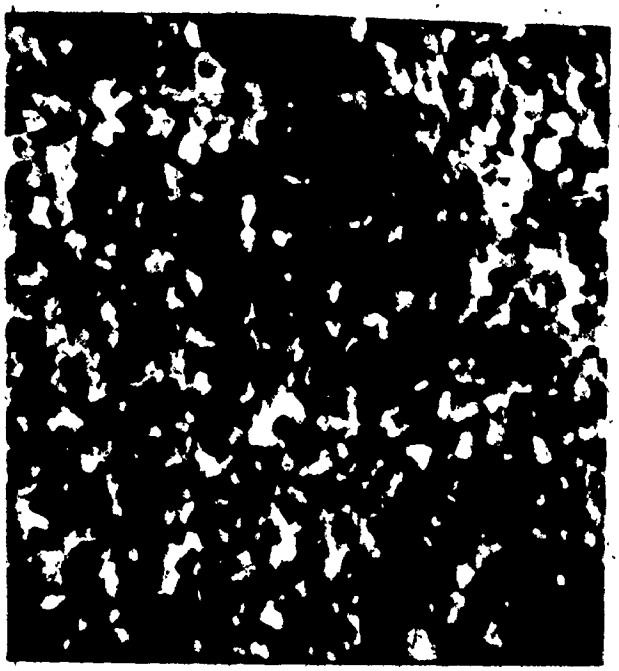

(x 3,650)

b

(x 6,500)

c

(x 3,500)

d

Fig. IV.5.2-5 a,b,c,d. Less pure nickel specimens oxidized for 2 hours at 800°: a. 2 hours continuous oxidation, b. 1 hour oxidation 1 hour annealing at 800° and 1 hour reoxidation, c. 20 minutes oxidation, 1 hour annealing at 800° and 1 hour forty minutes reoxidation, d. 20 minutes oxidation, 1 hour annealing at 900° and 1 hour forty minutes reoxidation.

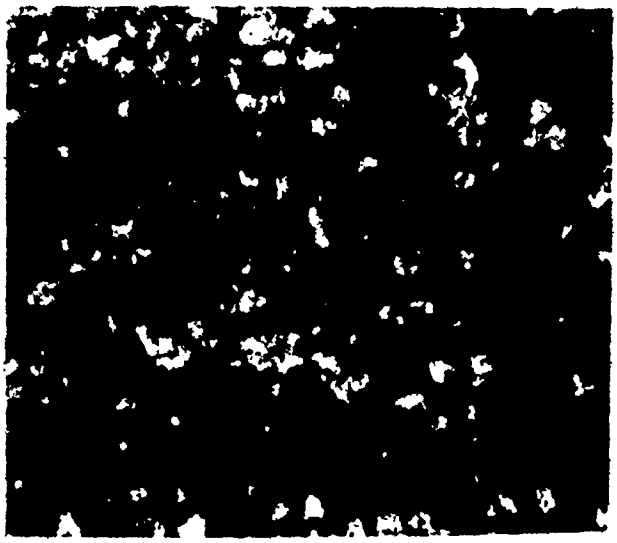

(x 3,4oo)

a

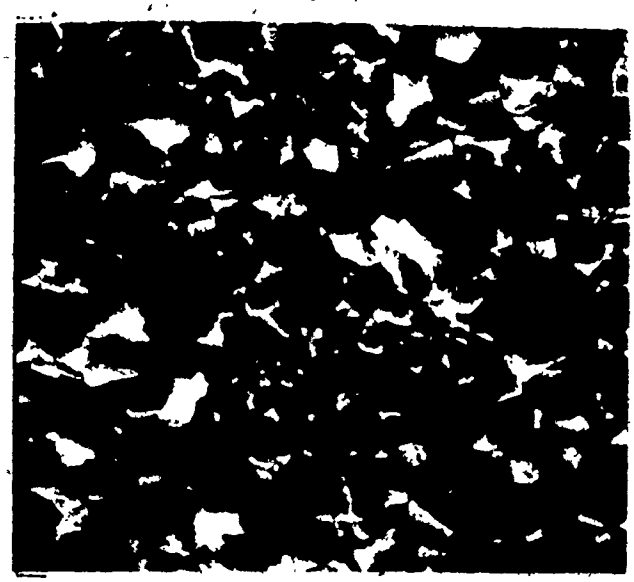

(x 3,5oo)

b

(x 3,5oo)

c

Fig. IV.5.3-1 a,b,c,d. Topographical aspect of nickel oxidized at 8oo°: a. 2o hours continuous oxidation, b. 2o minutes oxidation, 1 hour annealing at 8oo° and reoxidation, c. 1 hour oxidation, 2o hours annealing at 8oo° and reoxidation, d. 2o minutes oxidation of pure nickel, 1 hour annealing at 9oo° and reoxidation.

(x 1,800)

d

without a defined geometrical shape. The surfaces of the specimens obtained by oxidation interrupted by vacuum anneals exhibit completely different features. The remaining micrographs in (IV.5.3-1 represent oxide obtained by oxidation interrupted by vacuum anneals: (IV.5.3-1 b), 20 minutes oxidation, 1 hour annealing at 800°, followed by 20 hours reoxidation, (IV.5.3-1c) represents the surface of an oxide obtained by 1 hour oxidation at 800°, 20 hours annealing at 800° and 19 hours reoxidation; (IV.5.3-1d) represents the outer surface of nickel oxide obtained by oxidizing pure nickel for 20 minutes at 800°, 1 hour annealing at 900° and 20 hours reoxidation. The oxide in these micrographs is characterized by well developed grains of regular geometrical shape much larger in size than those of the scale obtained during continuous oxidation. The maximum size of these outer grains is between 2 and 3 μm.

Several less pure nickel and pure nickel specimens were oxidized for still longer periods of 70 hours during the continuous experiments and during the oxidation interrupted by vacuum anneals. Some features of the outer surface scales are revealed in the micrographs in fig. (IV.5.3-2 a,b,c,d,e and f). The micrographs (IV.5.3-2a and b) represent the topography of the scale obtained during 70 hours of continuous oxidation of less pure and pure nickel, respectively. Micrograph (IV.5.3-2 c) represents the scale obtained during 1 hour oxidation at 800°, 1 hour annealing at 900° and 70 hours reoxidation; (IV.5.3-2 d) represents a scale obtained by 10

minute oxidation at 800°,1 hour annealing at 800° and reoxidation; micrograph (IV.5.3-2 e) represents a scale obtained by 3 hours oxidation at 800°, 1 hour annealing at 800° and reoxidation for 70 hours, and (IV.5.3-2 f) is the topographical aspect of the sample obtained by 20 minutes oxidation at 800°, 1 hour annealing at 800° and 90 hours reoxidation of pure nickel. In the continuous oxidation of less pure and pure nickel, the oxide is characterized by the presence of a cellular structure and by the existence of well defined individual grains, many of them being elongated in shape, especially on the pure nickel specimen. The maximum size of these oxide grains is 2 µm and 4 µm respectivelly. All the scales obtained during the oxidation interrupted by vacuum anneals present an outer surface constituted of very well defined faceted grains with regular geometrical shape. The grains are much larger than in the case of the scales obtained during continuous oxidation. The maximum grain sizes range between 3.4 and 5 µm. A pure nickel sample oxidized continuously for the very long period of 240 hours gave rise to an oxide scale characterized by large outer grains up to 4 µm in size. The features of the outer layer scale are illustrated by the micrographs in fig. (IV.5.3-3). This micrograph also illustrates the presence of very well defined oxide grains of different size which exhibit the commencement of faceting.

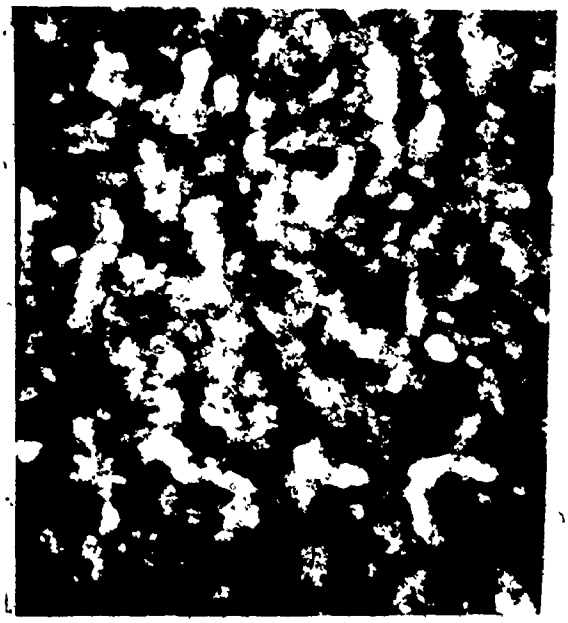

(x 3,400)

a

(x 2,500)

b

(x 3,500)

c

(x 3,500)

d

Fig. IV.5.3-2 a,b,c,d,e,f: Less pure nickel and pure nickel oxidized 70 hours at 800°: a. less pure nickel 70 hours continuous oxidation, b. pure nickel 70 hours continuous oxidation, c. less pure nickel 1 hour oxidation, 1 hour annealing at 900° and reoxidation, d. less pure nickel 10 minutes oxidation, 1 hour annealing at 800° and reoxidation, e. less pure nickel 3 hours oxidation, 1 hour annealing at 800° and reoxidation, f. pure nickel 20 minutes oxidation, 1 hour annealing at 800° and 90 hours reoxidation.

(x 3,500)

e

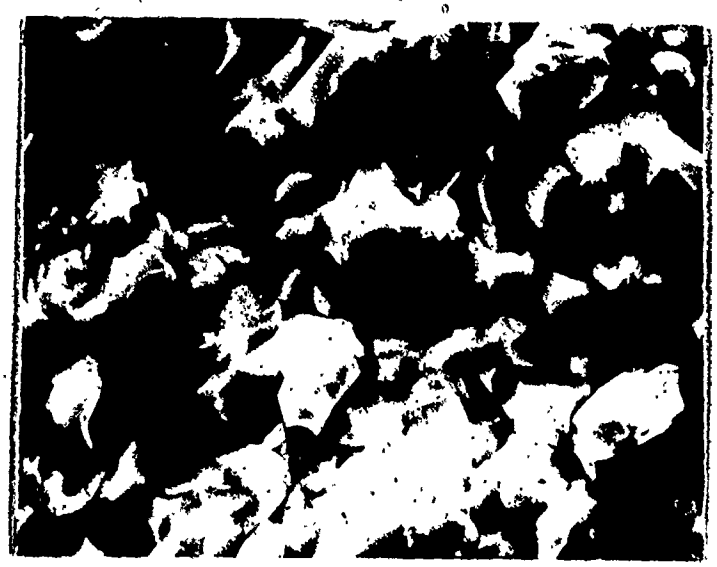

(x 5,000)

f

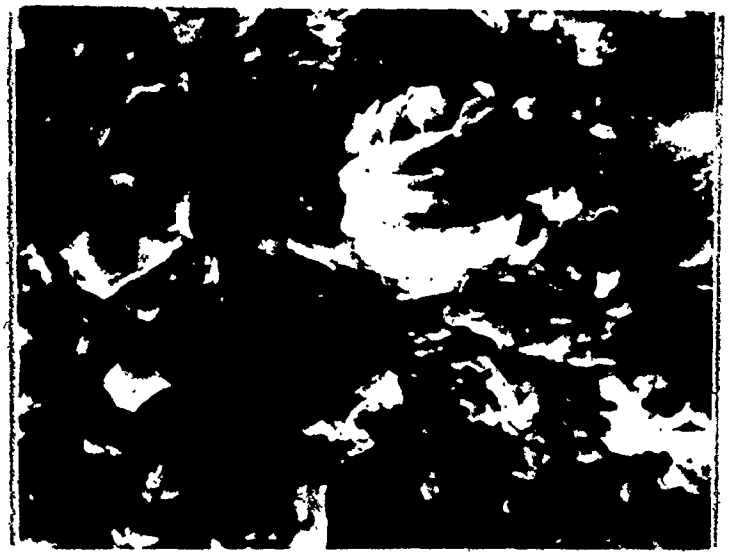

(x 5,000)

Fig. IV.5.3-3 Topographical view of pure nickel oxidized 240 hours at 800°.

### IV.5.4 Influence of Temperature on the Topographical Development of Nickel Oxide Scales

Experiments were carried out to determine if changing temperature influences the microstructure of nickel oxide obtained by continuous oxidation at 800°. Therefore the nickel specimen oxidized for 70 hours, which topographically is revealed by the micrograph in fig. (IV.5.3-2a), was reoxidized at 1000° for 30 hours. The outer surface of the scale is completely different in comparison to the surface of the scales obtained by continuous oxidation at 800°. There is some similarity only with the scale found during very long oxidation of 240 hours. The surface is completely faceted as is the surface of the oxide obtained during oxidation interrupted by vacuum annealing. Figure (IV.5.4-1a) represents the characteristics of the surface of this oxide. The oxide grains are much larger than those obtained by continuous oxidation reaching up to 10 μm. The surface of the grains seems to be concave or dished. The micrographs representing the outer surface of the oxide scale obtained by reoxidizing for 20 hours at 1000°, the nickel specimen oxidized 240 hours from fig. (IV.5.3-3) are presented in fig. (IV.5.4-1 b). The grains in this case were up to 11-12 μm in diameter. The surface of the nickel oxide scale is also characterized by well developed facets. One side of the nickel specimen used in this experiment was bare of oxide; thus this surface was only

(x 5,000)

a

(x 2,850)

b

(x 5,900)

c

Fig. IV.5.4-1 a,b,c
Influence of temperature on the topographical view of nickel oxide scale:

a. less pure nickel oxidized for 70 hours at 800° and reoxidized for 30 hours at 1000°,

b. pure nickel oxidized for 240 hours at 800° and reoxidized for 20 hours at 1000°,

c. Same as b but the micrograph presents the aspect of one bare side of the specimen oxidized only at 1000° for 20 hours.

oxidized for 20 hours at 1000° compared with the outer surface which was previously oxidized 240 hours at 800°. The topography of oxide formed on this bare surface is revealed by the micrographs in fig. (IV.5.4-1 c). The grain size, which reaches a diameter of 15 µm, is larger than the grain size of nickel oxide obtained by oxidizing pure nickel for 240 hours at 800° and reoxidizing for 20 hours at 1000°.

All these micrographs demonstrate that the "cellular" structure of the oxide formed at early stages of oxidation at 800° is transformed into a fine grained oxide at longer time due to a grain growth process. Subsequent oxidation at 1000° leads to development of coarse faceted grains due to enhanced grain growth process.

## IV.6 MICROSTRUCTURE OF THE NICKEL OXIDE SCALE: SCANNING ELECTRON MICROSCOPY OF CROSS SECTIONS AND FRACTURED SCALES

To understand the formation of the single or duplex nickel oxide scales obtained under the experimental conditions above described, the chronological development of the scales from early stage of oxidation up to 240 hours oxidation was followed by examining scale cross sections and fractured scales using scanning electron microscopy. It is suggested that discrepancies existing in the data reported in the literature are due to the lack of observations on the nickel oxide scale microstructures developed from the early stage of oxidation. Also discrepancies may have arisen from a lack of very careful

observation on the whole scale, especially in the case of polycrystalline nickel where the oxidation behaviour is an average of the behaviour of different metal grains characterized by different crystallographic orientations.

In attempts to understand the formation of the duplex scale, some observations were carried out of the scale formed at very early stages of oxidation within 10 minutes. Difficulties were encountered because the oxide less than 1 μm thick could not be successfully chemically etched to reveal the microstructure; also, nickel oxide was too adherent to nickel to be mechanically fractured. To observe the configuration of such a thin film, oxidized nickel specimens were bent several times until some oxide spalled; the microstructure of the retained oxide would then possibly be revealed under high SEM magnification upon tilting the specimen at different angles relative to the electron beam.

### IV.6.1 Microstructure of the Nickel Oxide Scale Obtained at Early Stages of Oxidation

To follow the formation of a duplex scale on less pure and pure nickel oxidized during a continuous oxidation experiment or oxidation interrupted by vacuum anneals at 800° for periods of 10, 20, 60 and 120 minutes, specimens were examined by scanning electron microscopy after cold mounting in resin and by fracturing the scale. Thus the micrographs in fig. (IV.6.1-1 a,b) represent features of nickel oxide obtained by 5 minutes continuous oxidation of pure nickel at 800°.

(x 9,400)

a

(x 9,400)

b

Fig. IV.6.1-1 a,b. Nickel oxide scale formed on pure nickel oxidized for 5 minutes at 800°. Fractured sample.

Despite the technical difficulties related to the small thickness of the oxide, it is possible to observe some common features. The scale consists of either one layer with elongated or equiaxed grains and another section of the scale appears to be formed of two layers. The micrographs in fig. (IV.6.1-2 a to g) represent features of the scale obtained by oxidation of less pure nickel and pure nickel for 20 minutes, 1 hour and 2 hours. All these micrographs indicate the presence of a duplex scale resulting from an inner equiaxed layer and a columnar outer layer. Micrographs from scale sections that are mainly equiaxed are given in figs. (IV.6.1-2 a,c and e). All these micrographs indicate as a general feature, the existence of the duplex scale even in the early stages of oxidation. It is also obvious that the thickness of a scale, the thickness of the inner and of the outer layer and the sizes of the grains in the outer layer differ within different cross sections of the scale obtained on the same nickel specimen. These features result from the influence of the grain structure of the nickel specimen.

The interface of separation between the inner and outer oxide layers becomes very precise at 2 hours of continuous oxidation. Despite the difference in various sections of the same scale, it is apparent that the outer layer becomes more columnar with increasing time of oxidation.

(x 6,000)

a

(x 8,400)

b

(x 9,100)

c

(x 11,000)

d

Fig. IV.6.1-2 a,b,c,d,e,f,g : Nickel oxide scale formed on less pure and pure nickel at 800°: a. and b. etched cross-sections of a less pure nickel oxidized for 20 minutes, c. and d. etched cross.section and fractured scale obtained by oxidation of less pure nickel for 1 hour, e. etched cross section of a pure nickel oxidized for one hour and f and g etched cross sections of less pure nickel oxidized for 2 hours.

(x 12,000)

e

(x 8,400)

f

(x 8,400)

g

Micrographs (IV.6.1-3 a, b,c,d,e) illusrtated features of the oxide scales obtained by oxidation followed by vacuum anneals. (IV.6.1-3 a) represents a cross section of the scale obtained on pure nickel by 5 minutes oxidation and 4 hours annealing at 800°. It is obvious that during this annealing period the scale appears more columnar. The micrographs of (IV.6.1-3 b and c) illustrate the etched cross sections of a scale obtained on less pure nickel by 20 minutes oxidation followed by 1 hour annealing at 900°. Some part of the scale is quite columnar (IV.6.1-3 b) while the other part of the scale is a double layer. Micrographs (IV.6.1-3 d and e) illustrate an etched cross section and a fractured scale obtained on less pure nickel by 1 hour oxidation followed by 1 hour vacuum anneal at 800°. Micrographs (IV.6.1-3 f) represent the cross sections of an etched scale on less pure nickel obtained by 1 hour oxidation at 800° and 1 hour annealing at 900°. These micrographs also demonstrate that as a result of annealing the interface between the two layers becomes sharper and that the grains of the outer layer become larger. The outer layer, moreover, transforms in some parts of the scale to a columnar structure only, as illustrated in micrographs (IV.6.1-3 a and b). It should also be emphasized that all micrographs illustrate an uneven thickness of the scale obtained under the same oxidation condition as a result of

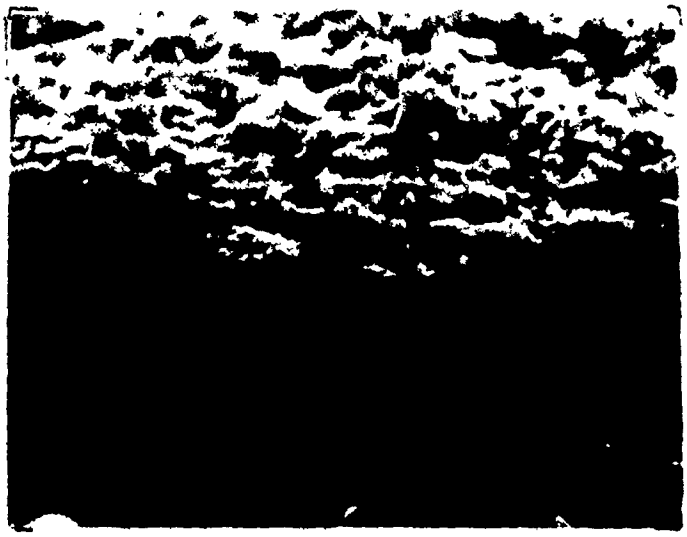

(x 9,000)

a

(x 6,700)

b

(x 18,200)

c

Fig. IV.6.1-3 a,b,c,d,e,f,g,h. Nickel oxide scale obtained at 800° by oxidation followed by vacuum anneals: a. fractured scale of nickel oxide obtained on pure nickel by 5 minutes oxidation and 4 hours annealing, b. and c. etched cross section of the scale obtained on less pure nickel by 20 minutes oxidation and 1 hour annealing at 900°, d. and e. etched cross section and fracture of the scale obtained on less pure nickel by 1 hour annealing at 800°, f. etched cross section of a scale obtained on less pure nickel oxidized for 1 hour and annealed for 1 hour at 900°, g. and h. etched cross section of a scale obtained on less pure nickel by 20 minutes oxidation, 1 hour annealing at 900° and 1 hour and 40 minutes reoxidation.

(x 9,1oo)

d

(x 1o,ooo)

e

(x 8,4oo)

f

(x 9,1oo)

g

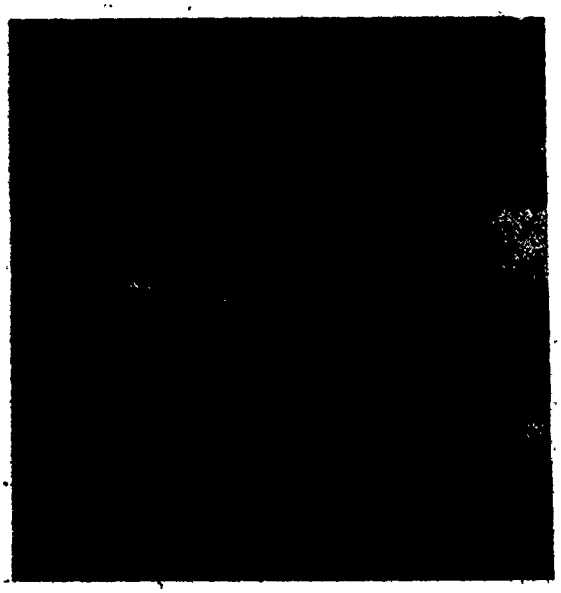

(x 9,1oo)

h

the influence of metal substrate orientation. The micrographs (IV.6.1-3 g and h) represent cross sections of the scale obtained by oxidizing less pure nickel for 20 minutes at 800°, annealing for 1 hour at 900° and reoxidizing for 1 hour and 40 minutes. Compared with the sample obtained during 2 hours of continuous oxidation, this scale exhibits a much more columnar outer layer and the interface between the two layers is sharper.

IV.6.2 Structure of Nickel Oxide Scales Obtained at Intermediate and Long Time Exposures: Cross Sections and Fractured Scales

Specimens obtained by oxidizing the less pure and pure nickel in continuous experiments and oxidation interrupted by vacuum anneals for longer periods of time up to 240 hours were examined to follow the morphological development of the nickel oxide scales. Thus micrograph (IV.6.2-1 a) represents an etched cross section of a scale obtained on less pure nickel by 70 hours continuous oxidation at 800°; micrograph (IV.6.2-1 b) represents an aspect of fractured scale obtained by 70 hours of oxidation of pure nickel at 800° and (IV.6.2-1 c) represents an etched cross section of the same scale. The micrographs (IV.6.2-1 a and c) illustrate the existence of the duplex layer with an outer layer characterized by long columnar grains. Due to the technical difficulties it was difficult

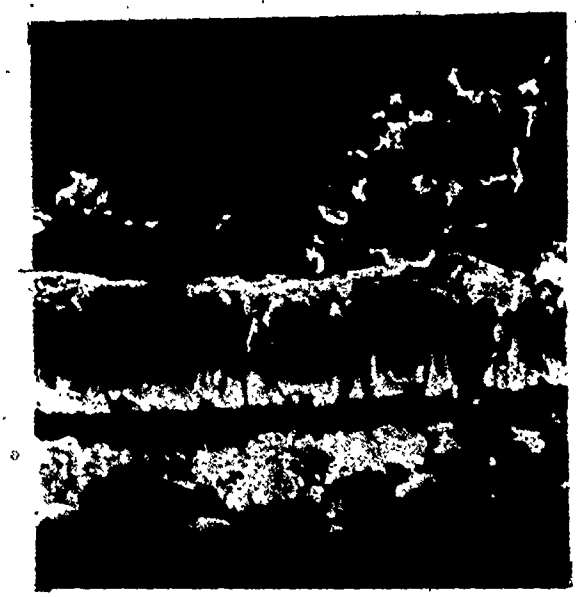

(x 5,200)

a

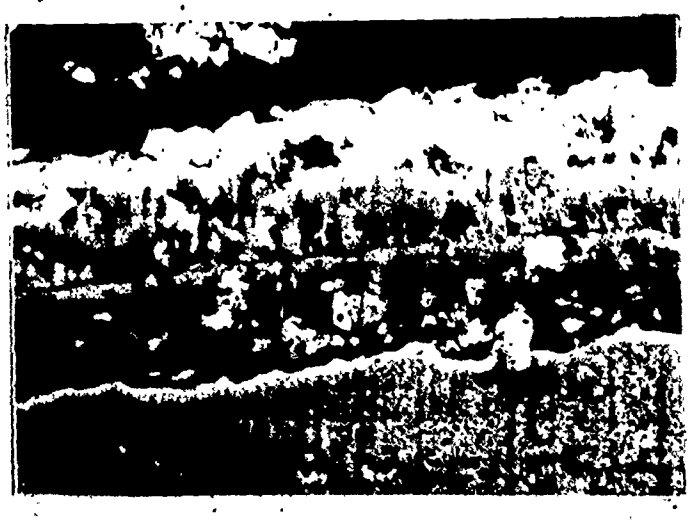

(x 3,000)

b

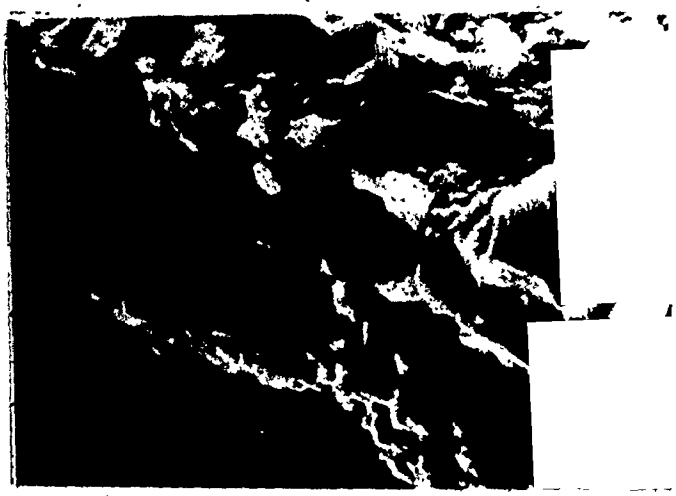

33°

(x 6,000)

c

Fig. IV.6.2-1 a,b,c: Nickel oxide scale obtained by oxidation of less pure and pure nickel at 800° for 70 hours. a. etched cross section of less pure nickel oxidized for 70 hours, b. and c. etched cross section and fractured nickel oxide obtained by oxidation of pure nickel at 800° for 70 hours.

to reveal the structure of the inner layer and to assign a size to its grains. The micrograph (IV.6.2-1 c) illustrates a scale section composed only of an equiaxed layer of nickel oxide.

The micrographs in figs. (IV.6.2-2 a, b and c) illustrate different features of the scale on pure nickel obtained by increasing the oxidation time to 240 hours. These micrographs should be compared with those previously given. All scale sections show that the outer layer has increased in thickness as a result of grain growth into the inner layer. This inner layer, as in micrographs (IV.6.2-2 a and b) is very small, approximately 1/4 or 1/5 of the outer layer thickness. In some sections of the scale, the inner layer is completely absent as in micrograph (IV.6.2-2 c). Several parts of the scale contain such a small number of equiaxed oxide grains so that it is difficult to consider the scale as having a duplex structure: micrograph (IV.6.2-2 a).

Observations made on fractured or etched cross sections of the scales obtained on less pure and pure nickel during oxidation experiments interrupted by vacuum anneals are illustrated in the following micrographs. Micrographs (IV.6.2-3 a and b) represent a fracture cross section of the scale obtained upon oxidizing less pure nickel for 3 hours followed by 1 hour annealing and 70 hours reoxidation at 800°.

(x 5,450)

a

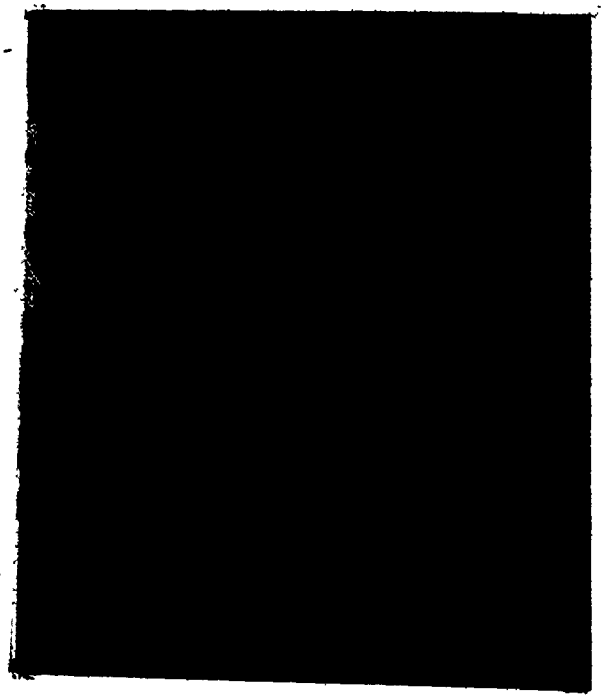

(x 2,950)

b

(x 11,000)

c

Fig. IV.6.2-2 a,b,c: Etched cross sections of a nickel oxide scale obtained by oxiation of pure nickel at 800° for 240 hours.

(x 4,5oo)

a

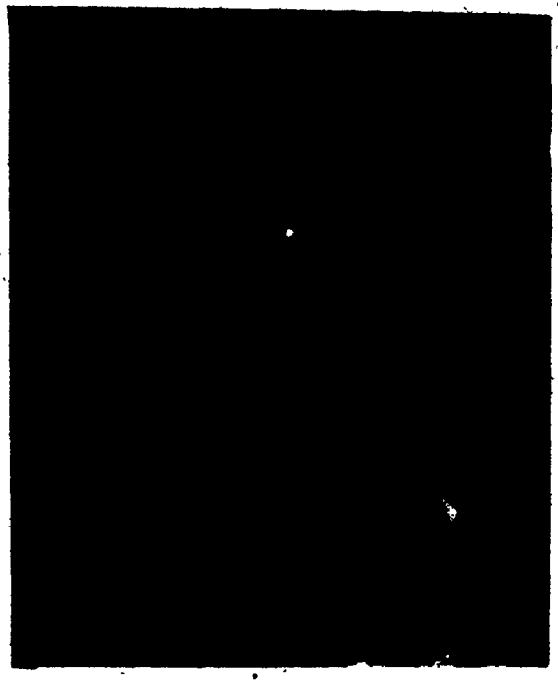

(x 4,5oo)

b

(x 4,1oo)

c

Fig. IV.6.2-3 a,b,c,d,e,f,g,h: Nickel oxide scale obtained by oxidation interrupted by vacuum anneals. a. and b. fractured nickel oxide scale obtained by oxidizing less pure nickel for 3 hours followed by 1 hour annealing and 7o hours reoxidation. c. fractured nickel oxide obtained by oxidizing less pure nickel for 2o minutes followed by two hours annealing at 8oo° and 7o hours reoxidation, d,e,f,g, etched cross sections of a scale obtained by 2o minutes oxidation of pure nickel, 1 hour ing at 8oo° 9o

(x 1,380)

d

(x 2,780)

e

(x 6,900)

f

(x 6,900)

g

Micrograph (IV.6.2-3 c) represents the same type of cross section of the scale on less pure nickel obtained during 20 minutes oxidation, 2 hours annealing and 70 hours reoxidation at 800°. Figs. (IV.6.2-3 d,e,f and g) represent different aspects of the etched cross section of a scale on pure nickel obtained by oxidizing for 20 minutes, annealing for 1 hour and reoxidizing for 90 hours at 800°. All these micrographs exhibit a common feature: the bilayer scale has been completely transformed in the majority of the scale into a single columnar layer. In micrographs (IV.6.2-3 c, f and g), it is possible to observe that the colmnar grains extend right from the metal surface all the way across the scale to the oxide-gas interface. There are some scale sections where the preferential growth of the oxide has proceeded more slowly leaving remnants of the inner layer, as on micrographs (IV.6.2-3 a and e).

### IV.6.3 Influence of Changing the Oxidation Temperature on the Nickel Oxide Scale Microstructure: Cross Sections and Fractured Scales

Micrographs (IV.6.3-1 a and b) represent two different parts of a fractured scale on less pure nickel obtained after reoxidation for 30 hours at 1000° of a specimen previously oxidized for 70 hours at 800°. (The scale obtained by continuous

(x 2,000)

a

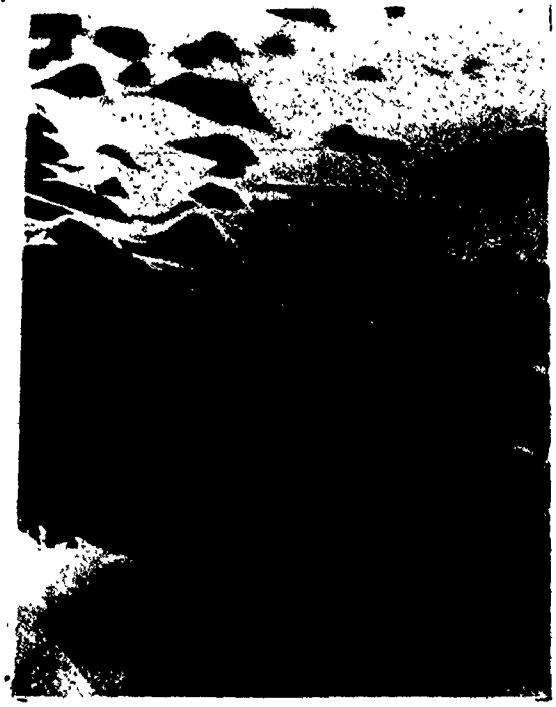

(x 2,000)

b

45°

(x 1,650)

c

(x 2,100)

d

Fig. IV.6.3-1 a,b,c,d: Influence of the temperature on the cross section of nickel oxide scales: a. and b. fractured scale of of nickel oxide obtained by oxidizing less pure nickel for 70 hours at 800° and reoxidized for 30 hours at 1000°, c.d. fractured and etched cross section of a sample obtained by oxidizing pure nickel for 240 hours at 800° and reoxidizing it for 20 hours at 1000°.

oxidation of less pure nickel for 70 hours at 800° is represented by micrograph (IV.6.2-1 a). It is obvious that reoxidation for 30 hours at 1000° causes the scale formed of two layers of oxide at 800°, to be completely transformed into a columnar scale. This transformation is brought about by the selective growth of the outer layer at the expense of the inner layer: micrographs (IV.6.3-1 a). In some other parts of the scale, micrographs (IV.6.3-1 b), the inner layer still exists due to slower grain growth. It is possible to observe that some of the columnar grains extend completely all the way from the metal surface up to the nickel oxide-gas interface: micrograph (IV.6.3-1 a).

The aspects of the scale on pure nickel obtained by reoxidizing for 20 hours at 1000°, the specimen oxidized for 240 hours at 800° are represented by the etched sections and fractured scales in micrographs (IV.6.3-1 c and d). These micrographs should be compared with those represented in micrographs (IV.6.2-2 a and b). Some parts of the scale are completely columnar extending from the metal to the oxide-gas interface.

In some other parts of the scale, very large diameter grains of an inner layer extend into the outer layer. Reoxidation at 1000° leads to oxide grains approximately twice as large in diameter as those initially obtained at 800°. After re-oxidation at 1000°, a distinct interface does not exist between the two layers. The scale is considered as formed from one layer characterized in some parts by a completely columnar layer, and in some other parts of a columnar layer formed from more than one grain extending across the thickness of the scale.

IV.6-4 Some Quantitative Results Obtained from Scanning Electron Microscopy Observations.

All the micrographs presented in the previous sections indicate that the structure of the nickel oxide scales obtained under different conditions is dependent upon the period of exposure, annealing and temperature of oxidation. Some attempts were made to interpret quantitatively these observations. It should be emphasized that many difficulties were encountered because of different factors affecting the results: 1) in the early stage of oxidation, it is difficult to assign a size to oxide grains of cellular structure from topological observations, 2) the thickness and size of the grains are difficult to measure because the high magnifications required to take pictures leads to poor focus, 3) at large thickness of the scale, the time of electroetching required to reveal microstructures also leads to attack of the resin mount and

hence poor resolution of observations. Besides these experimental factors, it should be taken into consideration that polycrystalline nickel samples were used for the experiments. Therefore each sample obtained under a set of experimental conditions presents different aspects that vary over regions of the sample as a result of the anisotropic properties of the oxidation process. To avoid these difficulties, each sample was investigated by taking many micrographs from which only representative examples were presented in the previous sections. Also several sections were taken of each sample. To give a quantitative interpretation to these observations, all the micrographs obtained in this investigation were used in order to obtain average values for calculations.

The results obtained in this manner are represented by the following graphs: IV.6.4-1, IV.6.4-2; IV.6.4-3 and IV.6.4-4. In fig. IV.6.4-1, the measurements of the total scale thickness, of outer and of the inner layer thickness, are given as a function of time in hours for the oxidation of pure nickel. It is obvious that variation of outer layer thickness is similar to that of the total layer thickness. The inner layer thickness shows only a small variation in thickness after the early oxidation stage but it decreases to practically zero upon changing the temperature of oxidation to 1000°.

The ratio of the thickness of the outer to inner layers is represented against oxidation time in fig. IV.6.4-2

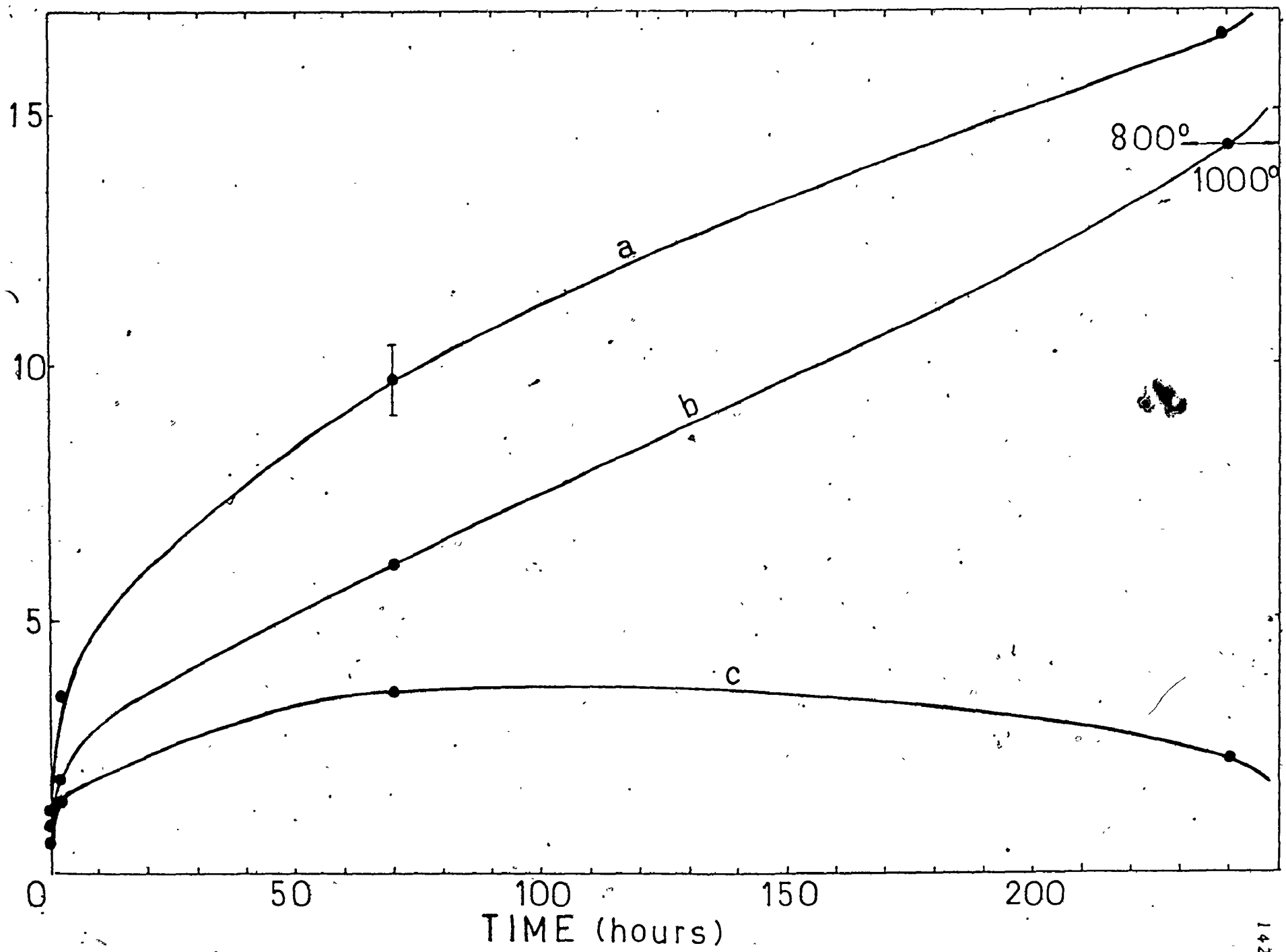


Fig.IV.6.4-1 Average oxide thickness versus time for oxidation of pure nickel.

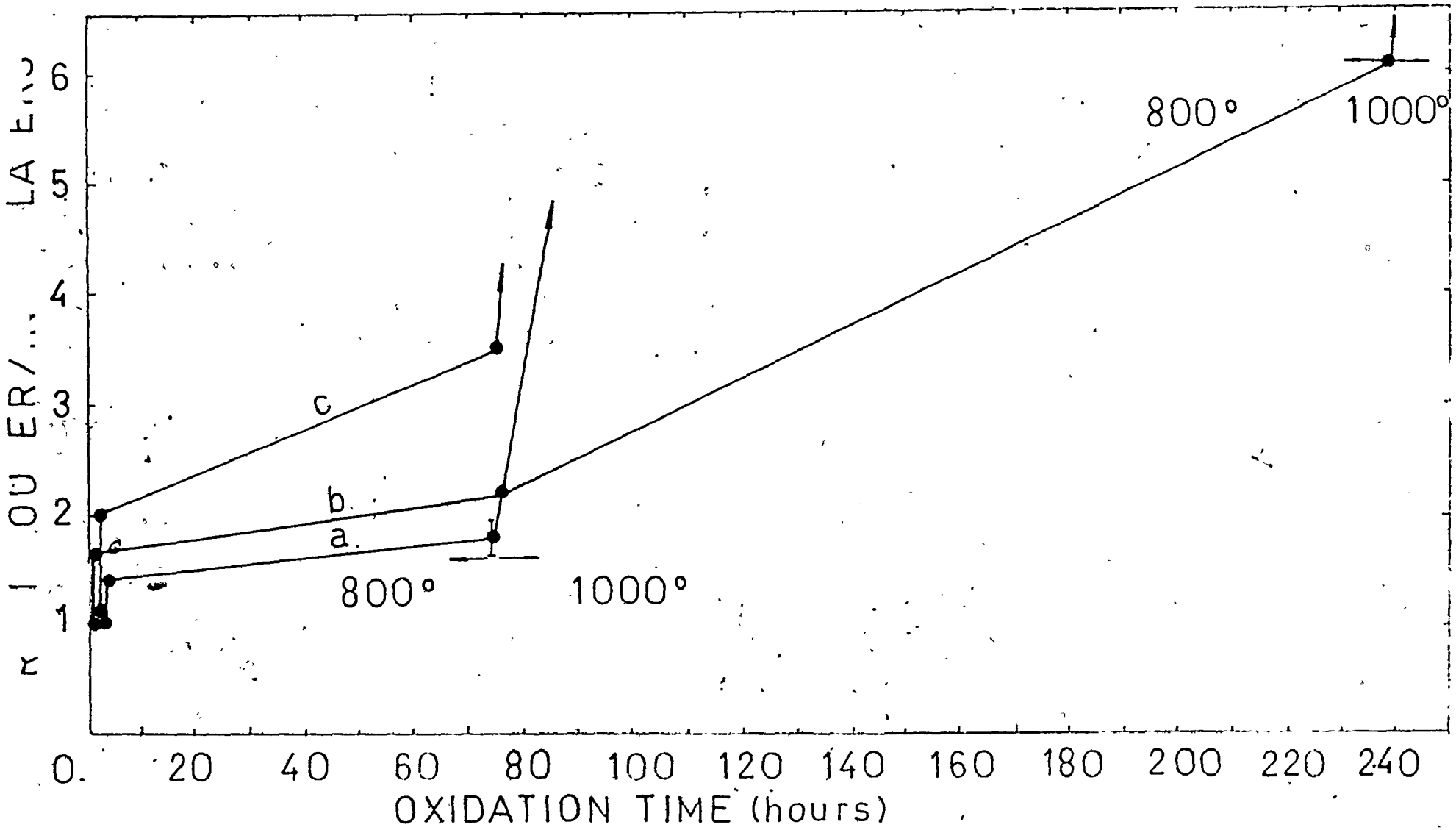


Fig.IV.6.4-2 Average ratio outer/inner layer versus time:
a: less pure nickel b: pure nickel
c: less pure nickel (oxidation interrupted by vacuum anneal.

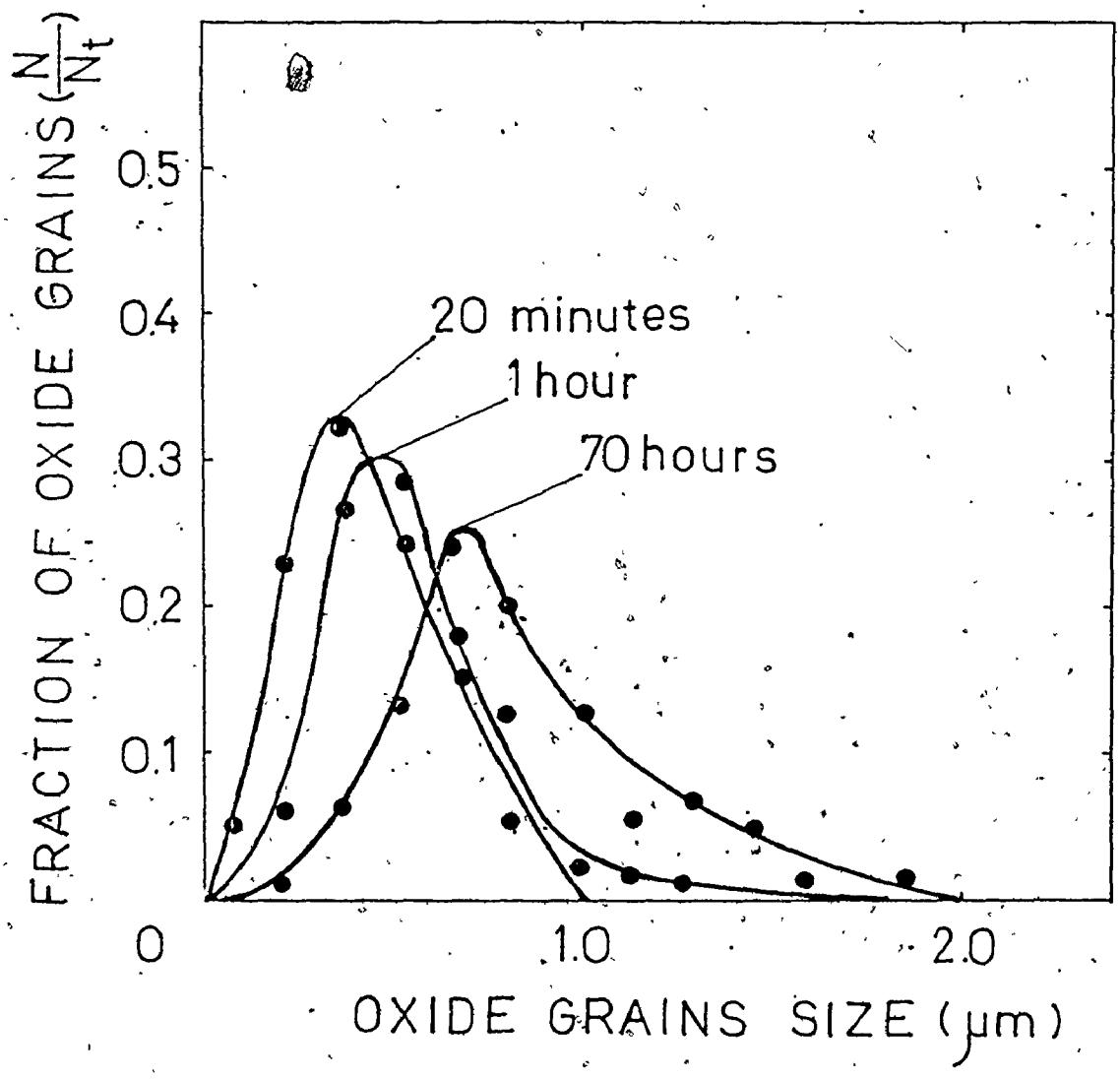


Fig. IV.6.4-3 Grain size distribution of nickel oxide formed on less pure nickel.

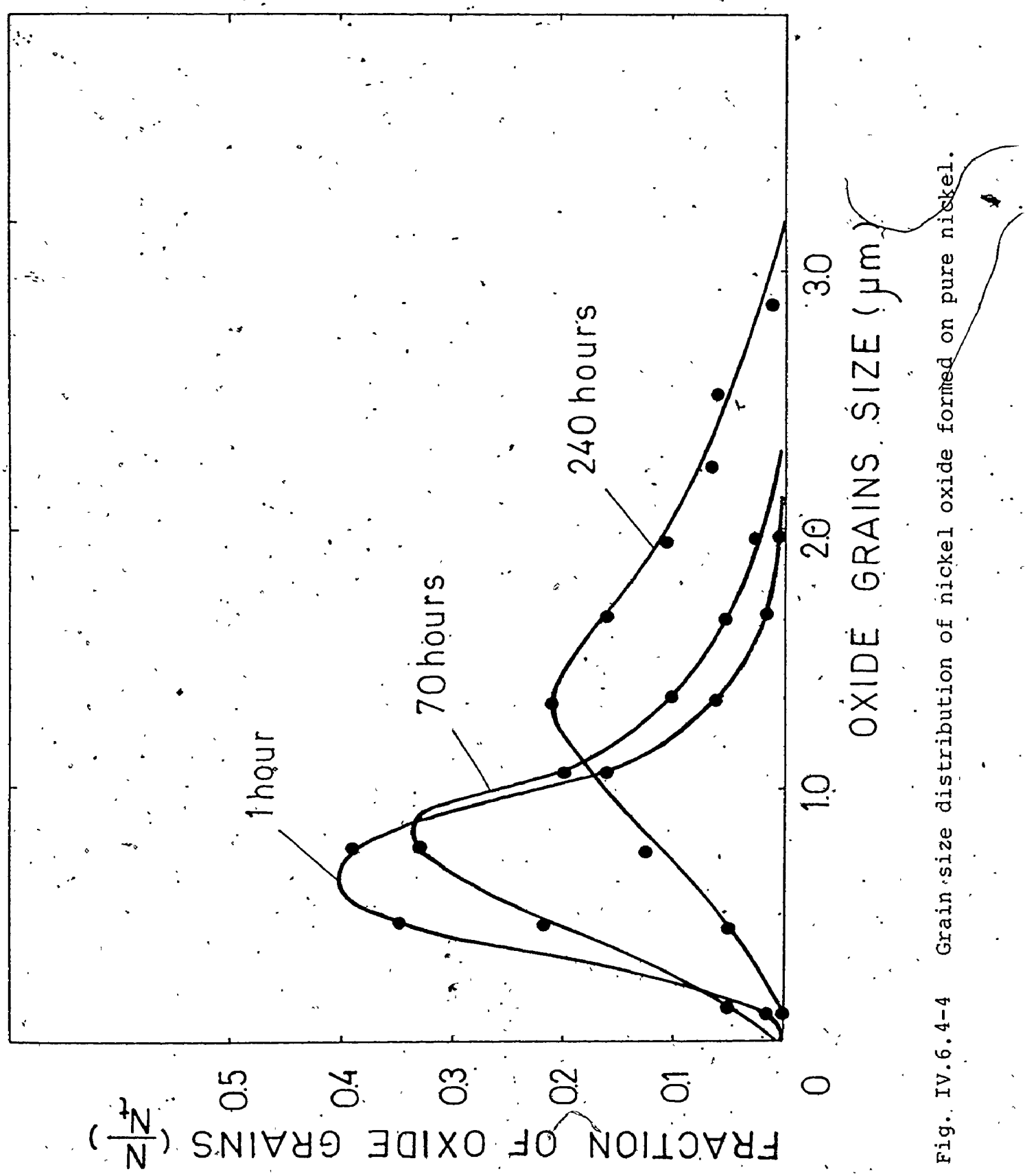


Fig. IV.6.4-4 Grain size distribution of nickel oxide formed on pure nickel.

a and b for less pure and for pure nickel continuously oxidized at 800° and 1000° and c for the scale obtained by oxidation interrupted by vacuum anneals of less pure nickel. This ratio increases with oxidation time. It increases still more when the temperature is changed from 800° to 1000° and also during the oxidation interrupted by anneals.

Figures (IV.6.4-3) and (IV.6.4-4) represent the size distribution of the grains in the outer layer of the nickel oxide scale on less pure and pure nickel obtained during continuous oxidation at 800°. The grain size in the outer oxide layer for both types of nickel increases with oxidation time. In the case of the oxide obtained during the experiments interrupted by vacuum anneals, the grains of the outer layers reach an average of 1.3 - 1.5 μm. During reoxidation at 1000° of the scale formed at 800°, the grain size of the outer layer attains 3 μm.

# CHAPTER V

# DISCUSSION

## V.1 INTRODUCTION

In the attempt to explain the formation of the duplex structure of the nickel oxide scale, an experimental investigation was carried out regarding the kinetics behaviour and the structural characteristics of the oxide scale formed during continuous oxidation and oxidation interrupted by vacuum anneals. The experimental results obtained were reported in the previous chapter. All these results indicated that there are some differences in the behaviour of the two types of nickel specimens from kinetics, texture and structure of scale points of view. It is the purpose of this chapter to explain these differences, relating them to the properties of nickel metal, to advance a model for the development of the duplex structure of nickel oxide scale based on the diffusion of nickel through lattice of nickel oxide and through the short circuit diffusion paths offered by the structure of the oxide and on structural changes occurring in this scale in time. The results obtained for grain growth of the oxide are used to calculate the contribution of grain boundary diffusion to the total transport of nickel during oxidation. The morphological development of the duplex

nickel oxide scale at 800° followed experimentally by sequences of cross sectioned scales and fractured samples will be discussed from the point of view of the possibilities of transforming this scale into a single layer scale. The results obtained during this investigation are also used to explain some of the controversial data reported in the literature regarding the duplex layer structure of the nickel oxide scale.

## V.2 OXIDATION KINETICS

The oxidation of nickel at temperatures exceeding 900° follows the model of parabolic oxidation developed by Wagner:

$$K_r(\text{eg/cm.sec}) = \bar{C}_{eq} \int_{a_0'}^{a_0''} D^*_{Ni} \cdot d/na_0 \qquad (V.2\text{-}1)$$

where the symbols have the meaning given in Chapter II.
A nonparabolic behaviour below 900° is a general feature of nickel oxidation kinetics as reported by different authors[10,32,63] and interpreted as reviewed in Chapter II.

The results obtained in this investigation by continuous oxidation of a less pure nickel and pure nickel at 800° and an oxygen pressure of 400 Torr were represented in figs. (IV.3-1 a,b,) as $\frac{\Delta\omega}{A}$ versus reaction time in minutes. These results illustrate that pure nickel oxidizes faster than does less pure nickel. At least this is a situation for the first hours of oxidation because the effective rate constant of oxidation calculated from the tangents to the parabolic plots in fig. (IV.3-2 a,b) of Chapter IV decreases in time slower in the case of less pure nickel than pure nickel.

The calculated effective parabolic rate constant of oxidation based on fig. (IV.3.2 a,b) are given in the following two tables:

Table V.2-1

Parabolic rate constant of oxidation: less pure nickel

| Time of oxidation (min) | 20 | 30 | 60 | 120 | 180 | 360 | 600 | 800 |
|---|---|---|---|---|---|---|---|---|
| $k_p$ $(mg^2.cm^{-4}.min^{-1})$ $\times 10^{+3}$ | 4.00 | 2.50 | 1.60 | 1.16 | 1.03 | 0.79 | 0.68 | |

Table V.2-2

Parabolic rate constant of oxidation: pure nickel

| Time of oxidation (min) | 20 | 30 | 60 | 120 | 180 | 340 | 400 |
|---|---|---|---|---|---|---|---|
| $k_p$ $(mg^2.cm^{-4}.min^{-1})$ $\times 10^{+3}$ | 7.00 | 3.10 | 2.50 | 1.90 | 1.64 | 1.13 | 0.86 |

Despite iron and cobalt impurities existent in less pure nickel, that could dope nickel oxide making it oxidize faster than pure nickel, this latter metal oxidized somewhat faster. This anomally can be explained by the different textures of the two types of nickel that influence the preferred orientation developed in the nickel oxide scale. If nickel oxide formed on pure nickel exhibits a preferred orientation characterized by the presence of high angle boundaries between the oxide crystallites, the oxidation rate will be enhanced. A comparison of the oxidation of the two types of nickel may result from a balance between the impurities content effect and the preferred orienta-

tion of the nickel and of the oxide scale, respectively. Cathcart et al.[70] working on nickel single crystals have found that there are differences in the oxidation rates of (111) and (100) planes of nickel. The oxide formed on the (100) nickel face contained a larger density of incoherent grain boundaries; this structure of the oxide, therefore, offered more short circuit diffusion paths for nickel transport through the oxide scale than in the case of the scale formed on the (111) nickel faces. Regarding this aspect of metal oxidation kinetics, some discrepancies existent in literature can be explained based on the texture characterization of the polycrystalline nickel used and/or the preferred orientation of the oxide. As an example, Phillips[71] reported that less pure nickel oxidizes faster than pure nickel between 700 and 1300°. Opposite to these experimental results, Gulbransen and Andrews[72] have found that the oxidation resistence of pure nickel at 750° was approximately the same as less pure nickel.

The attempts of assigning a value to m from formula

$$\left(\frac{\Delta m}{A}\right)^m = kt$$

by a double logarithmic plot ($\log \frac{\Delta m}{A}$ versus $\log t$) did not give any better representation of the results. Tables (V.2-1) and (V.2-2) and figures (IV.3-2 a) and (IV.3-2 b) from Chapter IV indicate that during oxidation of polycrystalline nickel at 800°, changes in the oxidation behaviour take place in time due to a change in the structure of the oxide scale formed. If these rate

changes are related to structural changes of the oxide scale, the decrease in time of effective parabolic oxidation rate constants, $k_p$, are to be explained by alterations in the orientation of the oxide grains and by a decreasing amount of grain boundaries available for nickel transport. Therefore the lower $k_p$ values during the oxidation of less pure nickel result from a slower rate of grain growth, and/or by the formation of an oxide that changes orientation in time.

The formation of an oxide scale rich in short diffusion paths that remain at constant density for the initial period of oxidation (approximately 20 minutes) account for the parabolic aspect of the curves in figs. (IV.3-1a) and (IV.3-1b) and also for the high values of the effective parabolic oxidation rate constants in comparison to the parabolic rational oxidation rate constant calculated from eqn. (V.2-1) using the self-diffusion coefficients of nickel. For comparison these values are given in Table (V.2-3).

Table V.2-3

Parabolic rate constant of oxidation of nickel (20 minutes)

| | |
|---|---|
| $k_p$ (less pure nickel) | $0.66\times10^{-10}$ $g^2$ $cm^{-4}$ $sec^{-1}$ |
| $k_p$ (pure nickel) | $1.1\times10^{-10}$ $g^2$ $cm^{-4}$ $sec^{-1}$ |
| $k_L$ (Wagner model) | $1.78\times10^{-14}$ $g^2$ $cm^{-4}$ $sec^{-1}$ |

To correlate the oxidation kinetics with the structural changes in the oxide, changing the "permeability" of the oxide to the reactants, the results obtained during oxidation interrupted by vacuum anneals at 800° of the two types of nickel were presented in figs. (IV.3-4), (IV.3-5), (IV.3-6) and (IV.3-7) and Tables (IV.3-5) and (IV.3-6). These results have common features. The oxidation curves are composed of two linear regions representing parabolic behaviour characterized by different oxidation rate constants, $k_p$, for oxidation before annealing and for oxidation after the oxide was vacuum annealed. All rate constants after annealing are smaller in value than those before annealing because the number of grain boundaries available for nickel transport was decreased by growth of the oxide crystallites.

Regarding the influence of the annealing conditions on the rate of oxidation, the following conclusions could be formulated from the experimental results. It is possible to remark that after 3 hours initial oxidation the effect of annealing on oxidation was very small. This signifies that the oxide aged to a large degree during this period. The effect of annealing on the oxide obtained during 20 minutes of oxidation was much stronger in decreasing the "permeability" of the oxide and resulting in much smaller oxidation rate. A different behaviour was exhibited by the oxide annealed after 10 minutes of oxidation. The effect was smaller than expected

in this case, as shown in fig. (IV.3-6). This unusual behaviour possibly results from thinning of the oxide film during vacuum annealing. Khoi et.al. [38] have shown that the air formed film on nickel single crystals is removed by vacuum anneals at 800°. They concluded that this behaviour was associated with oxygen dissolution from the oxide into metal. These vacuum anneals of the relatively thin oxide films during 10 minutes possibly decreases the action of the film as an effective diffusion barrier by decreasing its thickness. An increased time of annealing more effectively decreased the subsequent oxidation rate as shown in Table (IV.3-5). The relative rate constant of 6.8 obtained after 20 hours annealing of the oxide scale grown during one hour exposure should be compared with the value of the relative rate constant obtained during continuous oxidation of less pure nickel.

A strong effect on the subsequent rate of oxidation occurred upon increasing the annealing temperature. This could be seen from the values of 5.2 and 7.2 for the relative rate constants of oxidation that characterize oxidation for 1 hour, and 20 minutes initial oxidation, 1 hour annealing at 900° and reoxidation respectively. These results confirm those obtained by Perrow [63], that higher temperatures of oxidation increases the growth rate of crystallites in the oxide.

The experimental results regarding the oxidation of pure nickel, interrupted by vacuum anneals, indicated also that annealing decreases the rate of subsequent oxidation but its effect is less important than in the case of less pure nickel. To exemplify this difference the relative ratio of oxidation rate constants obtained under the same oxidation conditions for the two types of nickel are represented in Table V.2-4.

Table V.2-4

Comparison between kinetic behaviour of less pure and pure nickel during the oxidation interrupted by vacuum anneals at 900°

| Type of Experiment | Type of Nickel | $k_1/k_2$ |
|---|---|---|
| 1. Continuous oxidation | Less pure | 1.6 |
| 2. 20 minutes oxidation<br>1 hour annealing at 900°<br>Reoxidation | Less pure | 7.2 |
| 3. Continuous oxidation | Pure | 2.2 |
| 4. 20 minute oxidation<br>1 hour annealing at 900°<br>Reoxidation | Pure | 4.2 |

These findings suggest that the different preferred orientations of the oxide scales on the two types of nickel offer different degrees of nickel transport by short circuit diffusion and, also, that impurities in less pure nickel upon incorporation into the oxide retard grain growth. The annealing at high temperatures could possibly free the grain boundaries and lead

to faster growth of the oxide crystallites on less pure nickel, explaining the larger relative rate constants after annealing in comparison to the case of pure nickel.

The results discussed in this section are consistent with the conclusion that annealing of the oxide decreases the subsequent oxidation rate by having the same effect on the oxide as long time of exposure during continuous oxidation. Therefore the "loss in permeability" or changes in the oxide scale structure is due at least in part to the increase in oxide grain size.

## V.3 TEXTURE DEVELOPMENT OF THE NICKEL OXIDE SCALES

To characterize the scale textures the results of X-ray diffraction measurements were presented in figures (IV.4-1) to (IV.4-4) of Chapter IV. The X-ray recordings have shown that for oxide of 1 μm thickness there is no appreciable shift in the position of the diffracted peak. This was also confirmed by the results of Cathcart and Sartell and Li [90,53] related to the diffraction of nickel oxide obtained during nickel oxidation. Also the broadening due to the crystallite size as given by formula:[73]:

$$t = \frac{.9\lambda}{B\cos\theta} \qquad (V.3\text{-}1)$$

where t is the crystallite width, $\lambda$ is the wavelength of X-ray beam, $\theta$ is the Bragg angle and B is the width at half peak height, is negligible for the cases when t = 1000 Å. To repre-

sent the texture development, the texture coefficient of different planes versus oxidation time were plotted. This type of representation is suitable for following the chronological development of the nickel oxide scale on polycrystalline nickel since the nickel oxide thickness is an average value of different thicknesses of oxide formed on different metallic grains. Actually the oxide is relatively uniform in thickness because most X-ray results were obtained from thick scales.

Our experimental results demonstrated that the oxide scales are characterized by a preferred orientation that changes in time. This preferred orientation also depends on the nickel specimens and/or the type of experiment involving continuous oxidation or oxidation interrupted by vacuum anneals. The results reported in the literature as reviewed in Chapter II are mainly related either to the oxide orientations in the thin film range or to the scale formed on single crystal specimens. Gulbransen[44] observed preferred orientation in films formed on polycrystalline nickel above 500° as a result of a preferential growth process in the initial polycrystalline films. At higher temperature, in general at temperatures in the range 1000°-1200°, the few studies existent[45,47,74] indicate the formation of thick scales with a preferred orientation such that <100> NiO is parallel to the growth direction of the oxide. These observations are different than those of Perrow et al[63] on scales formed at 500-600° which indicate a development of a <110> fiber texture by recrystallization and growth

of the oxide nuclei. Regarding the results of Baur et al.[47] it is possible to realize upon careful examination of the authors' X-ray recordings (that their estimate of random orientation of nickel oxide formed at 850° and $p_{O_2}$ = 1 atm is actually a too gross simplification. Comparing their recordings with the ASTM intensity of nickel oxide lines, it is readily observed that the recorded (111) and (200) peaks have the same intensity as polycrystalline oxide but that the (220) peak has a higher intensity. To facilitate a comparison, we should mention that the (111) line of nickel oxide in the ASTM index has 90% relative intensity, (200) has 100% and (220) has a 57% relative intensity. Accordingly, the oxide scale is oriented on the (110) plane as also found by Perrow et al.[23].

To analyze our texture results, it is necessary to realize that the less pure and pure nickel specimens exhibit different preferred orientations. The less pure nickel exhibits a preferred orientation characterized by a texture coefficient of $P_{\{111\}}$=4.30 and very slightly on the (331) plane with the coefficient $P_{(331)}$ = 1 (Table IV.2-2). During continuous oxidation, the scales formed are characterized by an increasing texture coefficient of {111} planes up to 20 hours oxidation. After 20 hours oxidation, $P_{\{111\}}$ = 4.60. Following this stage there is a slight decrease in orientation on {111} family of planes with increasing exposure to oxygen, Fig. (IV.4-1) . This signifies that the oxide at the beginning of the reaction is predominantly characterized by a <111> texture. As oxidation

proceeds, (110) and (331) preferred orientations also appear. The texture coefficients of these planes become $P_{(110)} = 1.33$ and $P_{(331)} = 1.2$ after 70 hours of oxidation. These results demonstrate that the oxide tends to maintain a parallel orientation with the major {111} orientation of the metal surface and, moreover, that structural changes in the oxide lead to additional orientation of (110) and (331) oxide parallel to the metal surface.

Results are given in figure (IV.4-2) of previous chapter for the texture coefficients of the scales on oxidized specimens subjected to anneals and also to reoxidation. Those treatments lead to {111} planes of nickel oxide being maintained as a major orientation but the (110) and (311) orientations are less pronounced. There is, however, an increasing texture coefficient for the {100} orientations of nickel oxide resulting under these experimental conditions. It thus appears that the {111}, (311) and (110) oxide orientations are maintained in both continuous oxidation and oxidation interrupted by anneals; the (100) oxide orientation only appeared after anneals.

The pure nickel exhibits preferred orientations on {100} planes characterized by a texture coefficient $P_{\{100\}} = 4$ and very slightly on the (311) plane with $P_{(311)} = 1.2$. The continuous experiments indicate that the initial oxide is characterized by the existence of slight orientation on {111} planes and less on (110), (331) and (422) planes, fig. (IV.4-3).

These orientations agree completely with those results obtained on (100) nickel crystal face at short exposure[10]. Longer exposure and changing the temperature from 800° to 1000° lead to an increasing preferred orientation based upon (110), (331) and (211) oxide orientations. These orientations possibly represent both recrystallization and preferred grain growth because the major orientations of the metal surface are absent. The results from the oxidation experiments interrupted by anneals (fig. (IV.4-4)) also demonstrate that the (110) and (331) oxide orientations become much more preferred. A comparison of the results in figs. (IV.4-3) and (IV.4-4) also illustrates that vacuum anneals develop oxide texturing more rapidly than by continuous oxidation. These high orientations of the oxide on (110) plane could also explain the higher rate of oxidation on pure nickel. On oxidation of polycrystalline nickel, Perrow et al[23] found that the thicker part of the oxide scale was that characterized by an (110) oxide.

Therefore the major textures of the oxide scales on the less pure and pure nickels are the {111} and (110) orientations, respectively. Pure nickel oxidized at a rate more rapid than the less pure nickel even though the average grain size on this latter metal is slightly smaller, fig. (IV.2-3) . These findings suggest

that the (110) oxide orientation contains a larger density of incoherent boundaries permitting more rapid boundary diffusion of nickel. Confirmation for this suggestion is found from the transmission electron microscopy results of Perrow et al.[23] These investigators found that oxide film sections of (110) oriented oxide were thicker than those film sections exhibiting (111) orientation.

## V.4 STRUCTURAL DEVELOPMENT OF NICKEL OXIDE SCALE AT 800°

### V.4.1 Early Stages of Oxidation

Results were presented in the last chapter to demonstrate the morphological aspects of the outer surfaces of the nickel oxide scale based upon sequences of cross sections and fractured samples of the specimens obtained during continuous oxidation and during oxidation interrupted by vacuum anneals. A correlation is now presented on the development of the oxide scale with the metal properties by considering the role played by the oxide formed on the metal surface in early stages of the oxidation on the further development of the scale. General aspects of the specimens oxidized at 1000° and 800° and low pressure of oxygen, as presented in micrographs IV.5-1-1 to IV.5.1-3, will be discussed in this subsection.

The topographical views of the specimens oxidized at low oxygen pressure are important because they give information on two important aspects of oxidation: 1) the influence of temperature and oxygen pressures on the structure of the metal surface, and 2) the manner in which oxide growth on the metal surface is related to the metal structure.

Temperature influenced the metal grain size. The specimens oxidized at oxygen pressure of $5\times10^{-5}$ Torr and 1000° exhibited grains larger than the grains of specimens oxidized at 800°. The distribution curves for the grain size in each of the above specimens are represented in figs.(IV.2-3b) (IV.2-3c). These curves show that in the case of the specimen oxidized at 1000° the mean grain size is 170 μm, and in the case of the specimen oxidized at 800° the mean size is approximately 100 μm. Also the maximum grain size is approximately 500 μm in the case of the experiment at 1000° and it is approximately 300 μm in the experiment at 800°.

The specimen oxidized at 1000° and oxygen pressure of $5\times10^{-5}$ Torr exhibited thermal faceting. Since the metal is polycrystalline, the differently oriented grains represented different stages of this process. These situations, as revealed in the previous chapter, can be classified as:

1. a faceted surface completely free of isolated oxide growths,
2. a metal surface faceted or striated and accompanied by the presence of isolated oxide growth,
3. a specimen surface characterized by the coalescence of

oxide crystals that are aligned at relatively large density along metal striations,

4. a special situation occurs at the metal grain boundaries, especially at the twin boundaries.

These situations could be compared with those represented by Moreau and Bénard[75] on the oxidation of nickel-chromium alloys at high temperature. In their work selective oxidation led to formation of chromium oxide while in our case oxidation of pure nickel gives directly the influence of the orientation of the metal grains on oxide growth. The grains representing the first situation are characterized by a marked increase in surface relief caused by the formation of sharp surface striations. These striations result from "thermal etching" which has been reported by various authors for pure metals and alloys, but not on pure nickel to our knowledge[76,77,78].

There is no unified theory to explain this etching process but it is generally believed to be related to the presence of oxygen as an adsorbed or a thin oxide film on the metal surface modifying its equilibrium configuration such that a stepped structure arises of specific crystallographic planes of lower energy than a smooth surface of smaller area but of arbitrary orientation. It is important in our point of view that at high temperature in a slightly oxidizing atmosphere rearrangement of the surface atoms can occur due to their mobility to produce simple crystallographic planes of low indices. The striations in each metallic grain appear to form from long thin closely

spaced facets running from one boundary to the other boundary in the crystallographic direction characteristic of each grain. The surface appears then to be formed of two types of planes: one type characterized by low Miller indices and another more complex type of planes inclined to the other, which maintains the average orientation of the surface. For example, the results Rhead and Mykura[79] and Moore[80] indicated that for the silver-oxygen system at temperatures below its melting point, the (111) and (100) planes have surface free energy about 15% and 10% less than the value of a random surface. In the case of nickel[81], striations were observed on the (100) plane for tilt angles up to 1° 40' and on the (111) planes for angles up to 0° 30'. In this investigation some grains exhibited weak curved striations of small density, indicating that these grains approach low indices planes as in fig. (IV.5.1-1b). Each metallic grain exhibits generally only one set of parallel striations with some exceptions, fig. (IV.5.1-1f), when a second set appears having a different orientation. In the neighbourhood of the grain boundaries and especially at twin boundaries, fig. (IV.5.1-1d) and fig. (IV.5.1-1e) the striations change directions across the grain boundary. This situation is illustrated schematically in figs. (V.4.1-1) and (V.4.1-2).

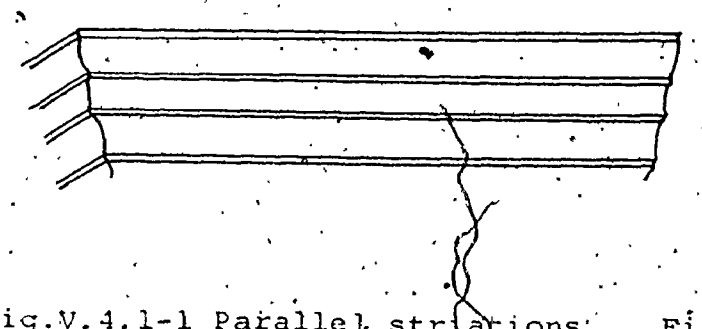

Fig.V.4.1-1 Parallel striations on a nickel grain

Fig.V.4.1-2 Two set of striations

In the second situation, isolated oxide crystallites approximately 2 μm in size were distributed on the metal surface striations. These crystallites have the same orientation and the same shape on the same metallic grains as in fig. (IV.5.1-1a), (IV.5.1-1d) and (IV.5.1-1e). The oxide crystallites form on the steps within the grains and sometimes at the grain boundaries. This situation could be illustrated schematically as in fig. (V.4.1-3).

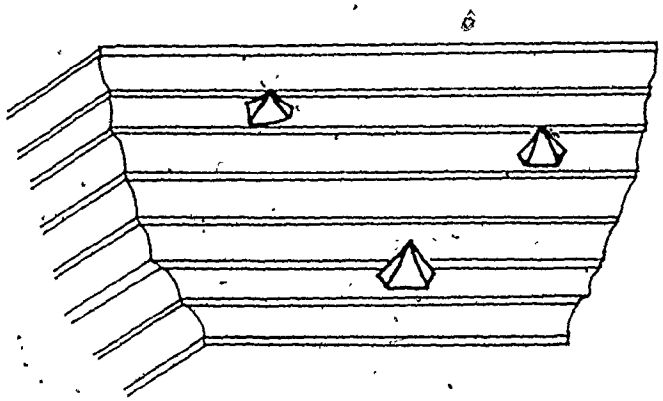

Fig. V.4.1-3 Formation of the oxide crystallites on a metallic grain.

The third situation is existent on those grains where islands of oxide crystallites form rapidly and coalesce forming parallel lines of oxide. The orientations and the shapes of these crystallites depends, as could be realized from fig. (IV.5.1-1d) and fig. IV.5.1-1g) on the metallic grain orientations. This situation is illustrated schematically in fig. (V.4.1-4 a).

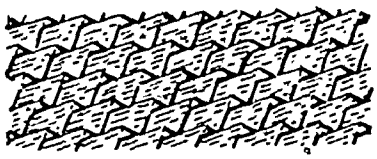

Fig. V.4.1-4 Formation of the islands of the oxide crystallites on a metallic grain

Between oxide crystallites which remain isolated it was possible to observe that the metal surface was rough with surface reliefs dependent again on the metal grain orientation.

A characteristic situation was revealed by the oxidation at the grain boundaries of the metal. Fig. (IV.5.1-1h) illustrates that the twin boundaries are completely free of oxide growths. This phenomenon was generally observed not only in the early oxidation stages and at higher temperature but also at later stages of oxidation as reported by Perrow[63]. This behavior can be explained due to the fact that a twin boundary is coherent characterized by a low surface energy. The grain boundaries are generally characterized by the fact that the striations abruptly change orientation from one grain to the other. Only a few grain boundaries contained active sites for the formation of oxide crystallites. Generally crystallites

frequently formed at the grain boundaries separating two grains characterized by high rates of formation of the crystallites. Conversely, at a grain boundary between two metal grains, one of which is oxidizing rapidly while the other is free of oxide crystallites, the crystallites form only in a band at the grain boundary laying on the side of the grain that is oxidizing rapidly as is shown in fig. (IV.5.1-1d). This situation indicates that at this temperature the grain boundaries are not preferentially sites for oxide formation . All observations indicated that the most important factor governing oxide growth in the early stages of oxidation is the crystallographic orientation of the metal grains.

The different situations described above demonstrate that the oxide crystallites formed on different metallic grains are of different orientation but with the same orientation on the same grain. Furthermore, coalescence of the oxide crystallites gave rise to coherent boundaries. The faceting of the metallic striations suggests that at this temperature and low oxygen pressure the surface mobility of metal atoms is sufficiently high to cause surface rearrangement to obtain a more stable configuration . The decrease in the surface energy apparently can be caused by both oxygen adsorption and formation of an oxide layer.

Oxidation of a nickel specimen at 800° and at a low oxygen pressure of $5\times10^{-5}$ Torr but for 18 hours presented completely different characteristics, as indicated by fig. (IV.5.1-2a) to fig. (IV.5.1-2g). The most important characteristic of

the micrographs is again the influence of the crystallographic orientation of the metallic grains. In this case, despite the longer exposure of the specimen to the same oxidation conditions the striations are not straight and regularly spaced as are those at 1000°. They appear curved with larger spacing and the relief effects are much smaller. This suggests that the mobility of the atoms at this temperature is much lower for rearranging the surface into a lower energy configuration. Prolonged exposure at this lower temperature gave rise to a larger fraction of the surface covered with well developed oxide crystallites. As shown by the micrographs presented in Chapter IV, fig. (IV.5.1-2b) to fig. (IV.5.1-2g) different oxidation features arose on different metallic grains depending again on crystallographic orientations.

Perhaps one of the most important characteristics at this lower temperature is that the metal grain boundaries are preferred sites for oxide formation . It was possible to observe that some of the grain boundaries were much more preferred for oxide formation than others especially those corresponding to a twin boundary. As illustrated by micrograph (IV.5.1-2b) the oxide formation rate was much higher at grain boundaries than on the metal grain surfaces. The oxide crystallites on a metal grain also exhibited different orientations at this lower temperature. Consequently the boundary

resulting between coalescing crystallites with a different orientation could be in this case incoherent boundaries.

These features explain characteristics of oxidation at intermediate temperatures below 1000°. The different situations represented by the difference in oxidation rate, oxide crystallite shapes and orientations on different metal grains, therefore, represent two important factors: 1) the orientation of the metal grain influences the rate of formation of oxide crystallites, and 2) the growth rates of the oxide crystallites are different on differently oriented metal grains. Also it appears that within the same grain there are sites favorable for nucleation, since areas of the same grain are covered by small crystallites that meet each other while other areas exhibit widely spaced oxide crystallites which develop slowly before meeting each other.

The specimen oxidized at 800° and the higher oxygen pressure of $5\times10^{-3}$ Torr for 45 minutes also confirms many of the above observations and conclusions. Results of these experiments were illustrated in figs. (IV.5.1-3 a,c,d,e). Schematically development of the nickel oxide layer could be represented as in fig. (V.4.1-5) to (V.4.1-7).

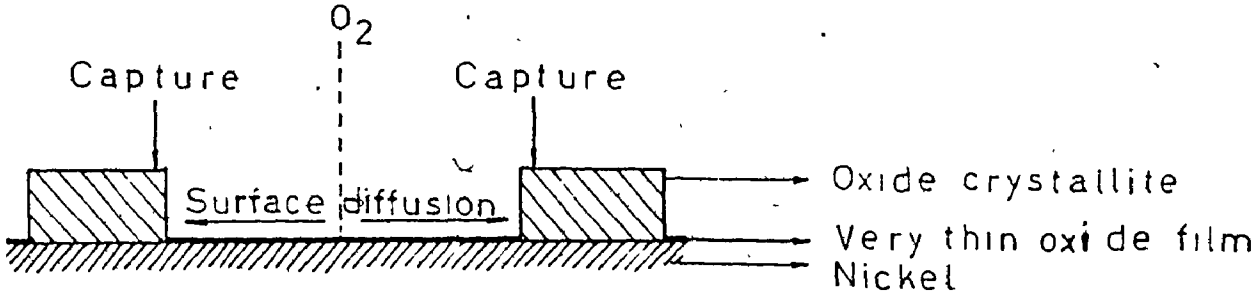


Fig. V.4.1-5 Formation of the oxide crystallites.

Upon nucleation of oxide, the crystallites grow in thickness and laterally. When the crystallites are widely spaced, continued nucleation leads to formation of new crystallites.

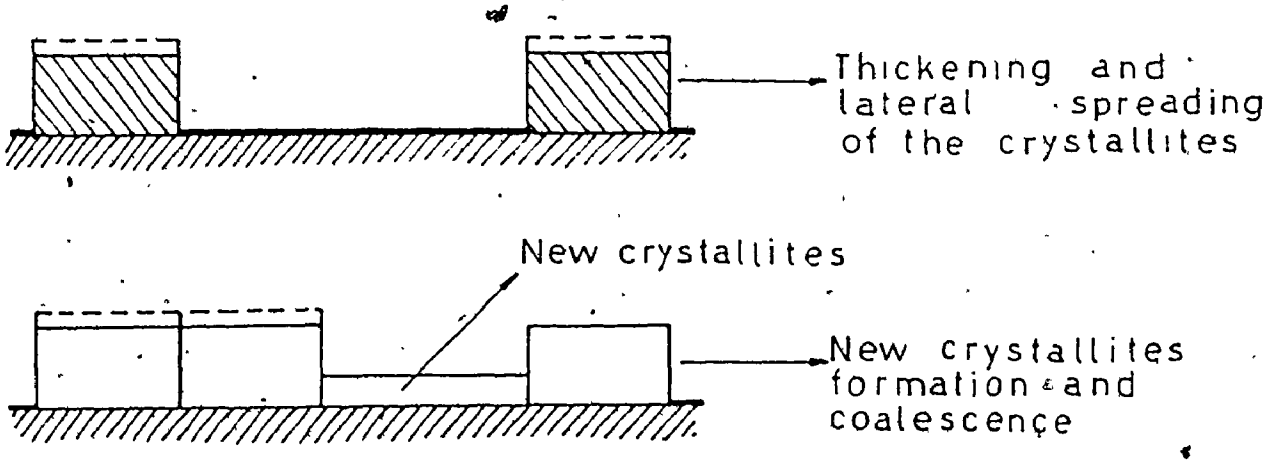


Fig. V.4.1-6 Coalescence of the oxide crystallites

When oxide crystallites meet each other, they coalesce to larger crystallites to form coherent and incoherent boundaries. Nickel has the possibility to diffuse preferentially through the grain boundaries formed between the impinging crystallites, especially those boundaries which are incoherent, to

react with oxygen. This is the beginning of the formation of "so-called" cellular structure.

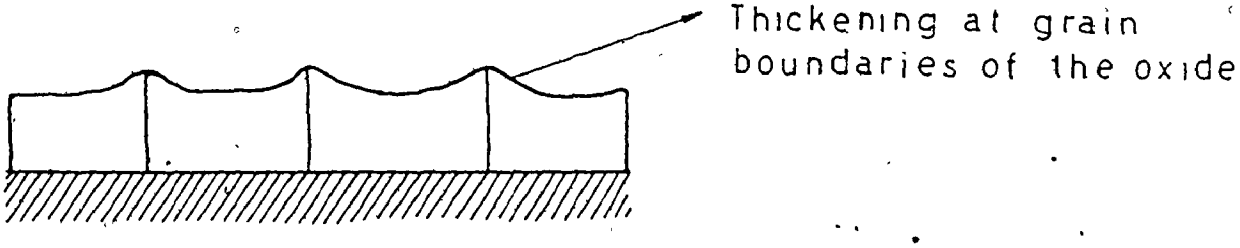


Fig. V.4.1-7 The formation of "cellular" oxide structure

These successive steps in the formation of the oxide crystallites up to coverage of the entire metal surface are best illustrated by the micrographs in fig. (IV.5.1-3 c,d,e). Another indication of the anisotropy of oxide growth is given by the grain size distribution of the oxide crystallites given in the previous chapter (fig. IV.5.1-4). This figure indicates the difference in the size of the crystallites on different grains. The average value is approximately the same but the size spread is different, on some grains the maximum size of the crystallites reaches 2,8 μm and on others only 1.9 μm.

V.4.2 Topographical Development of the Nickel Oxide Outer Surface During Oxidation at 800°

The development of the nickel oxide scale from the early oxidation stages under conditions of low oxidizing power as above described, to the oxide scale obtained in the normal condition of our experiments at 800° and an oxygen pressure of 400 Torr is illustrated by topographical aspects of the scales obtained during continuous oxidation and oxidation interrupted by vacuum anneals in micrographs (IV.5.2-1) to (IV.5.4-1). As discussed in the previous section, oxidation of pure nickel at 800° and low oxidizing power finally resulted in the formation of an oxide layer completely covering areas of the nickel surface as a result of oxide crystallites impinging on one another. This initial film was characterized by oxide thickening at the boundaries of the oxide crystallites. This aspect is generally called "cellular" structure. It is a general feature for the oxide obtained during continuous oxidation depending on temperature and time of oxidation. It is most pronounced especially at temperatures below 1000° and for exposure durations depending on temperature. This aspect was ~~still~~ detected at 900° by Caplan et al[51] but only for 30 minutes of oxidation. The same authors found this aspect at 20 hours of oxidation on annealed nickel at 700° as illustrated in fig. (V.4.2-1) and fig. (V.4.2-2).

Fig. V.4.2-1 and Fig. V.4.2-2 "Cellular" aspect of annealed nickel oxidized for 20 hours at 700°(51) and o.5 hour at 9oo°

This cellular aspect was found in our investigation on the oxidation of both less pure and pure nickel at 800° and an oxygen pressure of 400 Torr commencing at very short exposure of approximately 5-10 minutes. Micrographs (IV.5.2a) and (IV.5.2-4) as well as (IV.5.3-2b) indicate that this topographical aspect is characteristic under continuous oxidation exposures up to exposure times of 70 hours. The best examples of this cellular structure obtained during continuous oxidation were those presented in fig. (IV.5.2-2a,c) and (IV.5.2-5a). This structure results from localization of oxide growth at the

oxide crystallite boundaries upon impingement of these crystallites by lateral growth. It was not possible to assign sizes to the oxide crystallites at this stage of scale development since the chains or ridges of polycrystalline oxide appeared as an interconnected network.

The topographical aspect of the surface changed at times of oxidation extending beyond 70 hours. The outer surface mainly exhibited a fine grained appearance even though the cellular structure still could be detected. With respect to scanning electron microscopy, the oxide grains were of different sizes, some very fine and equiaxed while others were elongated and of larger size. It was still possible after 240 hours of oxidation to observe the oxide ridges on parts of the surface. Growth of these ridges laterally and vertically at grain boundaries ultimately led to development of the polycrystalline grains. The development of this polycrystalline structure from the cellular structure gave rise to individual oxide grains of different shape. Surface, volume and grain boundary diffusion are all involved in the development of this polycrystalline structure.

Topographical aspects of the oxide scales subjected to vacuum anneals and reoxidation exhibited features different from those of scales formed only by continuous oxidation. Two different types of topography could be distinguished by examining specimens subjected to oxidation and vacuum anneals

under different conditions and, on the other hand, specimens subjected to oxidation, annealing and reoxidation. As a general characteristic the scales obtained by oxidation and vacuum annealing showed the same topographical properties as those obtained only by oxidation for the same exposure period. The effect of annealing could be visualized from the respective micrographs as a decrease in the number of oxide ridges,

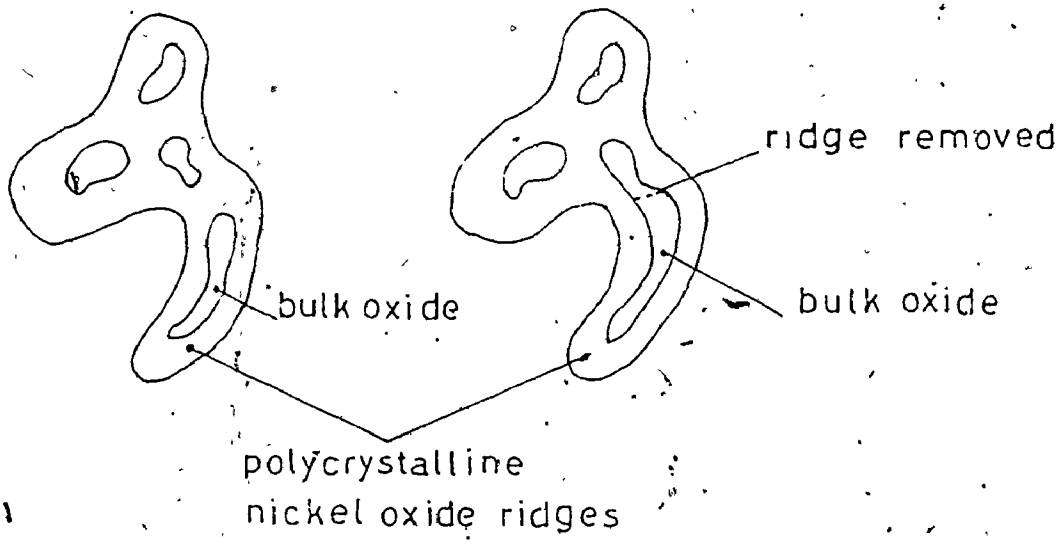


Fig. V.4.2-3 Effect of annealing on the outer surface of the oxide scale.

by coaleascence, as in fig. (V.4.2-3). Physically this coalescence was brought about by diffusion of nickel and oxygen. During normal oxidation, grain boundary diffusion of nickel led to continual growth of the oxide ridges. On considering this case

in 3 dimensional space, the structural changes give rise to a celullar structure which takes place by removal of branches due to their lateral and vertical thickening at the grain boundaries.

Annealing of the polycrystalline oxide scale decreases the number of grain boundaries available for diffusion. When reoxidation is commenced, nickel lattice diffusion will play a more effective role. Consequently larger faceted grains develop. This behaviour was characteristic as illustrated in all the micrographs representing the oxidation interrupted by vacuum anneals, figs. (IV.5.3.1 b,c,d) and (IV.5.3-2 c,d,e). The surface of the nickel oxide obtained on less pure nickel by oxidation interrupted by vacuum anneals is characterized by much more well developed and preferred oriented grains. To exemplify the transition from the cellular to faceted grain structure, micrographs are shown in figs. (V.4.2-4a and b) of two surface areas of oxide formed on pure nickel oxidized for 20 minutes, annealed for 1 hour and reoxidized for 40 hours at 800°.

Topographical aspects of the outer surface were completely changed upon increasing the temperature from 800° to 1000°. The fine grained oxide surface obtained at the lower temperature was changed to a well developed faceted large grained surface at the higher temperature.

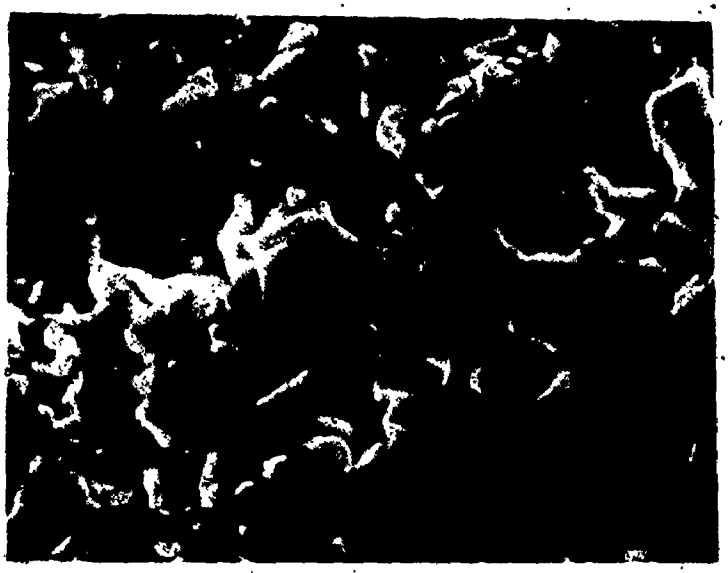

(x 4,750)

a

(x 9,500)

b

Fig. V.4.2-4a and b Topographical views of a nickel oxide in a pure nickel sample obtained by 20 minutes oxidation, annealing for 1 hour at 800° and 40 hours reoxidation.

The appearance of large well developed facets at this higher temperature was the most distinguishing feature, as illustrated by the micrographs in figs. (V.4.2-5 a and b) representing the outer surface of less pure nickel oxidized for 70 hours and

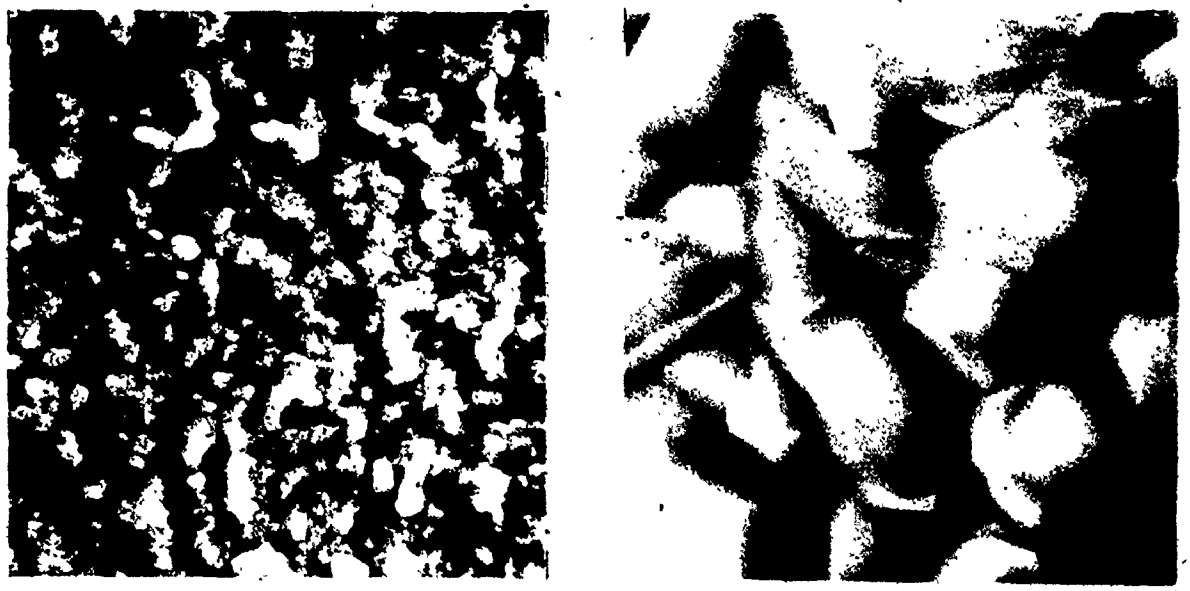

(× 3,400) (×, 5,000)

a b

Fig. V.4.2-5 a and b Comparison between the surface of the nickel oxide scale obtained upon oxidizing for 70 hours, less pure nickel (a) and sample reoxidized for 30 hours at 1000° (b).

reoxidized for another 30 hours at 1000°. From a topographical point of view, this surface is characterized by individual particles in the form of well developed grains with low connectivity.

The same topographical characteristics were represented by the pure nickel samples oxidized at 800° for 240 hours and then reoxidized at 1000° for 20 hours as shown in fig. (IV.5.4-1c). This demonstrates that at higher temperatures the cellular and intermediate stages of topographical development are not observed because of the larger reaction rate brought about by the higher mobility of nickel and on the more important role played by volume diffusion in respect to grain boundary diffusion. Considering these results on the topographical development of the external scale surface at 800° and 1000°, one may consider the scale as developing according to the following sequences:

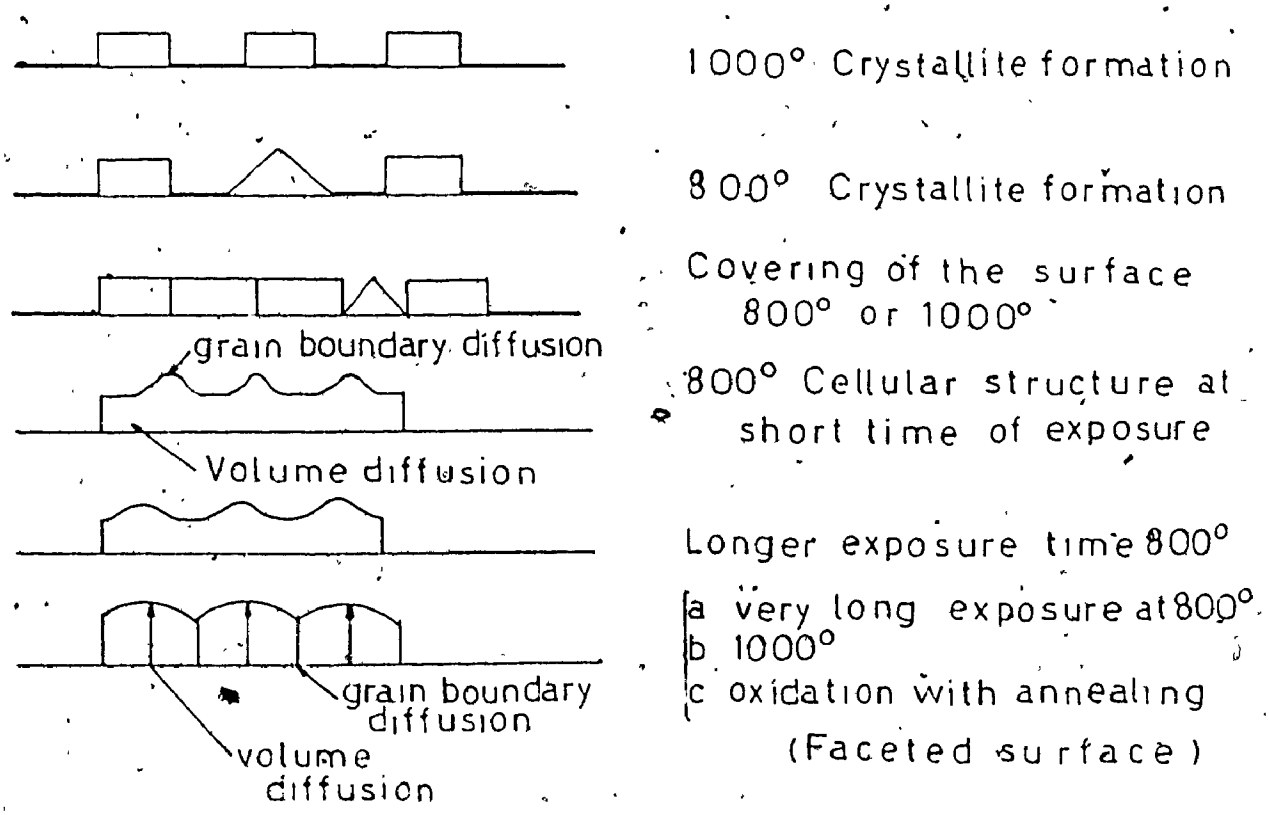


Fig. V.4.2-6. Topographical development of the outer surface of nickel oxide scale (schematic representation).

The observations reported by Caplan et al.[51] of the outer surface of the oxide scale found in the temperature range 700°-1200° also indicates that this mechanism may be applied for the topographical development of nickel oxide scales.

## V.5 STRUCTURAL DEVELOPMENT OF THE NICKEL OXIDE FORMED AT 800° AND AN OXYGEN PRESSURE OF 400 TORR

Sequences of electrochemically etched and fractured cross sections of oxide scales obtained during continuous oxidation and oxidation interrupted by vacuum anneals at 800° were presented in the previous chapter, fig. (IV.6.1-1) to fig. (IV.6.3-1). A notable observation was that these scales exhibited excellent adherence to the underlying metal. This feature was illustrated by optical micrographs of the samples oxidized for long times (70 hours and 240 hours) as shown in fig. (V.5-1 a) and fig. (V.5-1 b) respectively.

The first sequence of micrographs, figs. (IV.6.1-2 a) to (IV.6.1-2 g) indicate that in the early stage oxidation up to 2 hours of less pure and pure nickel a scale is formed which is nonuniform in thickness over the metal surface. These differences were accentuated in the very early exposure periods indicating again the influence of the metal structure on oxidation. For example, the thickness of the oxide layer formed after 20 minutes varied between 1.3 and 4

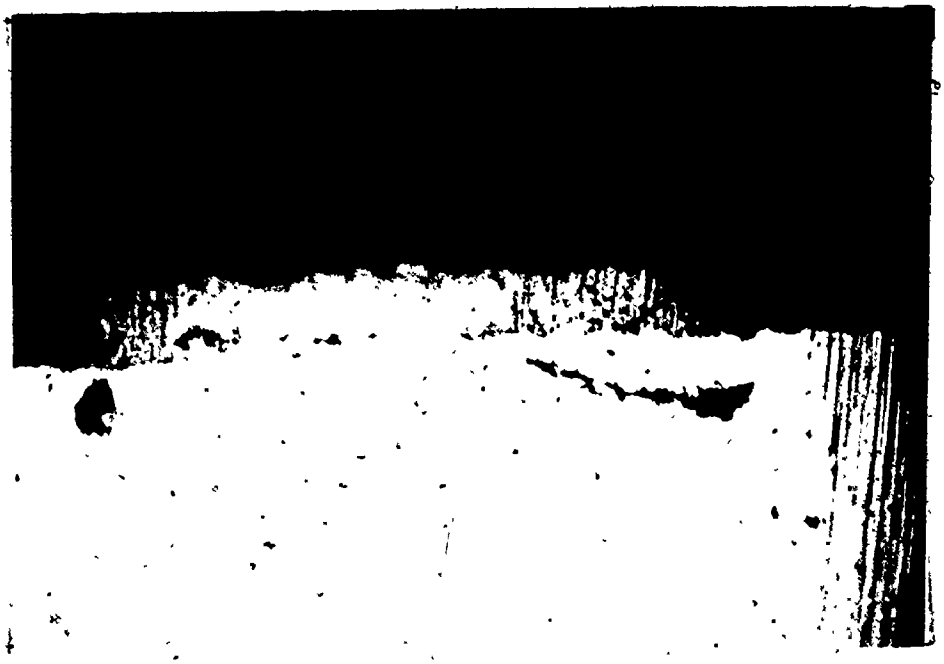

(x 800)

a

(x 800)

b

Fig.V.5-1 a,b: 70 hours a. and 240 hours b. oxidation of pure nickel at 800° (optical microscopy).

μm over the metal surface. After 70 hours the thickness varied between only 6.0 and 11 μm. Fig. (IV.6.1-2 b) and fig. (IV.6.1-2 c) represent two micrographs taken from different parts of a less pure nickel sample continuously oxidized for 2 hours at 800°. These micrographs indicate a difference in thickness of as much as one-half of the total thickness.

Another characteristic of all scales at different areas on the same sample was associated with the different ratio of outer to inner layer thickness and the grain size in the two layers. Due to the experimental difficulties, it was difficult to assign a size to the grains in the inner layer. Same aspects of the scale were revealed by Caplan et al.[51,82] as illustrated in fig. (V.5-2).

Fig. V.5-2 Oxide structure formed on C.P. nickel in 20 houra at 700° (cold worked nickel). (51)

It is obvious that there are differences in the total layer thickness, oxide grain size in the outer and inner layers as well as the ratio outer/inner layer over different parts of the scale.

The oxidation of pure nickel for 5-10 minutes, fig. (IV.6.1-1 a,b) gave rise initially to a scale characterized by the existence of single layer of equiaxed grains. Over several areas of the metal surface these grains exhibited a tendency to become more columnar. Other parts of the scale appeared to be formed of two layers (Fig. IV.6.1-1) but the interface between the two layers was diffuse. With increasing time of exposure, the outer part of the scale became more columnar. After 20 minutes of oxidation of less pure nickel, it was possible to distinguish the presence of the two layers: an inner one formed of equiaxed grains surmounted by an outer one formed of columnar grains. There were, however, some parts of the scale characterized by the presence of one layer predominately composed of equiaxed grains, fig.(IV.6.1-2a). At 1 hour oxidation of less pure and pure nickel the two layers were easily distinguished. The outer layer was columnar and an increase in grain size of this layer was evident. The micrographs of the scales oxidized for two hours were characterized by a very sharp interface between the two layers as indicated by fig. (IV.6.1-2f) and fig. (IV.6.1-2g)). Yet after 70 hours of oxidation, the scale was characterized by only a slight preferential growth of the inner layer so that some parts of the scale remained as one equiaxed layer. This aspect is shown in fig. (IV.6.2-1b). At longer time of oxidation, 240 hours, the oxide scale on pure nickel was characterized mainly by long well developed columnar grains, as illustrated in figs. (IV.6.2-2a to c). Parts of the scale

were completely columnar with grains extending all the way from the metal to the oxide/gas interface. In some other parts it was possible to observe both layers. It was evident, as illustrated in fig. (IV.6.2-2 a,b,c) that continuous oxidation for long exposures caused an increase in size of both the columnar and equiaxed grains in the oxide layers and that this behaviour was more pronounced in the scale formed on pure nickel. Possibly this slower rate of oxide grain growth in the scale on less pure nickel is caused by impurities pinning the grain boundaries of the oxide in the inner layer.

It appears that with increasing time of exposure the scale structure obtained during continuous oxidation at 800° changes from a bilayer scale composed of an inner equiaxed layer and one outer columnar layer, characterized by a diffuse interface of separation, to a duplex scale characterized by a sharp interface between the two layers. The preferential growth of columnar grains in the outer layer at intermediate time of exposure leads ultimately to sections of the scale which are completely columnar at very long exposure. All these stages are characterized by increasing oxide grain size in both scale layers, especially for pure nickel samples. Moreover, outward migration of nickel leads to nickel oxide formation at the scale-oxygen interface due to boundary and lattice diffusion of nickel in the scale. Scale growth is also characterized by preferential transformation of the equiaxed grains of the inner layer into the columnar grains by a process of grain growth.

These sequences are represented schematically in fig. (V.5-3).

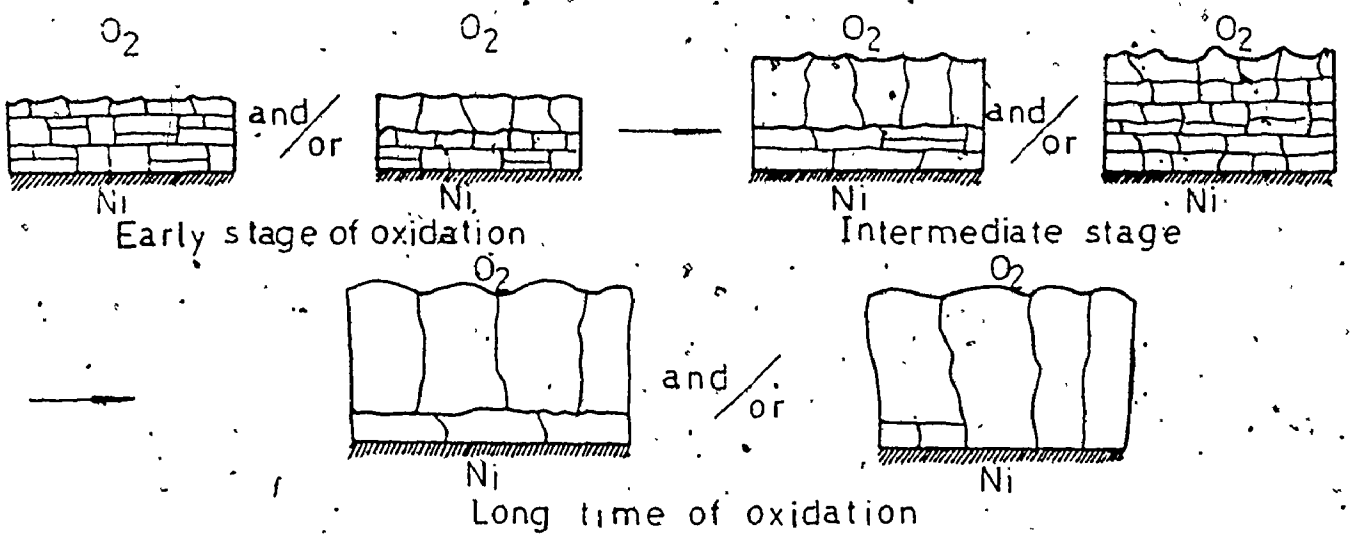


Fig. V.5-3 Transformation of the scale obtained in early stages of oxidation in a single columnar scale by long exposure to oxidation.

These observations are supported also by figs. (IV.6.4-1) and (IV.6.4-2) in the previous chapter, showing the quantitative results on the total outer and inner layer thicknesses and the changes in the ratio outer/inner layer for scales formed on pure and less pure nickel. These results, combined with the development of a well textured oxide scale, despite the polycrystalline aspect of the nickel specimens used, indicates that the formation of this duplex structured scale is at least a result of a preferential growth of the nickel oxide grains. Both types of nickel were characterized by a scale exhibiting a texture on the (111) plane at the beginning of the oxidation which changed during oxidation to a texture obtained on (110) and (331) planes. Therefore the parts of the scales exhibiting only the equiaxed layer could be associated with the absence of a preferred orientation. On the other hand,

the formation of one columnar well oriented scale with the oxide grains extending from the metal interface to the oxide-gas interface should be correlated with the much more preferred oriented structure as found in the texture measurements.

Annealing of the scales was shown to have an important effect on the structure of the nickel oxide scales. The interface of separation between the inner and outer oxide layers in scales formed at short exposures became more sharp as shown in fig. (IV.6.1-2f) and fig. (IV.6.2-1a). The outer layer became more columnar and the average ratio of outer to inner layer also increased. This effect was pronounced when the scales were annealed at the higher temperature of 900°. The increase in difference between the two layers was caused by an increase in the average oxide grain size not only in the outer layer but also in the inner layer. This increase in grain size was less rapid in the scale formed on the less pure nickel samples. However, preferential growth of the columnar oxide in scales on both types of nickel gave rise to scale sections consisting entirely of columnar grains. The increase in oxide grain size could be correlated with the kinetic measurements for scale growth as illustrated in Table (V.5-1). Reoxidation of the scale obtained by oxidation at 800° and annealing at 900° was characterized by a decrease in the effective oxidation rate constant by 7 times compared with a decrease of 1.3 resulting during continuous oxidation. More advanced grain growth by high temperature annealing led to

less short circuit diffusion paths available for nickel transport. Annealing of the oxide scales obtained during short exposure times to oxygen also played an important role on the final structure of the scales obtained after this reoxidation. All the micrographs presented in the previous chapter, figs. (IV.6.2-3a) to (IV.6.2-3g) demonstrated that the structure of such scales is changed by grain growth processes more drastically than in the scales obtained by the same exposure time to oxygen during continuous experiment. Some parts of the scales, annealed and reoxidized, were completely columnar with the grains extending from the underlying metal to the outer scale

Table V.5-1

Comparison between the average ratio outer to inner layer obtained during continuous oxidation and oxidation interrupted by vacuum anneals

| Type of Ni | Type of Experiment | Average ratio outer/inner layer |
|---|---|---|
| Less pure Ni | Continuous (70 hours) | 1.7 |
| Less pure Ni | Oxidation interrupted by vacuum anneals (70 hours) | 2.7, 4.5 and completely columnar scale |
| Pure Ni | Continuous (70 hours) | 2.2 |
| Pure Ni | Oxidation interrupted by vacuum anneals (90 hours) | quite completely columnar |
| Pure Ni | Very long continuous oxidation (240 hours) | 4-6 or completely columnar |

surface. The sizes of grains in the outer and inner layers were also increased in the scales obtained on both types of nickel .

The changes in the ratio of outer to inner layer for the structure of the scales obtained under continuous exposure and the same type of experiment interrupted by vacuum anneals are illustrated in table (V.5-1). These results again indicate that interruption of oxidation by vacuum anneals has the same effect of the morphological development of the scales as long time continuous oxidation (240 hours for pure nickel) as indicated by fig. (IV.6-2). There is an increase in the grain size of the oxide and a transformation of the scale from a bilayer to columnar structure.

Changing the oxidation temperature from 800° to 1000° produced a drastic effect on the bilayer structure of the scale. The micrographs (IV.6.3-1a) to (IV.6.3-1d) are illustrative of this effect. The scale becomes columnar in the case of the sample of pure nickel oxidized continuously for 240 hours and this specimen reoxidized for 20 hours at 1000°. These changes were even more drastic in the case of the sample of less pure nickel oxidized for 70 hours and then reoxidized for 2 hours at 1000°. Two micrographs are given below to illustrate this transformation. It should be mentioned that the sample in figs. (V.5-3 a and b) did not exhibit a completely columnar structured scale. Some other parts of the scale of this reoxidized sample as indicated in fig. (IV.6.3-1b) remained as two layers

with the thickness of the inner layer remaining the same as that at 800°. An important characteristic again was the increase in the size of the grains in both layers.

One of the most important characteristics of all the oxidation phenomena was the influence of the crystallographic orientation of the nickel grains on the development of the oxide scales. Those metallic grains having a crystallographic orientation favoring a high formation rate for oxide crystallites formation but a slow rate for growth of the oxide were characterized by the formation of a scale that initially showed one equiaxed layer which only slowly transformed into a bilayer scale. The metallic grains characterized by a low rate of oxide formation but by a relatively high rate of preferential growth transformed most rapidly into a columnar structured scale.

(x 5,200) a

(x 2,000) b

Fig. V.5-3 a and b Comparison between nickel oxide scale obtained after 70 hours oxidation of less pure nickel. a) (etched cross section) and same sample reoxidized at 1000° for 30 hours (b) (fractured).

## V.6 OXIDATION MODEL

### V.6.1 Introduction

The oxidation curves given in fig. (IV.3-2 a and b) for less pure and pure nickel plotted according to the parabolic equation:

$$\left(\frac{\Delta W}{A}\right)^2 = k_p t + c \qquad \text{(V.6.1-1)}$$

where the symbols have the significance indicated in Chapter II, show that parabolic behaviour is not obeyed. Consequently Wagner's mechanism based only on lattice diffusion is not applicable to nickel oxidation under our working conditions. The conclusions resulting from the discussion of the experimental results, subsections V.3 and V.4 of this chapter, demonstrate that the influence of structural changes occurring in the oxide scale during oxidation ranging from preferred oxide orientation possibly recrystallization and grain growth play important roles in the oxidation mechanism. Therefore a model to explain this nonparabolic oxidation of nickel at 800° should take into account diffusion of nickel through the oxide lattice and via structural defects in the scale which decrease in density with the exposure time due to a grain growth process. Grain growth is commonly placed as a double logarithmic plot of grain size versus time according to the general equation given by Beck[83].

$$D_t^n - D_o^n = k_3 t \,, \qquad \text{(V.6.1-2)}$$

where $D_t$ is the grain size of the oxide crystallites at time t, $D_o$ is the initial grain size and $k_3$ is the rate constant of growth.

Graphical representation of the average grain size of nickel oxide formed on less pure nickel and pure nickel, figs. (V.6.1-1) and (V.6.1-2), demonstrates that n equals approximately ly 6 and 2. An analysis therefore can be only made to explain the decreasing oxidation rate of the pure nickel specimens with increasing exposure time by taking into account the presence of structural defects in the oxide scale by the model proposed by Perrow et al.[23] and applied by Khoi et al.[28] to single crystal nickel oxidation at temperatures ranging between 500 and 800°.

As shown in Chapter II, this model consists of defining an effective diffusion coefficient in which both lattice diffusion and diffusion via paths of low resistance offered by structural defects contribute to nickel transport across the oxide scale. These defects could be grain boundaries or dislocations. The diffusion coefficient based on random walk analysis, derived by Hart[25]

$$D_{eff} = D_\ell(1-f) + D_B f \qquad (V.6.1-3)$$

where $D_\ell$ and $D_B$ are the diffusion coefficients defining lattice and line defect transport, and f is the fraction of sites lying in the low resistence paths is valid only

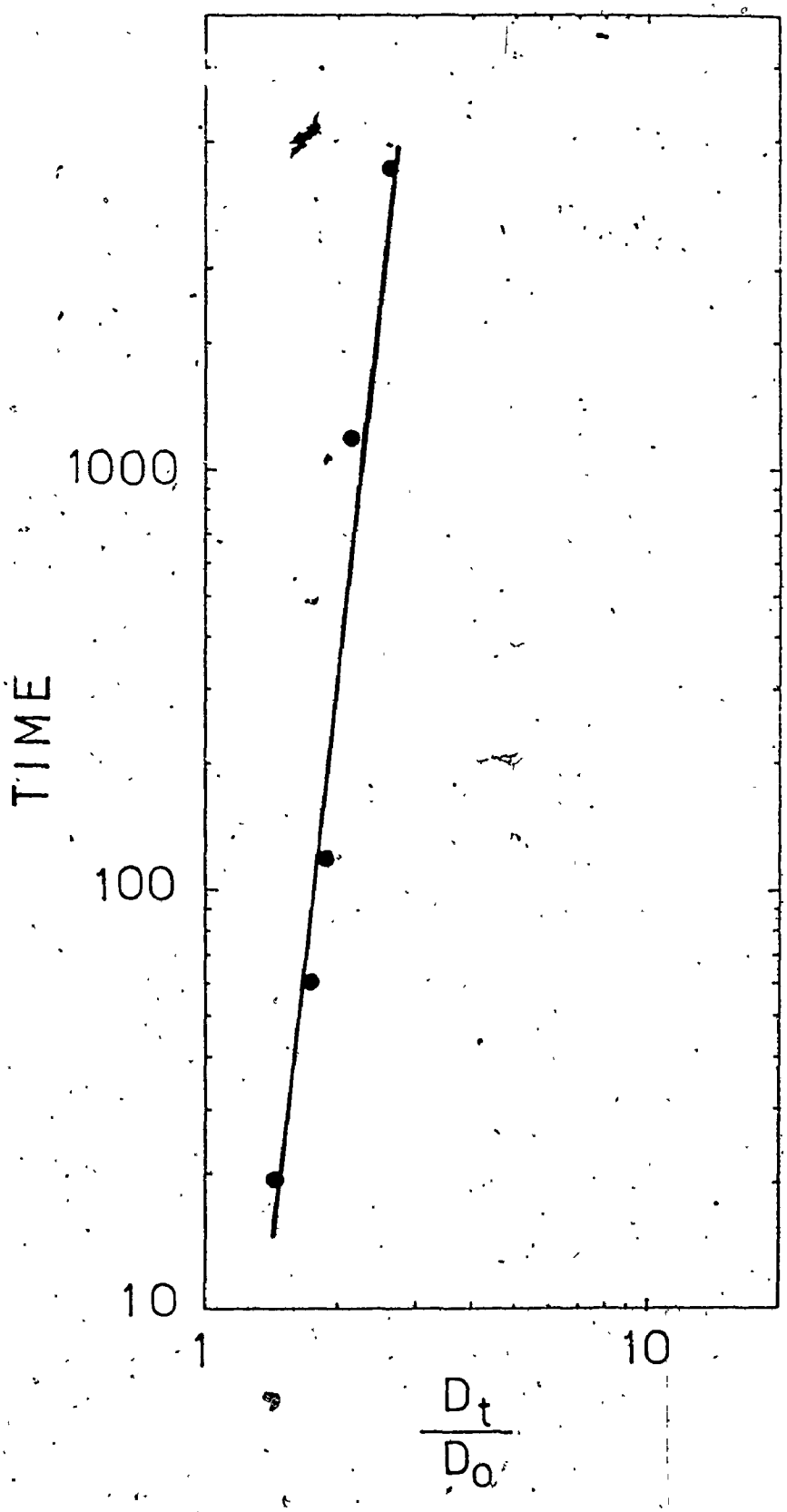


Fig. V.6.1-1 Double logarithmic plot of oxide grain size versus time for less pure nickel.

$(D_t^n - D_o^n = k_3 t)$

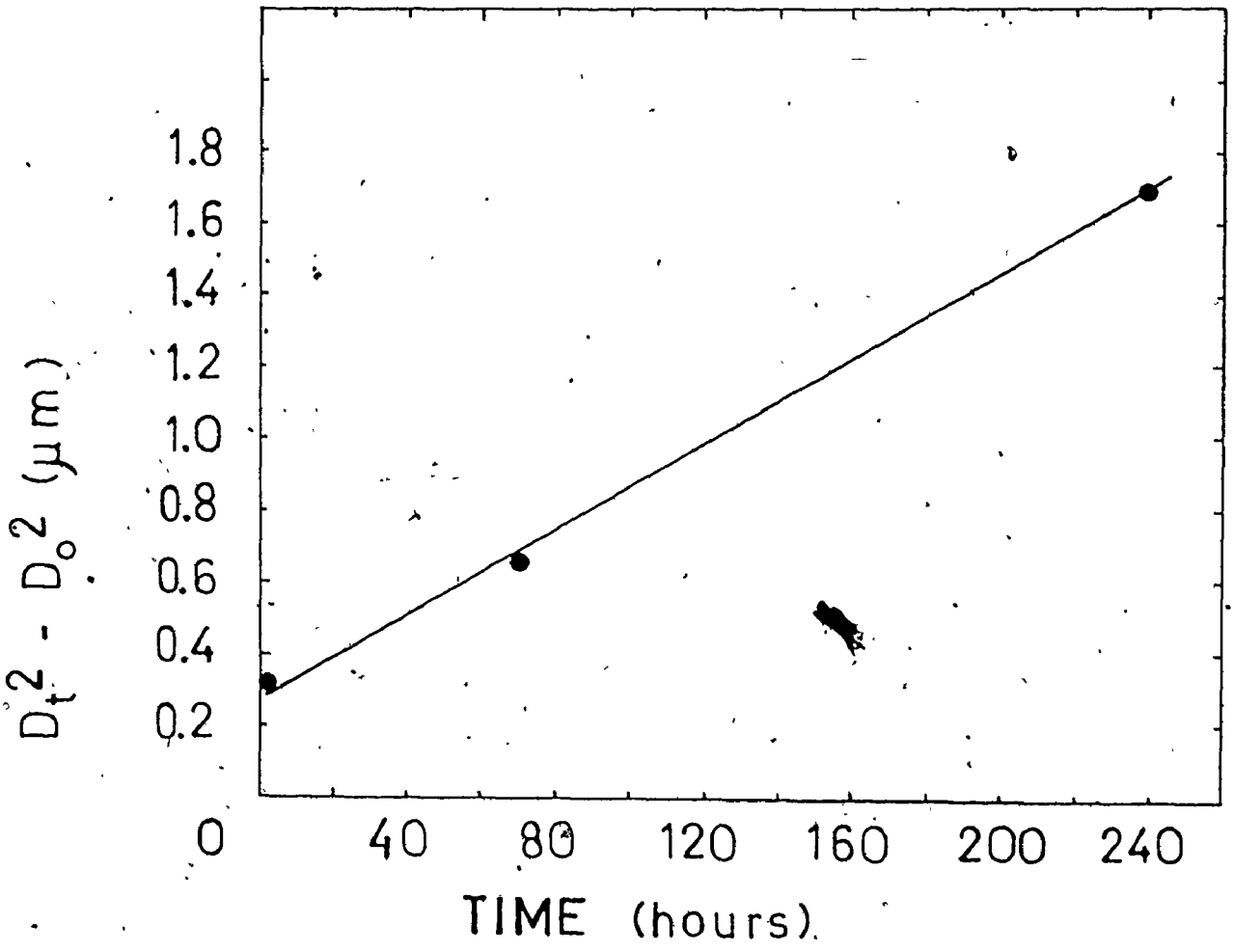


Fig.V.6.1-2 Oxide grain size ploted versus time for pure nickel, ($D_t^2 - D_o^2 = k_3 t$)

if $2(D_\ell t)^{1/2} > \ell_d$ where $\ell_d$ is the spacing of the defects. In our case the spacing between boundary paths corresponds to the oxide grain size. Even for the largest grains of nickel oxide obtained by oxidation of pure nickel at 800° for long times of exposure this condition is met considering a diffusion coefficient for nickel in nickel oxide of approximately $10^{-14}$ $cm^2/sec$[19]. The factor f is a time dependent parameter defining the fraction of diffusion sites situated at boundaries. A simple expression for this parameter based upon an array of oxide grains is

$$f(t) = \frac{2d}{D_t}$$

where $D_t$ is the diameter of the grain at time t and d is the width of the grain boundary.

V.6.2 Test of the Oxidation Model

As indicated in Chapter II, the plot of

$$\frac{1}{(\frac{dx^2}{dt} - k_L)^2} \text{ vs } t \qquad \text{(V.6.2-1)}$$

should yield a straight line. In this expression $\frac{dx^2}{dt}$ is equivalent to the instantaneous effective parabolic rate $k_p(t)$ calculated as tangents to the oxidation curve, represented in the parabolic form, at different times and $k_L$ is the Wagner's parabolic rate constant for lattice diffusion. For the present calculation $k_L$'s value computed by Khoi et al.[38] were used. Using as values for $\frac{dx^2}{dt}$ those given

in table (V.2-2) for pure nickel the graphical representation of

$$\frac{1}{\left(\frac{dx^2}{dt} - k_L\right)^2}$$

against time followed a linear relation, fig. (V.6.2-1). The slope of this line is

$$S = \frac{k_3}{4k_B^2 d^2}$$

and the intercept is

$$I = \frac{D_o^2}{4k_B^2 d^2}$$

where letters and constants have the significance previously given in Chapter II. The results of these calculations, along with the experimental curve, illustrated in fig. (V.6.2-2) show that the experimental results are well reproduced by this model invoking nickel diffusion via lattice and structure defects in the scale.

It should be emphasized that this kinetic model, developed by Perrow et al[23] and Khoi et al[38] is based on the assumption that the concentration of defects are decreasing in time due to recrystallization and grain growth processes. This assumption was based on the experimental data of changing of the oxide crystallite size in time at 500° and 600° for the oxide obtained on polycrystalline and single crystal nickel specimens, respectively. The curves of crystallite size[38,23] versus time obtained by these authors were representative of

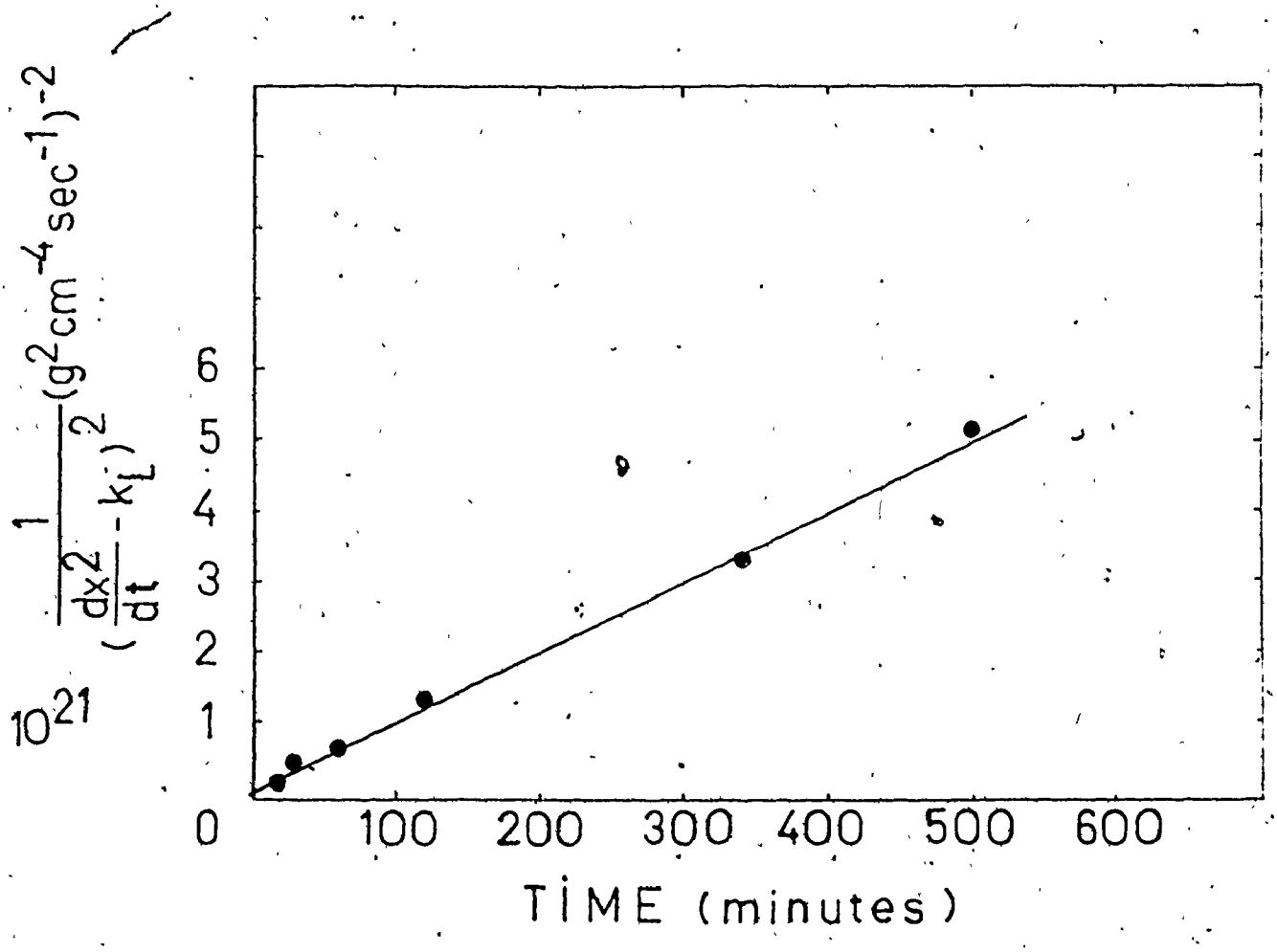


Fig. (V.6.2-1) Plot of $\frac{1}{(\frac{dx^2}{dt} - k_L)^2}$ versus time for the oxidation of pure nickel.

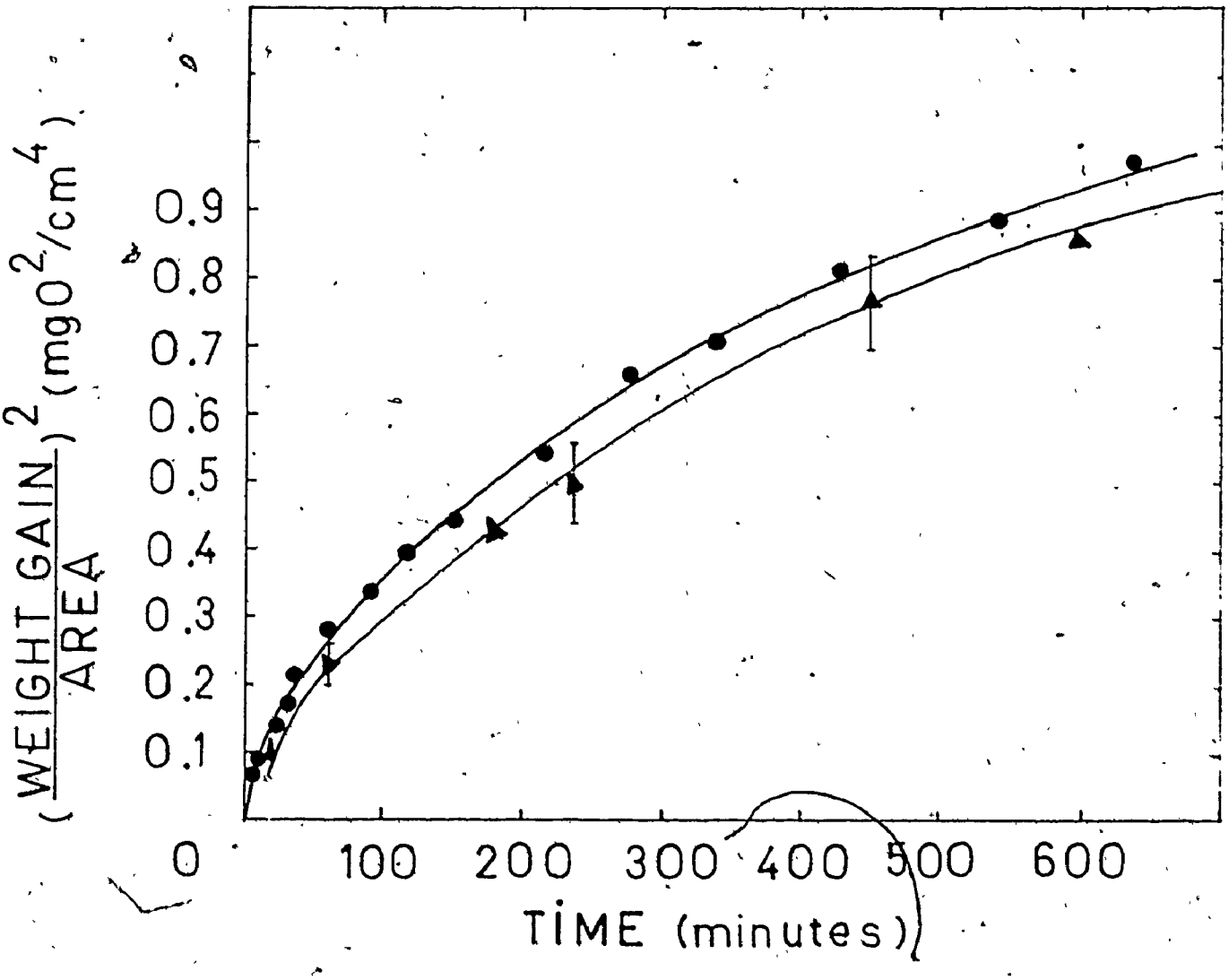


Fig. (V.6.2-2) The experimental (o) and the calculated curve for the oxidation of pure nickel, (Δ).

recrystallization and grain growth based on the fact that the crystallite size remained constant at 100 - 150 Å at the beginning of oxidation for periods ranging between 40 to 90 minutes.

In our case, because of higher temperature of oxidation, 800°, it was not possible to assign an accurate size to the oxide for the period of oxidation under 1 hour. Therefore direct evidence was not found for the existence of this period in which the grain size remained constant. However, the high parabolic rate constant of the oxidation in the first 20 minutes of oxidation of both types of nickel correlated with its further decreases with oxidation time associated with a corresponding increase in grain size of the oxide are an indication that the oxidation rates are correlated at least with oxide grain growth. This conclusion is also supported by the texture measurements that show an increasing orientation of the oxide scale in time. It is possible that recrystallization takes place also but this stage could not be determined in our condition of higher temperature. Especially in the case of less pure nickel, the initial oxide orientation was parallel as influenced by the preferred orientation of the underlying metal, and subsequently characterized by this same parallel orientation and an additional orientation on the (110) plane.

V.6.3 The Grain Boundary Oxidation Diffusion Constant for Nickel Oxide Grown on Pure Nickel

Two methods were used to determine the values for the boundary diffusion constants.

1) from the expression, previously discussed in Chapter II,

$$k_B = \frac{k_p(t) - k_L}{f(t)} \qquad (V.6.3\text{-}1)$$

where $k_p$'s values are taken from table (V.2-2) and f(t) is calculated from the experimental measurements of the grain size of the oxide and,

2) using the value of $S = \frac{k_3}{4k_B^2 d^2}$, the value of the slope determined from the curve in fig. (V.6.2-1). The results of these calculations are indicated in table (V.6.3-1).

Table V.6.3-1

Boundary diffusion oxidation constants for the oxide on pure nickel

| Time of oxidation | $k_p(t) - k_L$ ($g^2 cm^{-4} sec^{-1}$) | f(t) | $k_B$ ($g^2 cm^{-4} sec^{-1}$) | $k_B/k_L$ |
|---|---|---|---|---|
| 1 hour | $0.35\times10^{-10}$ | $3.3\times10^{-3}$ | $10^{-8}$ | $4.5\times10^5$ |
| 70 hours | $0.12\times10^{-10}$ | $2.4\times10^{-3}$ | $5\times10^{-9}$ | |

The $k_B/k_L$ ratio is approximately the same magnitude previously determined for nickel single crystals oxidized at same temperature, 800°, by Khoi et al.[38]. A value of $k_B = 1.5\times10^{-9}$ $g^2 cm^{-4} sec^{-1}$ was determined using the slope, S, which is in good agreement with the values in the table considering the experimental errors in averaging oxide grain size in the

scales formed on the polycrystalline metal samples.

V.6.4 Calculation of the Oxide Grain Size Based on the Proposed Oxidation Model

The model proposed above could also be tested by attempting to calculate the average oxide grain size from the experimental values of the instantaneous rate constant at different times and to compare these values with those experimentally measured from S.E.M. Considering the expression

$$\frac{k_p(t)}{k_p^o} = \alpha = \frac{D_o}{D_t} = \frac{f(t)}{f^o} \qquad \text{(V.6.2-3)}$$

where $k_p(t)$ is the instantaneous oxidation rate constant at time t, $k_p^o$ is taken as the limiting tangent on the parabolic oxidation curve as time approaches 0 and $D_o$ and $D_t$ have the significance above stated, $D_t$ was calculated, for 1 hour oxidation. As illustrated in table (V.6.2-3), the observed and calculated average grain sizes are in good agreement.

Table V.6.4-1 Calculation of the oxide grain size on pure nickel.

| Oxidation time (hours) | Observed crystallite size (μm) | Calculated Crystallite size (μm) |
|---|---|---|
| 1 hour | 0.62 | 0.70 |

V.6.5 Concluding Remarks on the Kinetic Model for Oxidation of Nickel at 800°

The above calculations indicate that the presented model is a good first approximation for relating the oxidation kinetics with the structural changes occurring in the oxide

scale on pure nickel. Certainly the model exhibits extreme limitations. This simple model could not be applied to growth of the oxide scale on less pure nickel because the grain growth approximates to a 6th power relationship. In this case, the grain growth phenomena was largely confined to the outer layer in the duplex structured scale. Considering the kinetic results it is possible also to remark that the oxidation rate constant decreased more slowly as a result of this lower rate of grain growth of the oxide. The texture of the oxide indicated only in the later stages of exposure a distinctly preferred (110) orientation. In the case of pure nickel, which oxidized at a more rapid rate, the oxide exhibited this same preferred orientation at early exposure time which became much more pronounced with continuing time.

## V.7 REMARKS ON THE FORMATION AND DEVELOPMENT OF THE NICKEL OXIDE SCALE

A primary aim of this investigation was to obtain systematic observations on the development of the oxide scale and correlating the morphology of the oxide formed at the early stages of oxidation with the structure of the metal and the influence of this morphology on the reaction rate and subsequent development of the scale microstructure. Although it has been well established that the oxidation behaviour

of a metal depends on the structural characteristic of its surface, the results of this investigation yield new conclusions. The kinetics, texture and scanning electron microscopy measurements have demonstrated that oxide growth on polycrystalline nickel depends on the orientations of the nickel surface.

Despite the fact that the nickel specimens were polycrystalline and of two types based upon impurity contents, they could be characterized by {111} and {100} preferred orientations, respectively. This difference in texture was reflected by the difference in oxidation kinetics and by the difference in the structural development of the oxide scale. It was also found that the texture of the nickel in itself influenced the formation and growth of the oxide and the resulting mosaic structure of the early stage oxide films. This latter structure, in turn, influenced the oxidation kinetics governed by short-circuit diffusion. Temperature was also shown to exert a strong influence on the microstructural development and growth of the oxide scales.

Comparing the results from the early stages of oxidation at 1000° and 800° and the same oxygen pressure, it was possible to confirm qualitative aspects of general findings regarding epitaxial growth of oxides on metals. At higher temperature the oxygen supersaturation is small and correspondingly the formation rate is low compared with that at lower temperature. Epitaxy was therefore much more pronounced

at 1000° and fewer grain boundaries were formed. At 1000° the oxide on each metal grain exhibited a preferred orientation related to the metal orientation. This favored the formation of large oxide grains characterized by coherent boundaries. At 800° the larger oxygen supersaturation produced a larger number of smaller grains characterized by incoherent boundaries. These boundaries led to a larger degree of short-circuit nickel diffusion through the scale.

Our experimental results also emphasize that oxide growth on the same polycrystalline nickel specimen in the early stages of reaction is at different stages of development due to the anisotropy of reaction on the metallic grains of different orientations. Formation of oxide crystallites is followed by their growth laterally and in thickness. From the scanning electron microscopy observations it appears that tne oxide crystallites markedly thicken before the metal surface is completely covered with oxide. It was also shown that new oxide crystallites form at regions between isolated oxide growth already formed. Lateral and vertical growth of oxide finally led to a network of grain boundaries which offered low resistance paths for nickel diffusion. This marks the beginning of the formation of the oxide "cellular structure" Nickel is transported preferentially at the low resistance boundaries resulting in oxide thickening at the grain boundaries. The outer surface consequently exhibits connected ridges of oxide giving the cellular aspect.

In cross sections, the scales were characterized by the presence of one equiaxed layer or two layers but the interface of separation was often very diffuse. The presence of one or two layered scales depended upon two factors: the rate of formation of the oxide crystallites and the rate of their growth. The distinction between the two layers became more resolvable by the increasing columnar aspect of the outer layer. This stage was characterized by a preferred (110) orientation for oxide on pure nickel and by a parallel orientation for the oxide on less pure nickel. All the experimental evidence indicated that the grains of the outer layer increased with oxidation time altering also the ratio of outer to inner layer. In time the interface between the two layers became more sharp. Some parts of the same nickel sample exhibited the presence of the two oxide layers whilst some other areas exhibited a very slow rate of preferential oxide grown and hence a thickness of outer columnar grains which was often barely distinguishable. With longer exposure time, the equiaxed and columnar oxide grains increased in size. The grains in the outer layer in general grew at a more rapid rate and this was more noticeable for the oxide formed on pure nickel. For example, very long time oxidation of pure nickel led to sections of the scale showing columnar grains extending from the metal-oxide to the gas-oxide interface.

Generally the experimental results at 800° reported in the literature have indicated the presence of a bilayer scale or single equiaxed oxide layer but never the presence of a single columnar scale. The results from this investigation, however, have demonstrated that all of the above types of scales can form at 800° dependent mainly on the grain orientation of the metal and the exposure time. During this investigation, moreover, the bilayer scale was transformed into a single columnar layered scale by four methods:

- Oxidation for short time at 800° followed by annealing especially at 900° transformed parts of the scale into a columnar layer.
- Oxidation at 800° followed by vacuum annealing and reoxidation transformed scales obtained on both less pure and pure nickel into one single layer scale.
- Oxidation at 800° for long time, 70 hours when only a bilayer scale is present, followed by reoxidation at 1000° transformed parts of the scale into a completely columnar layer.
- Very long time of oxidation, 240 hours, at 800°, gave rise to only one layered scale of nickel oxide characterized by columnar grains. It should be again emphasized that due to the polycrystalline characteristics of the nickel specimens, some parts of a scale remained bilayer but there was no experimental evidence of increasing thickness of the inner scale.

## V.8 CONCLUDING REMARKS ON THE MECHANISM OF MORPHOLOGICAL DEVELOPMENT OF THE NICKEL OXIDE ON NICKEL AT 800°

As presented in the literature review, a unique mechanism has not been available to account for the diverse experimental results on bilayer scale formation. These discrepancies in the experimental results can be explained at least in part by the lack of systematic observations on the development of the scale in time, and also to lack of careful preparation of the oxide scale cross sections for detailed examination. As an example, Berry et al.[48] concluded from their micrographs that nickel oxidation at 800° for 100 hours gave rise to a single layer scale. However, the scale was not etched and the microstructural details of the scale were not revealed in these micrographs.

The oxidation mechanisms developed by different investigators have been based to a great extent on the interpretation of results from inert marker experiments. In the majority of cases the inert markers have been found at the metal/oxide interface after oxidation when only one columnar layer is present[88] and within the bilayer scale when two layer scales are formed[53,85,86]. These measurements must be cautiously interpreted because of the secondary processes which can disturb the location of the marker. For example, the location of the marker within a scale is often considered as an indication of the inward diffusion of the oxidant. Several investigators have shown, however, that this result can be obtained by the "flow" of the

scale around the marker owing to the plasticity of the scale[87]. Also the dimension of the inert markers must be carefully considered, especially in the case of nickel oxidation at our range of temperature because of the relatively small thickness of fine-grained nickel oxide scale obtained.

The bilayer characteristic is a common feature of the oxide scales formed at temperatures in the range 300-800°, especially on nickel, copper; cobalt and iron. The attempts to explain these results were reviewed in Chapter II. The majority of these attempts is based on the oxide dissociative mechanism. The calculations of the maximum oxygen arrival in the crack formed at metal/oxide interface, by the dissociation of the initially formed oxide, demonstrate that an inner layer could not grow until gas has access to the metal through microchannels formed in the oxide scale[60]. As soon as oxygen can enter from the external gas new oxide crystals could be nucleated. Our experimental evidence as well as that represented by different other investigators indicates that nickel oxide forms an adherent scale to the underlying nickel without formation of microchannels. In the case of nickel oxide growth based upon the dissociative mechanism, the oxidation rate can be calculated from the oxide dissociation pressure by the Langmuir expression:

$$\frac{d\omega}{dt} = P_{O_2}^{D} \left(\frac{M}{2\pi RT}\right)^{1/2}$$

$$\frac{d\omega}{dt} = \left(\frac{32}{2\pi \times 0.082 \times 1000}\right)^{1/2} = 2\times10^{-17}\ g^{0}/cm^{2}.sec.$$

This rate is insignificatn in comparison to the actual oxidation o rate.

Several investigators[89,90] considered that oxidation reduction impurities such as carbon and hydrogen arising from the metal or atmosphere will result in a higher oxygen activity in cavities existent at the metal-oxide interface or in voids existent throughout the oxide scale. Oxygen transport in the pores could then lead to formation and growth of a porous inner layer. In the case of nickel[51,91], voids were observed to form only at high temperatures, 1100°-1300°, in the oxide scale. To explain the stability of these voids, Graham and Caplan[91] in a study of the oxidation of nickel with different contents of carbon have demonstrated that these voids contain carbon dioxide at appreciable pressure and that the amount of cavity formation was related to the carbon content of nickel. Some of our micrographs indicated the presence of a small degree of porosity in the inner layer and voids located at the oxide boundaries in the columnar layer. Emphasis is not placed, however, on the inward migration of oxygen by these voids since the microstructural observations and growth of both types of scale were consistent with outward migration of nickel. The small degree of porosity appeared rather to be

simply related to the morphological development of the grains which could be equiaxed or columnar on the differently oriented grains of the polycrystalline nickel.

Rhines and coworkers[54,92] consider that nickel migrates at high temperatures through the lattice of nickel oxide and oxygen diffuses inward through grain boundaries of an initial columnar oxide to react with oxygen within the scale. This feature gives rise to a swelling of the scale as discussed in Chapter II. This swelling is considered to give rise to stress; subsequent recrystallization of the oxide near the metal gives rise to equiaxed grains but this mechanism gives no indication how the ratio outer to inner layer is changing with exposure time. Our results show that at temperatures less than 1000° the equiaxed oxide layer is the first to form and that this equiaxed layer can be converted to a columnar layer by long times of exposure and annealing. Therefore, the oxide grain size increases as a result of the annealing during an oxidation exposure and is not due to the formation of the new oxide at the grain boundaries. In addition the formation of outward extending polycrystalline oxide ridges at the oxide grain boundaries from very initial periods of oxidation demonstrate that boundary diffusion of nickel rather than oxygen plays a dominant role in the growth and development of the oxide scale.

It should be understood that our investigation develops one of the most important aspects of metal oxidation, generally observed by all investigators in the field, in that the grain growth of the oxide influences the oxidation mechanism and morphological development of the scales.

# CHAPTER VI

## GENERAL CONCLUSIONS

Some general conclusions follow from our experimental investigations:

1) The structure of the polycrystalline metal influences the oxidation behaviour due to its texture, grain size and impurities. The influence of the texture of polycrystalline nickel on its oxidation behaviour could lead to results that have practical application.
2) The structure of metal influences the mosaic structure of the oxide formed which, in turn, affects the contribution of short circuit paths to nickel transport through the scale during its growth.
3) Nickel oxide forms at 1000° and is characterized by a low nucleation rate and high growth rate. Consequently, metal-oxide epitaxy is much more favored than at 800°. As a result the oxide formed at 1000° is characterized by few boundaries which in character are more coherent than those formed at 800°.
3) An oxide cellular structure develops during the early stages of the reaction as a result of oxide thickening at grain boundaries due to nickel migration through diffusion sites offered by these grain boundaries. The ridges of oxide forming the cellular structure broaden and merge as the

oxidation proceeds. This structure subsequently develops distinct grains which are distinguishable by the virtue of their tendency to thermally facet. This tendency is most apparent on the scales obtained during oxidation intercepted by vacuum anneal.

4) The oxide scales formed on both impure and pure nickel after the very early stage of exposure exhibit a single equiaxed layer and/or a duplex layer in which the columnar layer is barely distinguishable depending on the recrystallization and the preferential growth of oxide formed on different crystallographically oriented metallic grains. As oxidation proceeds, the outer columnar layer consumes the inner equiaxed layer and at very long oxidation time some sections of the scale are formed of one columnar layer.

5) Our mechanism of duplex oxide layer formation is supported by two major experimental findings;

   a) The bilayer scale was transformed experimentally into a single columnar scale by four methods.

   b) During annealing of the scales, structural changes in the oxide scale due to a grain growth process takes place as indicated by the kinetic measurements, texture determinations and grain size observations. These experiments also indicated that the increasing temperature rather than increasing time played a more predominant role in the kinetics of grain growth.

6) The deviation in the oxidation rates from parabolic relationships was a result of the structural changes in the oxide scale in time which affects the number of the short diffusion paths available for nickel transport. It should be emphasized that the large decreasing effective rate constant for scale growth in time cannot be explained simply by a decreasing number of grain boundaries, since the orientation relationships between the oxide grains influence the effectiveness of boundaries for nickel transport.

# CHAPTER VII

## RECOMMENDATIONS FOR FUTURE WORK

Some possibilities for further work to extend our model describing scale growth would be as follows:

1) To extend our type of experiments to temperatures above 1000° in order to realize the sequences in the development of the nickel oxide scale and to understand the appearance of the inner equiaxed oxide layer in these conditions.
2) Experiments using inert and radioactive isotopes should be initiated in order to actually determine the relative amounts of metal and oxygen transport through differently structured oxide scales on nickel.
3) Attempts should be made to obtain direct measurements of the magnitudes of the effective diffusion coefficients for nickel in nickel oxide films and scales of different crystallite sizes and dislocation distributions using a radioactive nickel isotope.
4) Some types of experiments could be made on some other metals, e.g. cobalt, that exhibit some double layer structure. This type of investigation has an advantage since the more rapid oxidation rate of cobalt yields the possibility to readily obtain observations on development of the single layer and bilayer structure.

## APPENDIX A

## MATHEMATICAL ANALYSIS OF THE OXIDATION MODEL

To describe the nonparabolic behaviour of pure nickel during the oxidation at 800° and $p_{O_2}$ = 400 Torr the model proposed by Perrow et al[23] and developed by Khoi et al[38] was used.

The detailed mathematical analysis[10] of this model is presented in the following section. Using Wanger as a model for an ideal parallel layer of growing oxide, the rate of thickening $\frac{dx}{dt}$ can be expressed as:

$$\frac{dx}{dt} = V_{eq} \frac{K_r}{x} \qquad (A-1)$$

where $V_{eq}$ is the volume equivalent of the oxide, x is the thickness and $K_R$ is the parabolic rational rate constant. Substituting in the value for $K_r$ for NiO, after making the appropriate assumptions and using the proposed effective diffusion coefficient, we have:

$$\frac{dx}{dt} = \Omega D_{eff} \frac{\Delta c}{x} \qquad (A-2)$$

where Ω is the volume of the oxide per nickel ion. Replacing the $D_{eff}$ term by its equivalent[10], this equation may be expressed as:

$$\frac{dx}{dt} = \Omega \frac{\Delta c}{x} [D_L(1-f) + D_B f] \qquad (A-3)$$

because f << 1 and the above expression can be approximated to:

$$\frac{dx}{dt} = \Omega \frac{\Delta c}{c} D_L + \Omega \frac{\Delta c}{x} D_B f(t) \qquad (A-4)$$

which yields upon integration:

$$x^2 = 2\Omega \Delta c D_L t + 2\Omega \Delta c D_B \int f(t)dt. \qquad (A-5)$$

By differentiating $X^2$ with respect to t,

$$\frac{dx^2}{dt} = 2\Omega \Delta c D_L + 2\Omega \Delta c D_B f(t) . \qquad (A-6)$$

The expression $\frac{dx^2}{dt}$ is equivalent to the instantaneous effective parabolic rate constant $K_p(t)$, at time t. The values for $K_p(t)$ can be obtained by taking the tangents to the oxidation curves plotted in parabolic form. The expression $2\Omega \Delta c D_L$ is the Wagner's parabolic rate constant for lattice diffusion and is fixed for a given oxygen pressure. The term $2\Omega \Delta c D_B$ is the line defect contribution to the overall transport of the reactant. This expression is assumed also to be constant for a given oxygen pressure. We can thus define

$$K_L = 2\Omega \Delta c D_L \qquad (A-7)$$

and

$$K_B = 2\Omega \Delta c D_B . \qquad (A-8)$$

Substituting in the expression for $K_L$ and $K_B$ in equation (A-6) we obtain:

$$K_p(t) = K_L + K_B\, f(t) \quad . \qquad \text{(A-9)}$$

Clearly in the absence of short circuit diffusion, $f(t) = 0$ and the above relation is reduced to:

$$K_p(t) = K_L$$

or

$$\frac{dX^2}{dt} = K_L \quad \text{and} \quad X^2 = K_L\, t + C \qquad \text{(A-10)}$$

which is the familiar parabolic growth rate equation for a reaction product layer governed by lattice diffusion of the reactant.

The authors have considered $f(t) = \frac{2d}{D_t}$, where $D_t$ is the diameter of the grain at time t. Considering that grains grow during oxidation following the general expression for grain growth derived by Beck[83]

$$D_t^2 - D_o^2 = k_3 t \quad \text{or} \quad D_t = (k_3 t + D_o^2)^{1/2} \quad , \qquad \text{(A-11)}$$

where $D_o$ is the initial grain size and $k_3$ is the growth constant, the expression for $f(t)$ became:

$$f(t) = \frac{2d}{(k_3 t + D_o^2)^{1/2}} \quad . \qquad \text{(A-12)}$$

The combination of equation (A-9), (A-10) and the above

value for f(t) gives the following expression

$$\left(\frac{dX^2}{dt} - K_L\right) = K_B \frac{2d}{(k_3 t + D_o^2)^{1/2}} \quad \text{(A-13)}$$

Squaring both sides and taking the inverse, we obtain:

$$\frac{1}{\left(\frac{dX^2}{dt} - K_L\right)^2} = \frac{k_3}{4K_B^2 d^2} t + \frac{D_o^2}{4K_B^2 d^2} \quad \text{(A-14)}$$

A plot of $\frac{1}{\left(\frac{dX^2}{dt} - K_L\right)^2}$ versus t should yield a straight line with a slope $S = \frac{k_3}{4K_B^2 d^2}$ and an intercept $I = \frac{D_o^2}{4K_B^2 d^2}$.

To test this model the authors have derived an expression relating the thickness (weight gain) to the exposure time from the parameters obtained in the mathematical analysis, namely the slope S and the intercept I .

Substuting the expression of $f(t) = \frac{2d}{(D_o^2 + K_3 t)^{1/2}}$ into the expression:

$$X^2 = K_L t + K_B \int f(t)\, dt \quad \text{(A-15)}$$

and performing the integration, the following expression is obtained:

$$X^2 = K_L t + \frac{4K_B d}{k_3} \sqrt{D_o^2 + k_3 t} - \frac{4K_B d}{k_3} \quad \text{(A-16)}$$

Noting that the intercept $I = \frac{D_o^2}{4K_B^2 d^2}$ and the slope $S = \frac{k_3}{4K_B^2 d^2}$, the above equation can be simply written as:

$$X^2 = K_L t + \frac{2}{S}\left(\sqrt{I + St} - \sqrt{I}\right) . \qquad \text{(A-17)}$$

Thus an expression for $X^2$ in terms of a constant $K_L$ and two experimentally determined values S and I was derived. A test of the model thus consists of calculating $X^2$ from the values of $K_L$, S and I and comparing these values with the experimentally observed values. The good agreement of the experimental and calculated curves will support this proposed model and will allow the ratio of the boundary diffusion .

## APPENDIX B

## CALCULATION OF THE PARABOLIC OXIDATION RATE CONSTANT

To compare the kinetic experimental results obtained on nickel oxidation at 800° with those data based only on self diffusion of nickel through nickel oxide scale conforming to Wagner's model, the value of $k_p = 1.78 \times 10^{-14}$ $g^2\ cm^{-4}\ sec^{-1}$ was used. This value was taken from Khoi's[10] analysis regarding the evaluation of $k_p$ at temperatures below 1000°).

## APPENDIX C

## EXPERIMENTAL ERRORS AND LIMITATIONS

The experimental errors involved in the quantitative measurements of some of the parameters discussed in this thesis are considered in the following section.

### Oxidation kinetics

The results from the investigations on the oxidation kinetics were obtained on a continuously recording Cahn microbalance. The weight gains were expressed in $mg/cm^2$ and time in minutes, vibrations, oxygen flow in the reaction tube and electromagnetic fields inside the furnace caused small oscillations of the sample which were recorded on the recording chart. The maximum oscillation was ± 0.17 mg representing a negligible error of approximately 3% in determination of the weight gain. The errors associated with the initial period of reaction were eliminated by weighing the specimen before and after oxidation on a Metler microbalance. There are some factors influencing the experimental results such as accuracy of temperature and oxygen pressure, size of samples, position of the sample in the hot zone of the furnace. For this reason all the kinetics measurements were repeated at least twice to check the reproducibility of experiments.

From the oxidation kinetics plotted in the parabolic form the value of the effective parabolic rate constant $k_p(t)$

at a given time were calculated by taking tangents to these curves. The errors in $k_p$ determination are directly related to the experimental reproducibility. In fig. (C-1) the initial parabolic part of the oxidation curve is given for three of the runs effectuated at 800° for less pure nickel. The experimental reproducibility is in the range from 5 to 14% from the arithmetical average value.

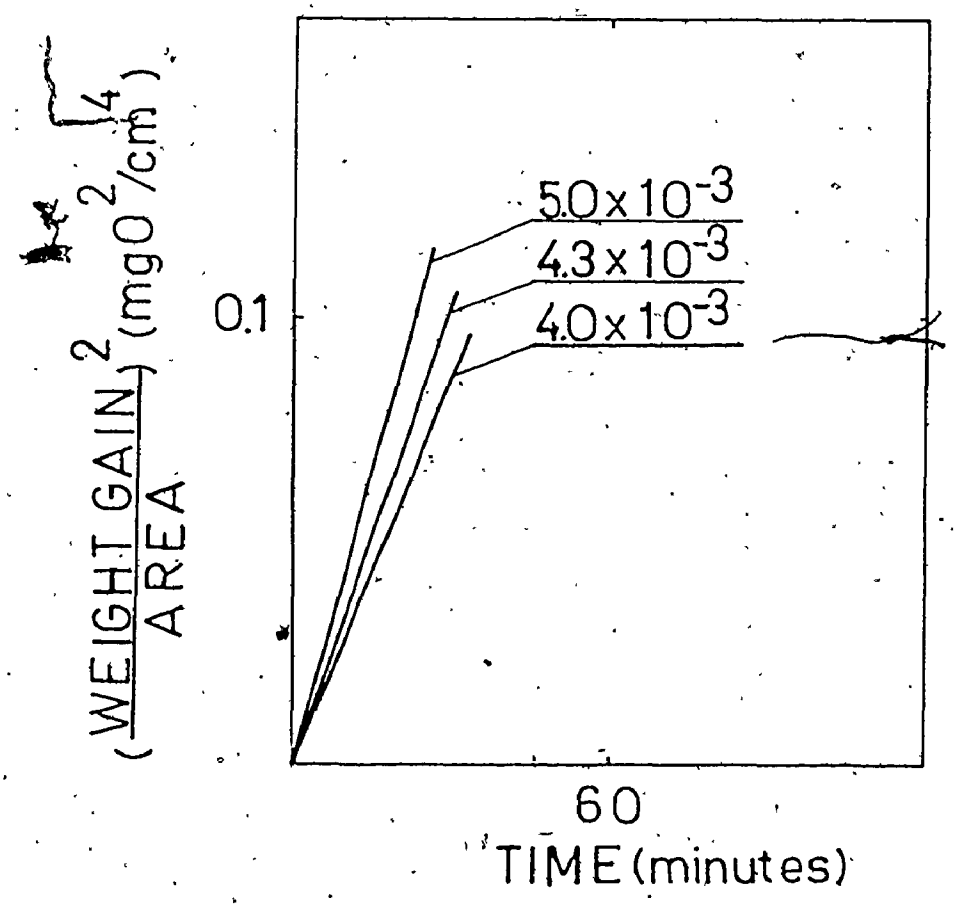


Fig. C-1. Plot of $(\frac{\text{weight change}}{\text{area}})^2$ versus time for three experimental curves (twenty minutes of oxidation of less pure nickel at 800°).

Determination of given grain size distribution

Determination of grain-size distribution requires measurements of each individual grain so each grain can be sized. In order to arrive at a distribution for grain size one divides the entire range of existing size into size intervals. Every size class has associated with it a frequency $f_i$, which indicates the number of grains N in the size interval i divided by the total number of grains measured:

$$f_i = \frac{N}{N_t}$$

The arithmetic scale is the simplest arrangement of size classes. Each class interval i has the same absolute width $\Delta$ and the lowest size class (i=1) begins at zero. This interval width $\Delta$ should be chosen to divide the overall range into an appropriate number of intervals. In geometric scaling the class limits are arranged in geometric series with a modul $\alpha$, so that the ratio of the upper to the lower class limit for each size class takes the same value, i.e. $\alpha$. The class width is then proportional to the class limits. To represent the distribution, the cumulative or relative frequency distribution curves could be used. In this investigation the relative curve distribution was preferred because it is more sensitive to the shape of the distribution. Here the frequency $\Delta P_i$ divided by the class width $X_i - X_{i-1}$

termed the relative frequency $p_i$ was plotted against the class limits as a continuous curve. The following quantities in figure (C-2) are generally used to characterize the size of the planar features: a) Nassenstein's diameter, Martin's diameter, c) Feret's diameter, d) the projection and e) the maximum chord length in the scanning direction[93]. During this

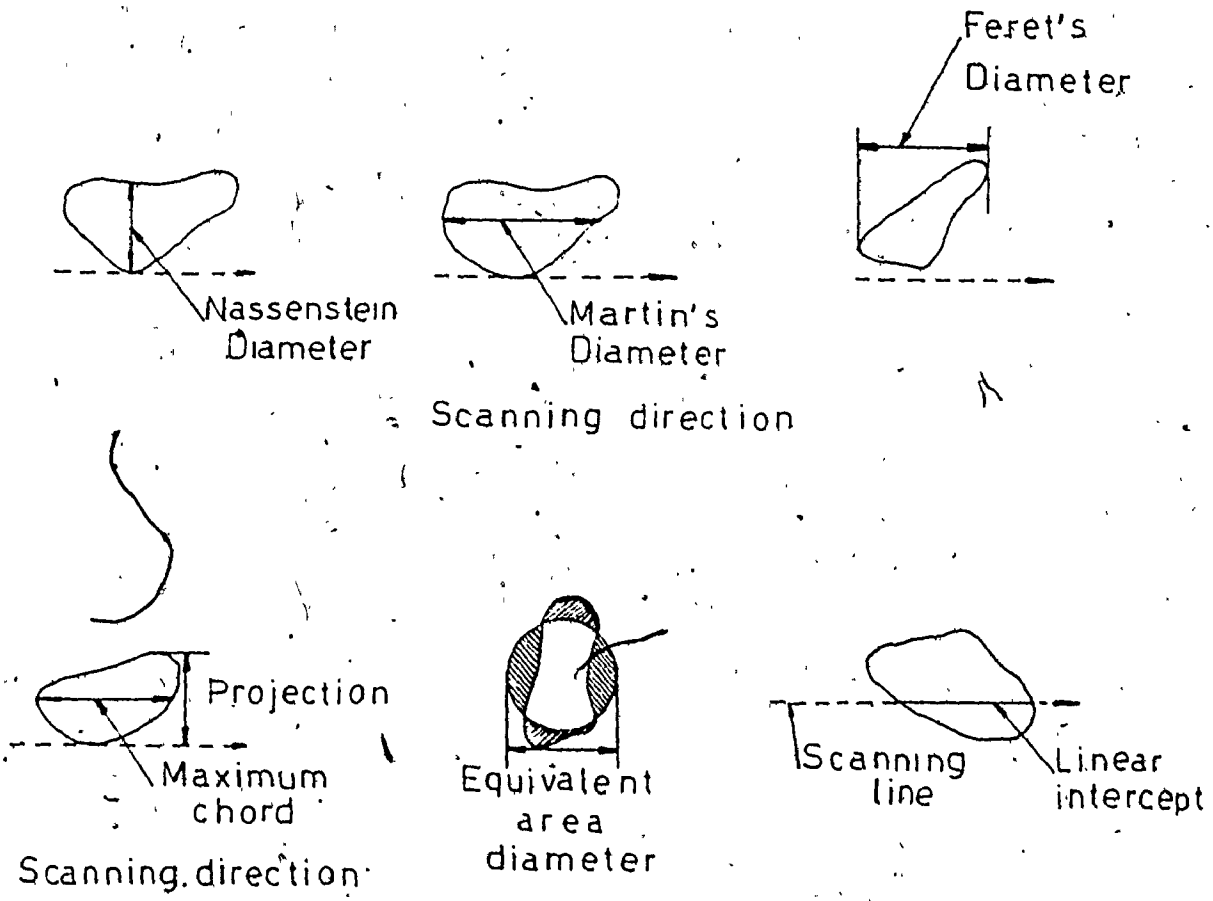


Fig. C-2. Quantities for sizing irregular planar features.

investigation a linear intercept and a Feret's diameter were used for grain size measurements of nickel oxide in the outer layer and for metal grains and for oxide crystallite sites formed in the early stages of oxidation[94] respectively. The linear intercepts method has the advantage that no approximations are involved in measurements since linear intercepts of features having any shape are read directly from lined scans. This method is easy to apply to plane cross section. The distribution of the internal areas and their equivalent diameters is to be preferred for projections in transmission or scanning electron microscopy, especially for the distribution of the crystallites size in the thin film of nickel oxide. There are effects of overlapping of crystallites causing errors in the sampling. There are some methods[95] of calculation to avoid these errors but for our purpose it was not necessary to consider them. Also there are some factors affecting the experimental measurements, as for example in the early stages of oxidation the size of the grains is difficult to measure because of the high magnification required, leading to poor focus and also at large thicknesses of the scale the time of electroetching required to reveal microstructures also leads to attack of the resin mount and hence poor resolution of observations. To obtain the grain size distribution from the cross sections at different times of oxidation many micrographs from the same.

types of specimens were used for size measurements. Also several sections were taken of each specimen. The sizes of crystallites were measured to an accuracy of 0.5 mm in size. Generally this uncertainty could reach 20% taking into account all experimental variables.

Measurements of the thickness of the oxide layers

Because of the polycrystallinity of the specimens used during this investigation and because of the anisotropy of the oxidation process, the thicknesses of the total outer and inner layers presented in fig. (IV.6.4-1) are an average value of the layers measured on many micrographs. From the arithmetic average of the total layer the layers formed only of equiaxed or columnar layers were excluded. Only the total layers composed of inner and outer layers are averaged. Considering the experimental difficulties in obtaining good microsections the uncertainty in measuring the total layer is about 16% for oxide layer obtained upon short exposure considering a magnification of 10000 and a thickness of 3.5 mm with an imprecise of reading of about 5 mm. This allowance of 5 mm was considered especially for etched cross sections when the micrographs don't give good indication of the interface metal-oxide.

## REFERENCES


1. O. Kubaschewski and B. C. Hopkins, Oxidation of Metals and Alloys, Butterworths, London 1962.
2. J. Bénard, Oxidation des Metaux, Gauthier-Villard, Paris, 1962.
3. Per Kofstad, Nonstoichiometry, Diffusion and Electrical Conductivity in Binary Metal Oxides, Wiley, New York, 1972.
4. J. Bardolle and J. Bénard, Rev. Met. 49, 613 (1952).
5. V. Martius, Can. J. Phys. 35, 466 (1955).
6. D. W. Pashley, Adv. Phys. 5, 173 (1956).
7. J. H. van der Merve, Discuss. Farad. Soc. 5, 201 (1949).
8. K. R. Lawless, J. W. Young and A. T. Gwathmey, J. Chem. Phys. 53, 667 (1956).
9. L. B. Garmon, Ph.D. Thesis, University of Virginia, U.S.A. (1966).
10. N. M. Khoi, Ph.D. Thesis, McMaster University, Canada (1972).
11. S. P. Mitoff, J. Phys. Chem. 35, 882 (1961).
12. H. G. Sockel and H. Schmalzried, Ber. Bunsenges. Physik. Chemie, 72, 745 (1968).
13. Y. D. Tretyakov and R. A. Rapp, Trans. AIME, 245, 1235 (1969).
14. W. C. Tripp and N. M. Tallan, J. Am. Cer. Soc. 53, 531 (1970).

15. I. Branski and N. M. Tallan, J. Chem. Phys. 49, 1243 (1968).

16. R. Lindner and Å. Åkerström, Disc. Farad. Soc. 23, 133 (1957).

17. M. T. Shim and W. J. Moore, J. Chem. Phys. 26, 802 (1957).

18. J. C. Choi and W. J. Moore, J. Phys. Chem. 66, 1308 (1962).

19. L. M. Volpe and J. Reddy, J. Chem. Phys. 53, 1117 (1970).

20. S. M. Klotsman, A. N. Timofeyev and I. Sh. Trakhtenberg, Fiz. Metal, Metalloved, 14, 428 (1962).

21. K. Fucki and J. B. Wagner, Jr., J. Electrochem. Soc. 112, 384 (1965).

22. M. O'Keefe and W. J. Moore, J. Phys. Chem. 65, 1438 (1961).

23. J. M. Perrow, W. W. Smeltzer and J. D. Embury, Acta Met. 16, 1209 (1968).

24. T. Homma, N. N. Khoi, W. W. Smeltzer and J. D. Embury, Oxidation of Metals 3, 463 (1971).

25. E. W. Hart, Acta Met. 5, 597 (1957).

26. H. Uhlig, J. Pickett and J. MacNairn, Acta Met. 7, 111 (1959).

27. H. J. Engel, K. Hauffe and B. Ilschner, Z. Electrochem. 58, 478 (1954).

28. K. Hauffe, L. Pethe and R. Schmidt, J. Electrochem. Soc. 115, 456 (1968).

29. K. Boreskov, Discuss. Farad. Soc. 41, 263 (1966).

30. C. Wagner, Corros. Sci. 10, 641 (1970).

31. I. M. Ritchie, Proc. Roy. Soc. (London) A299, 371 (1967).

32. M. J. Graham and M. Cohen, J. Electrochem. Soc., 119, 879 (1972).

33. C. Wagner in Atom Movements, ASM, Ohio, 153 (1959).

34. R. Herchl, N. N. Khoi, T. Homma and W. W. Smeltzer, Oxidation of Metals, 4, 35 (1972).

35. E. A. Gulbransen and F. K. Andrew, J. Electrochem. Soc. 104, 451 (1957).

36. M. J. Graham, D. Caplan and M. Cohen, J. Electrochem. Soc. 119, 1265 (1972).

37. S. Matsunaga and T. Homma, Oxidation of Metals, 10, 361 (1976).

38. N. N. Khoi, W. W. Smeltzer and J. D. Embury, J. Electrochem. Soc. 122, 1495 (1975).

39. L. E. Collins and O. S. Heavens, Proc. Phys. Soc. B70, 265 (1957).

40. M. Otter, Z. Naturforschung 14a, 355 (1959).

41. D. F. Mitchell, P. B. Sewell and M. Cohen, Surface Science 61, 355 (1976).

42. H. Pu. C. Chien-ti and K. Ke-hsin, Scientia Sinica 14, 632 (1965).

43. E. A. Gulbransen, Rev. Met. 45, 286 (1948).

44. E. A. Gulbransen and J. W. Hickman, Tech. Pub. 2068, Am. Soc. Mining and Met. Engrs. (1946).

45. D. L. Douglas, Corros. Sci. 8, 665 (1968).

46. A. Goswami, Nature (London) 191, 160 (1961).

47. J. P. Baur, R. W. Bartlett, J. N. Ong, Jr. and W. M. Fassell, Jr., J. Electrochem. Soc. 110, 185 (1963).

48. L. Berry and J. Paidassi, C. R. Acad. Sci. Paris 258, 2810 (1964).

49. J. Paidassi and L. Berry, C. R. Acad. Sci. Paris, 262, 1553 (1966).

50. R. Hales, Corros. Sci. 12, 555 (1972).

51. D. Caplan, M. J. Graham and M. Cohen, J. Electrochem. Soc. 119, 1205 (1972).

52. B. Ilschner and H. Pfeiffer, Naturwissenschafter 40, 603 (1953).

53. J. D. Sartell and C. H. Li, J. Inst. Metal, 90, 92 (1961).

54. F. N. Rhines and J. S. Wolf, Met. Trans. 1, 1701 (1970).

55. N. Terao, Jap. J. Appl. Phys. 10, 1256 (1971).

56. T. Ueno, Trans. JIM, 14, 267 (1973).

57. T. Ueno, Trans. JIM, 15, 167 (1974).

58. T. Ueno, Jap. J. Appl. Phys. 13, 725 (1974).

59. T. Ueno, Jap. J. Appl. Phys. 13, 773 (1974).

60. A. Dravnicks and H. J. McDonald, J. Electrochem. Soc. 94, 139 (1948).

61. N. Birks and H. Rickert, J. Inst. Metals, 91, 308 (1962).

62. S. Mrowec, Corros. Sci. 7, 563 (1967).

63. J. M. Perrow, Ph.D. Thesis, McMaster University (1967).

64. J. S. Dunn, J. Inst. Met. 46, 25 (1931).

65. J. L. Meijering and U. J. Verheijke, Acta Met. 7, 331 (1959).

66. J. J. Van der Broeck and J. L. Meijering, Acta Met. 16, 375 (1968).

67. T. Yamashina and T. Nagamatsuya, J. Electrochem. Soc. 111, 249 (1964).

68. G. B. Harris, Phil. Mag. 43, 113 (1952).

69. ASTM, card file of X-rays diffraction data.

70. J. V. Cathcart, G. E. Petersen and C. J. Sparks, Jr., J. Electrochem. Soc. 116, 664 (1969).

71. W. L. Phillips, Jr., J. Electrochem. Soc. 110, 1014 (1963).

72. E. A. Gulbransen and K. F. Andrew, J. Electrochem. Soc. 101, 128 (1954).

73. B. D. Cullity, Elements of X-rays diffraction, Addison-Wesley, Reading, Mass. 118 (1959).

74. C. E. Lowell, S. I. Grisaffe and D. L. Deadmore, Oxidation of Metals 4, 91 (1972).

75. J. Moreau and J. Bénard, J. Inst. Met. 83, 87 (1954-1955).

76. J. Moreau and J. Bénard, J. Chem. Phys. 53, 787 (1956).

77. C. F. Elam, Trans. Farad. Soc. 32, 1604 (1936).

78. J. Moreau and J. Bénard, Compte Rendus, 284, 1658 (1959).

79. G. E. Rhead and H. Mykura, Acta Met. 10, 843 (1962).

80. A. J. W. Moore in Metal Surfaces, Structure, Energetics and Kinetics, Seminar of American Society of Metals, pg. 155 (1962).

81. H. Mykura, Acta Met. 9, 570 (1961).

82. M. J. Graham, G. I. Sproule, D. Caplan and M. Cohen, J. Electrochem. Soc. 119, 883 (1972).

83. P. A. Beck, J. Appl. Phys. 19, 507 (1948).

84. G. C. Wood, T. G. Wright and J. M. Ferguson, Corros. Sci. 5, 645 (1965).

85. L. Czerski, S. Mrowec and T. Werber, Arch. Hutnictwa 3, 25 (1958).

86. S. Petit and E. S. Felton, J. Electrochem. Soc. 111, 135 (1964).

87. S. Mrowec and T. Werber, Acta Met. 8, 819 (1960).

88. W. W. Smeltzer, J. Electrochem. Soc. 103, 209 (1956).

89. G. B. Gibbs and R. Hales, Corros. Sci. 17, 487 (1976).

90. R. J. Hussey, G. I. Sproule, D. Caplan and M. J. Graham, Oxidation of Metals 11, 65 (1977).

91. M. J. Graham and D. Caplan, J. Electrochem. Soc. 120, 769 (1973).

92. F. N. Rhines and R. G. Connell, Jr., J. Electrochem. Soc. 124, 1122 (1977).

93. H. E. Exner, Int. Met. Reviews, 17, 25 (1972).

94. R. DeHoff - Quantitative Microscopy, McGraw-Hill Book Company (1968).

95. J. E. Hillard, Trans. MEt. Soc. AIME, 224, 906 (1962).